Extending Depletion Flocculation Phase Behavior Models to Partially Soluble and Aggregating Colloids—Asphaltenes

by

Sayyid Sajjad Pouralhosseini

A thesis submitted in partial fulfillment of the requirements for the degree of

Doctor of Philosophy

in

Chemical Engineering

Department of Chemical and Materials Engineering

University of Alberta

Abstract:

Mixtures of colloids + non-adsorbing polymers + good solvents are well known to exhibit multiphase behaviors that are driven by the depletion flocculation mechanism where one phase, designated a colloid gas, is largely comprised of polymer and solvent, while the other phase, designated a colloid (liquid or solid), comprises largely solvent + colloid. Qualitative aspects of this behavior are well-understood and quantitative models for the phase behavior of mono-dispersed hard-sphere particles + mono-dispersed non-adsorbing polymers in good solvents, such as the Fleer–Tuinier[1] model are well established. In this work, a generalization of the Fleer–Tuinier model for cases where the fraction of colloid that is soluble in a solvent and the size distribution of colloid particles both vary with global composition is described. The impacts of temperature variation, and mean polymer size, on phase diagrams are also treated theoretically and validated experimentally.

By incorporating the Ostwald–Freundlich equation, which links the size of nanoparticles to their solubility in the parameterization of the modified Fleer–Tuinier model, the number of parameters that must be identified by fitting experimental data is minimized. Envisioned applications and illustrations are drawn from the hydrocarbon energy sector where, for example, self-assembled nano-aggregates, known as asphaltenes, pose production, pipelining, and refining challenges. The solubility, mean size and size distribution of these self-assembling species are well known to be dependent on global composition. Quantitative fits to measured phase diagrams for Maya[2] and Athabasca asphaltenes + polystyrene (non-adsorbing polymer) + toluene (good solvent) at 298 K at fixed polymer mean molar mass are obtained for both mixtures. Variations of the two-phase to single-phase boundaries, critical points, and tie lines with changes in temperature at fixed polymer size and with polymer

mean size at fixed temperature are then predicted and the outcomes compared with data. The modeling approach, data fitting procedure, and the quality of the predictions, for these illustrative examples, are presented. The importance of these results with respect to the broader development of depletion flocculation models for applications where partially soluble and aggregating colloids arise is discussed.

REFERENCES

(1) Khammar, M.; Shaw, J.M. Liquid–Liquid Phase Equilibria in Asphaltene + Polystyrene + Toluene Mixtures at 293 K. *Energy Fuels* **2012**, 26 (2), 1075–1088.

(2) Fleer, G.J.; Tuinier, R. Analytical Phase Diagrams for Colloids and Non-adsorbing polymer. *Adv. Colloid Interface Sci.*, **2008** 143, 1-47.

Preface:

Chapter 2 of this thesis will be combined with Chapter 3, and will then be submitted as S. Pouralhosseini, F. Eslami, J.A.W. Elliott, J.M. Shaw, "Simulating Depletion Flocculation in Asphaltene + Toluene + Polystyrene Mixtures" to the Journal of Fluid Phase Equilibria. I was responsible for the modeling calculations and analysis as well as the manuscript composition. F. Eslami assisted me with the manuscript composition and Ostwald–Freundlich equation calculations. J.A.W Elliott was the supervisory co-author and was involved with concept formation and manuscript editing.

Chapter 4 has been accepted as S. Pouralhosseini, M. Alizadehgiashi, and J.M. Shaw, "On the Phase Behavior of Athabasca Asphaltene + Polystyrene + Toluene Mixtures at 298 K" at Energy & Fuels. I was responsible for the data collection and analysis as well as the manuscript composition. M. Alizadehgiashi assisted me with the manuscript composition.

Chapter 5 has been accepted as S. Pouralhosseini and J.M. Shaw, "On the Temperature Independent Colloidal Phase Behavior of Maya Asphaltene + Toluene + Polystyrene Mixtures" at Energy & Fuels.

It is noteworthy to mention that none of these journal papers and chapters would have been possible without J.M. Shaw's assistance with concept formulation and manuscript editing.

Dedication

To my parents and my supervisor, I couldn't have done this without you.

Thanks you for all your support along the way.

Acknowledgements

It is a genuine pleasure to express my deep sense of thanks and gratitude to my supervisor, Professor Shaw. His dedication and keen interest above all his overwhelming attitude to help his students played the main role in completing my work. His timely advice, meticulous scrutiny, and scientific advice have helped me to a great extent to accomplish this task.

I owe deep gratitude to Professor Elliott, for her keen interest on me during my graduate study. Her prompt inspirations with kindness, enthusiasm, and dynamism enabled me to complete my PhD.

I also thank profusely for the time and the effort the members of the supervisory and examining committees have spent on reviewing this thesis. Gratitude is also extended to Dr Petersen for the insightful discussions.

I am extremely thankful to my parents, brothers, and friends for their unlimited and wholehearted support.

I also thank Mildred Becerra, Linda Kaert, Amin Pourmohammadbagher, and Marc Cassiede.

I gratefully acknowledge financial support from the sponsors of the NSERC Industrial Research Chair in Petroleum Thermodynamics: the Natural Sciences and Engineering Research Council of Canada (NSERC), Alberta Innovates Energy and Environment Solutions, BP Canada, ConocoPhillips Canada Resources Corp., Nexen Energy ULC, Shell Canada Ltd., Total E&P Canada Ltd., Virtual Materials Group.

Table of Contents

List of Tables

List of Figures

Chapter 1: Introduction

1. Colloids

In this thesis, the colloidal behavior of asphaltenes is the central theme. IUPAC[1] defines colloids as supramolecular particles having at least one dimension of between 1 nm and 1 μm dispersed in a gas or liquid medium.[2-3] Just as the pressure of an atomic gas is affected by the interactions between the atoms, the physical properties of a colloidal dispersion depend on the interaction between particles. Apart from such similarities, there are also distinct differences between colloids and atoms. In contrast to pair interactions between atoms, interactions between particles can be tuned by changing particle type, solvent, temperature, addition of electrolytes, polymers or other colloidal particles, or by particle surface modification.

Colloidal dispersions can be found in a wide range of environments and products. Industrial examples include emulsions (mayonnaise), foams (shaving cream), surfactant solutions (shampoo) or polymer latex dispersions such as paints.[4-7]

2. Colloidal Interactions

The interaction forces acting between colloidal particles in suspensions play an important role in determining their properties and their behaviors in a range of environmental and industrial processes. In this introduction, the colloidal forces between particles including van der Waals forces (attraction), electrical double layer forces (repulsion), and steric forces (repulsion) are briefly reviewed. In colloidal dispersions, the van der Waals attraction between colloidal particles is opposed by a repulsion originating from either electrical double layers or steric hindrance.

2.1 van der Waals Attraction

In physical chemistry, the van der Waals interaction is the sum of weak London dispersion forces and stronger dipole-dipole forces. This intermolecular attraction arises from a cooperative oscillation of electron clouds when the molecules are proximate. Colloidal particles consist of atoms/molecules. When two colloidal particles in a medium are at close range, the van der Waals interaction between all atoms contributes to an effective attraction termed the colloidal van der Waals interaction. This attraction arises from the sum of atomic van der Waals interactions. The dielectric properties of the colloidal particles and the medium (solvent) determine the strength of the particle-particle interaction. Temperature is one of the parameters that affect van der Waals attraction. Lowering temperature results in stronger attraction.

2.2 Electrical Double Layer Attraction

A charged colloidal particle is surrounded by a medium with an inhomogeneous distribution of ions. Co-ions bearing the same charge as the colloids are depleted from the colloid surface and counter ions bearing opposite charge adsorb at the surface. Far from the colloidal surface the concentrations of the two ion types attain a constant averaged value. The inhomogeneous layer is called the double layer and its thickness depends on the bulk ion concentration in the medium. A double layer is composed of three parts: surface charge, the stern layer, and a diffuse layer. The electrical potential within the double layer has the maximum value on the particle surface (Stern layer). The potential decreases with the increase of distance from the particle surface and reaches the minimum value of zero at the boundary of the double layer. When a particle moves in a dispersion medium, a layer of the surrounding liquid is attached to the particle. The boundary of this layer is called the slipping plane. Zeta potential, the

value of the electric potential at this plane, is a very important parameter in the theory of interaction of colloidal particles.

When two double layers overlap, a repulsive pair potential develops which leads to a repulsive pressure. Dispersed like-charged colloids hence repel each other upon approach due to screened-Coulomb or double layer repulsion. Adding ions to the medium screens the charges on the colloidal surfaces and results in weaker repulsion.

2.3 Stern Layer Interaction

Colloidal dispersions can be stabilized by molecular chains attached to particle surfaces.[8] These chains can be either part of the molecules comprising the particle or a polymer attached to the surface of the particle. As two colloidal particles protected with chains approach one another the local osmotic pressure increases dramatically in addition to the steric hindrance of the chains on the surfaces of both particles. This competition between the chains for the same volume leads to a repulsive interaction.[9] Chains on the surface of particles can contribute to a (significant) repulsive interaction between particles. When the attached polymers or molecule chains on two particles overlap, the osmotic pressure between the surfaces strongly increases which leads to a repulsive interaction between the particles as illustrated in Figure 1.1.

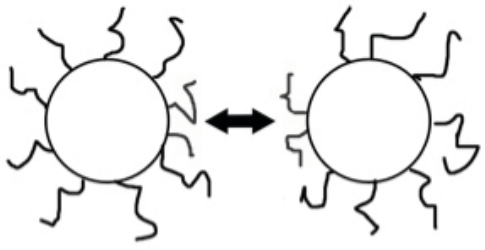

Figure 1.1 *Steric repulsion between two colloidal particles.*

3. Depletion Flocculation

When colloidal particles are mixed with non-adsorbing polymers, negative adsorption then causes an effective depletion layer near the surface of the particles due to a loss of configurational entropy of a polymer chain in that region. The attractive interaction between particles arises from the presence of depletion layers. A few colloidal particles in a non-adsorbing polymer solution are shown in Figure 1.2. Depletion layers are indicated by the dotted circles around the black colloidal particles. When the depletion layers overlap, the free volume available for the polymer chains increases. It follows that the free energy of the polymers is minimized by states in which the colloidal particles are at close vicinity. This phenomenon is just as if there were an attraction between the colloidal particles even while the colloid–polymer and direct colloid–colloid interactions are both repulsive.[10]

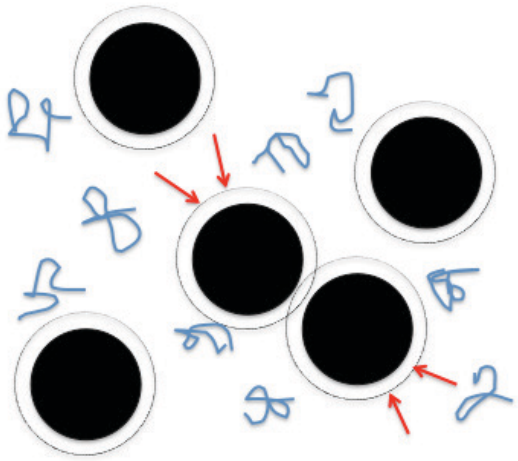

Figure 1.2 *Colloidal particles in a medium that also includes a non-adsorbing polymer. Dashed circles around the particles show depletion layers. When there is no overlap between depletion layers, the osmotic pressure on the spheres due to the polymers is isotropic. When the depletion layers overlap, the osmotic pressure on the spheres is asymmetric; Red arrows show the unbalanced osmotic pressures.*

4. Phase Separation of Colloidal Particles + Medium + Polymer Mixtures

When a dispersion containing colloidal particles is mixed with a medium including polymers, two kinds of instabilities can occur as illustrated in Figure 1.3: bridging flocculation (1) caused by adsorbing polymer or phase separation arising from the depletion force (2). The instability type encountered depends on whether the polymers adsorb on particle surfaces. Polymer adsorption can occur when contact between the colloidal particle surface and the polymer segments is energetically favorable to such a degree that the loss of configurational entropy is compensated.[8] When the amount of adsorbing polymer is insufficient to fully cover all available surface area on the colloids, bridging flocculation occurs (Figure 1.3).[11] By contrast, non-adsorbing polymers can induce phase separation by the mechanism of depletion flocculation (Figure 1.3). Any study on colloid–polymer mixtures should be preceded by an analysis of whether polymers adsorb or not. Analysis of the composition of the two phases formed can also be used to verify whether a depletion interaction is responsible for phase separation. It is also possible to investigate whether a polymer adsorbs onto a colloid by measuring the friction coefficient that a sphere experiences by for instance sedimentation or dynamic light scattering.[12-13] In this work, phase separation arises from depletion flocculation. Polystyrene does not adsorb on the surface of asphaltene particles.

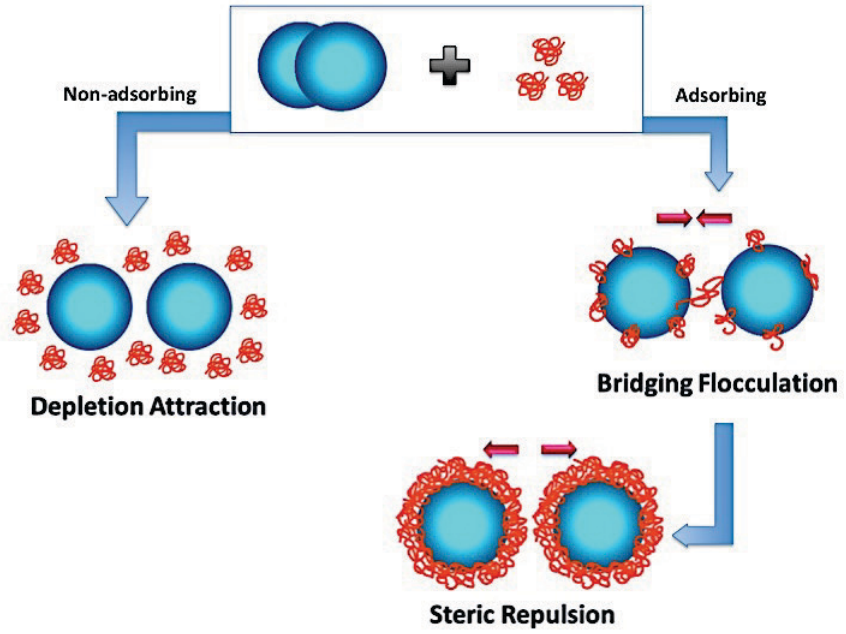

Figure 1.3 *Efects of polymer addition to the mixture of colloidal particles.*

5. Asphaltene Colloids

Asphaltenes are an ill-defined and self-aggregating petroleum fraction presenting numerous challenges from the perspective of measuring and modeling their behaviours in hydrocarbon resources or resource fractions from which they are partitioned physically or chemically, and in organic solvents once they are partitioned. Aphaltenes are defined as a molecular solubility class on the basis of macroscopic filtration measurements (ASTM D4055). However, this definition is at odds with the increasing and diverse collection of experimental data highlighting the nanostructured nature of asphaltenes.[14-17] Prior experiments on asphaltene filtration suggest that the size distribution of asphaltene colloidal particles in both crude oils and concentrated toluene solutions is bounded with nominal sizes ranging from ~ 1.5 to ~ 100 nm.[18-24] Colloidal mixtures undergo phase separation by adding a polymer.[25-26] The depletion

flocculation arising on addition of non-adsorbing polymers to asphaltene + toluene mixtures dictates that asphaltenes or a fraction of them must be colloidal.[27]

6. Polymer Addition to Mixtures Including Asphaltenes

Polymer addition is a way to control asphaltene sedimentation. Chang et al.[18] found that increasing the polarity of the amphiphile head group of a polymer strengthens the attractive force of amphiphiles to asphaltenes in alkane solvents and therefore improves asphaltene stabilization—preventing sedimentation. An amphiphile without a polar group namely nonylbenzene did not have an effect on asphaltene stability. Hashemi et al.[28] explored the effect of adding polyolefin amide alkeneamine polymeric dispersants and alkylated phenol on asphaltene sedimentation in mixtures of oil + heptane. The sedimentation of asphaltenes was delayed due to a decrease in asphaltene particle size and change of interactions between asphaltene particles. Recently, after investigation of the flocculation of asphaltenes in organic solvents caused by polymeric compounds, Lima et al.[25] suggested that the most suitable polymers to change asphaltenes stability contain polar groups that can interact with asphaltenes. Two types of polymers were studied: polycardanol with different molar masses and sulfonated polystyrene with various degrees of sulfonation. Their observation was that both sets of polymers behave as dispersants at higher concentrations and flocculants at low concentrations. The reason was the relative amount of polymer polar groups available for interaction with asphaltene polar groups. Increasing polymer concentration increased the number of asphaltene–polymer interactions which initially increased the number of asphaltene aggregates associated to the polymer but a large amount of asphaltene–polymer association was thought to cause less asphaltene–asphaltene association and therefore less

aggregates were susceptible to flocculate. It was reported that polystyrene without polar groups did not modify asphaltene behaviour in dilute solutions.[25] This result from the literature, showing the dilute composition range investigated[30-31] is different from the behavior for the impact of a non-adsorbing polymer (polystyrene) in a good solvent (toluene) on concentrated stabilized colloidal particles (asphaltenes) shown by Khammar and Shaw.[27, 32-33] While the two-phase behavior of this mixture at room temperature was identified, a robust model describing asphaltene + polystyrene phase behavior is not available.

7. Free Volume Theory

A volume theory to calculate phase behaviour of colloid + non adsorbing polymer mixtures + solvent mixtures was proposed by Lekkerkerker et al.[34] Their model is not valid for the full range of R_g/R_s ratios where R_g is the polymer radius of gyration and R_s is the particle radius. Fleer–Tuinier[35] extended this approach using free volume theory to address this problem. The Fleer–Tuinier model is a hard sphere (temperature independent) monodispersed model and cannot be used directly for polydispersed colloids such as asphaltenes in toluene because: 1) asphaltene average particle size changes with concentration, 2) part of the asphaltenes are soluble in toluene and depending on concentration the rest is colloidal, and 3) asphaltenes are not hard spheres and there are interactions between particles that are impacted by composition and may be impacted by temperature. These interactions must be calculated or measured so that the Fleer–Tuinier model can be modified.

8. Objectives

The main hypothesis in this thesis is that asphaltenes are not completely soluble in organic solvents i.e. part of asphaltenes are colloidal. In chapter 2, the fraction of colloidal particles of asphaltene versus asphaltene concentration in toluene is obtained. In addition, the size change of these particles with concentration is a question for this part. This phase behavior and property knowledge is of importance to design novel processes and calibrate the modified model. So in the next chapter, it was necessary to validate the predictions and theoretical findings using another conceptually similar model, the Ostwald–Freundlich equation. Expansion of our knowledge about other asphaltene sample phase behaviors and properties is the theme of chapter 4. In chapter 4, Athabasca asphaltene phase behavior in the mixture of toluene + polystyrene was tested and compared to data for Maya asphaltenes. In the last part of this thesis, the effect of temperature on the phase behavior of asphaltene particles in toluene in the presence of polystyrenes is tested theoretically and experimentally. The interactions between particles and temperature effects on the size of particles and polymers need to be tested to explore the temperature effect on the behaviour of interest.

9. Thesis Outline

In chapter 2, the Fleer–Tuinier model is modified according to Maya heavy oil asphaltene features and a property model is developed to predict asphaltene average size and solubility in toluene. Validation of the predicted results for asphaltene average size and solubility by the Ostwald–Freundlich equation are presented in Chapter 3. In Chapter 4, experimental results and property predictions related to phase behavior of Athabasca asphaltene + toluene + polystyrene are presented. The effect of temperature on phase boundaries of asphaltene +

toluene + polystyrene is explored theoretically and experimentally in Chapter 5. Finally, conclusions and future work are presented in the last chapter.

REFERENCES

(1) Everett, D.H. Manual of Symbols and Terminology for Physicochemical Quantities and Units, Appendix 2: Definitions, Terminology and Symbols in Colloid and Surface Chemistry, Pure Appl. Chem. 1972, 31, 579-638.

(2) Everett, D.H. Basic Principles of Colloid Science, The Royal Society of Chemistry 1988, 243-244.

(3) Russel, W.B.; Saville, D.A.; Schowalter, W.R. Colloidal Dispersions Cambridge Universtity Press, USA, 1999.

(4) Zimmerman, S.; Minton, A. Macromolecular Crowding - Biochemical, Biophysical, and Physiological Consequences, Annu. Rev. Biophys. Biomol. Struct. 1993, 22, 27-65.

(5) Neu, B.; Wenby, R.; Meiselman, H. J. Effects of Dextran Molecular Weight on Red Blood Cell Aggregation, Biophys. J., 2008 95, 3059- 3065.

(6) Doublier, J.; Garnier, C.; Renard, D.; Sanchez, C. Proteinpolysaccharide Interactions, Curr. Opin. Colloid Interface Sci. 2000, 5, 202-214.

(7) Hughes, D.; Robb, I.; Dowding, P. Stability of Copper Phthalocyanine Dispersions in Organic Media, Langmuir 1999, 15, 5227-5231.

(8) Fleer, G.J.; Cohen Stuart, M.A.; Scheutjens, J.M.H.M.; Cosgrove, T.; Vincent, B. Polymers at Interfaces, Chapman & Hall, New York, 1993.

(9) Fischer, E.W. Elektronenmikroskopische Untersuchungen zur Stabilität von Suspensionen in Makromolekularen Lösungen, Kolloid Z 1958, 160, 120-141.

(10) Vrij, A. Polymers at Interfaces and the Interactions in Colloidal Dispersions, Pure Appl. Chem. 1976, 48(4), 471-483.

(11) Evers, O.A.; Scheutjens, J.M.H.M.; Fleer. H.J. Statistical Thermodynamics of Block Copolymer Adsorption. Part 2.—Effect of Chain Composition on the Adsorbed Amount and Layer Thickness, J. Chem. Soc. 1990, 86,1333-1340

(12) Golz P.M. Dynamics of Colloids in Polymer Solutions, Ph.D. Thesis, University of Edinburgh, 1999.

(13) Gögelein, C.; Nägele, G.; Buitenhuis, J.; Tuinier, R.; Dhont, J.K.G. Polymer Depletion-Driven Cluster Aggregation and Initial Phase Separation in Charged Nanosized Colloids, J. Chem. Phys. 2009, 130, 204905.

(14) Yarranton, H.W. Investigation of Asphaltene Association with Vapor Pressure Osmometry and Interfacial Tension Measurements, Ind. Eng. Chem. Res. 2000, 39(8), 2916-2924.

(15) Yarrranton, H.W.; Ortiz, P.D.; Barrera, D.M.; Stasik, E.N.; Barre, L.; Frot, D.; Eyssautier, J.; Zeng, H.; Xu, G.; Dechaine, G.; Becerra, M.; Shaw, J.M.; McKenna, A.M.; Mapolelo, M.M.; Bohne, C.; Yang, Z.; Oake, J. On the Size Distribution of Self-Associated Asphaltenes, Energy Fuels 2013, 27(9), 5083-5106

(16) Nikooyeh, K.; Shaw, J.M., On Enthalpies of Solution of Athabasca Pentane Asphaltenes and Asphaltene Fractions, Energy Fuels 2013, 27(1), 66-74.

(17) Zhang, Y.; Takanohashi, T.; Shishido, T.; Sato, S.; Saito, I. Estimating the Interaction Energy of Asphaltene Aggregates with Aromatic Solvents. Energy Fuels 2005, 19(3), 1023-1028.

(18) Mostowfi, F.; Indo, K.; Mullins, O.C.; McFarlane, R. Asphaltene Nanoaggregates Studied by Centrifugation. Energy Fuels 2009, 23, 1194-1200.

(19) Espinat, D.; Fenistein, D.; Barre, L.; Frot, D.; Briolant, Y. Effects of Temperature and Pressure on Asphaltenes Agglomeration in Toluene. A Light, X-ray, and Neutron Scattering Investigation. Energy Fuels 2004, 18, 1243-1249.

(20) Barre, L.; Simon, S.; Palermo, T. Solution Properties of Asphaltenes. Langmuir 2008, 24, 3709-3717.

(21) Sheu, E.Y. Small Angle Scattering and Asphaltenes. J. Phys.: Condens. Matter 2006, 18, 2485-2498.

(22) McKenna, A.M.; Blakney, G.T.; Xian, F.; Glaser, P.B.; Rodgers, R.P.; Marshall, A.G. Heavy Petroleum Composition 2. Progression of the Boduszynski Model to the Limit of Distillation by Ultrahigh Resolution FT-ICR Mass Spectrometry. Energy Fuels 2010, 24, 2939–2946.

(23) Zhao, B.; Shaw, J.M. Composition and Size Distribution of Coherent Nanostructures in Athabasca Bitumen and Maya Crude Oil. Energy Fuels 2007, 21, 2795-2804..

(24) Ching, M.J.T.M.; Pomerantz, A.E.; Andrews, A.B.; Dryden, P.; Schroeder, R.; Mullins, O.C.; Harrison, C. On the Nanofiltration of Asphaltene Solutions, Crude Oils, and Emulsions. Energy Fuels 2010, 24, 5028-5037.

(25) Lima, A.F.; Mansur, C.R.E.; Lucas, E.F.; Gonzalez, G. Polycardanol or Sulfonated Polystyrene as Flocculants for Asphaltene Dispersions. Energy Fuels 2010, 24, 2369-2375.

(26) Myakonkaya, O.; Eastoe, J. Low Energy Methods of Phase Separation in Colloidal Dispersions and Microemulsions. Adv. Colloid Interface Sci. 2009, 149, 39-46.

(27) Khammar, M.; Shaw, J.M. Liquid–Liquid Phase Equilibria in Asphaltene + Polystyrene + Toluene Mixtures at 293 K. Energy Fuels 2012, 26 (2), 1075–1088.

(28) Chang, C.L.; Fogler, H.S. Stabilization of Asphaltenes in Aliphatic Solvents Using Alkylbenzene—Derived Amphiphiles 1. Effect of the Chemical - Structure of Amphiphiles on Asphaltene Stabilization. Langmuir 1994, 10, 1749-1757.

(29) Hashmi, S.M.; Quintiliano, L.A.; Firoozabadi, A. Polymeric Dispersants Delay Sedimentation in Colloidal Asphaltene Suspensions. Langmuir 2010, 26, 8021-8029.

(30) Noda, I.; Higo, Y.; Ueno, N.; Fujimoto, T. Semidilute Region for Linear-Polymers in Good Solvents. Macromolecules 1984, 17, 1055-1059.

(31) Luckham, P. Measurement of the Interaction Between Adsorbed Polymer Layers—The Steric Effect, Adv. Colloid Interface Sci. 1991, 34, 191-215.

(32) Wang, S.; Liu, J.; Zhang, L.; Xu, Z.; Masliyah, J. Colloidal Interactions between Asphaltene Surfaces in Toluene, Energy Fuels 2009, 23, 862- 869.

(33) Khammar, M.; Shaw, J.M.; Estimation of Phase Composition and Size of Asphaltene Colloidal Particles in Mixtures of Asphaltene + Polystyrene + Toluene at 293K and Atmospheric Pressure. Fluid Phase Equilib. 2012, 332,105-119.

(34) Lekkerkerker, H.N.W.; Poon, W.C.K.; Pusey, P.N.; Stroobants, A.; Warren, P.B. Phase Behaviour of Colloid + Polymer Mixtures. Europhys. Lett. 1992, 20, 559-564.

(35) Fleer, G.J.; Tuinier, R. Analytical Phase Diagrams for Colloids and Non-adsorbing Polymer. Adv. Colloid Interface Sci. 2008, 143, 1-47.

Chapter 2: Simulating Depletion Flocculation in Asphaltene + Toluene + Polystyrene Mixtures

ABSTRACT: Polymers are added to crude oils to modify asphaltene aggregate behaviour during oil production. Typically, these polymers sorb on multiple asphaltene aggregate surfaces simultaneously and cause flocculation. Recently, polystyrene, a non-adsorbing polymer, was shown to cause asphaltene + toluene mixtures to split into two stable phases, one polymer-rich and one asphaltene-rich, due to depletion flocculation. In this work, the phase behaviour of polystyrene + Maya pentane asphaltene + toluene mixtures is simulated using a modified Fleer–Tuinier model, where the monodispersed and composition invariant mean size requirement for the particles is relaxed but the polystyrene, with mean molar masses of 393,000 and 700,000 g/mole, is approximated as monodispersed. The distribution of asphaltenes between molecular and aggregated species, and the mean and distribution of the size of aggregated asphaltenes with global composition in toluene, are not known a priori. Consequently, the variation of the fraction of asphaltenes participating in the depletion flocculation mechanism and variation of their mean size with overall composition are key parameters in the modified Fleer–Tuinier model. The proposed model provides quantitative fits to measured two-phase to single-phase boundaries, and liquid–liquid critical points. The computed variation of the fraction of asphaltenes participating in the depletion flocculation mechanism, and the mean size of the asphaltenes with overall composition, are shown to be consistent with measured enthalpy of solution measurements, and with measured relative phase volumes within the two-phase region.

Key words: Non-adsorbing, Polymer, Aggregation, Size, Solubility

1. Introduction

Addition of non-sorbing polymers to colloidal suspensions is one way to cause them to split into two phases. One phase, rich in colloid, is referred to as a colloid liquid, and the other phase, rich in polymer, is referred to as a colloid gas.[1-3] The mechanism, known as depletion flocculation, comprises four steps:

1. Formation of a polymer free layer around individual colloidal particles
2. Development of an osmotic pressure, at the boundary of the polymer free zone as a consequence of this depletion
3. Formation of largely polymer free but solvent rich flocks as the polymer free layers of particles overlap
4. Separation of the fluid into bulk phases as flocks combine.

The local physics/chemistry surrounding individual particles is illustrated in Figure 2.1, and the overall separation process is illustrated in Figure 2.2. These figures serve to introduce key terms and concepts. For further details readers are referred to a recent book by Lekkerkerker and Tuinier.[4]

An osmotic equilibrium theory for depletion flocculation was developed by Lekkerkerker et al.[5] for the prediction of the phase behaviour of such ternary mixtures. According to this theory, polymer partitioning between phases is taken into account and the depletion layer thickness δ surrounding nanoparticles with radius R_s is considered to be proportional to the radius of gyration R_g of the polymer. Their model, valid when $R_g/R_s<1$ (colloid limit) and where polymer concentration is below the overlap concentration ($\varphi/\varphi_{ov}<1$), was extended by

Fleer–Tuinier[6] using free volume theory to include all polymer size-to-particle-radius (R_g to R_s) ratios.

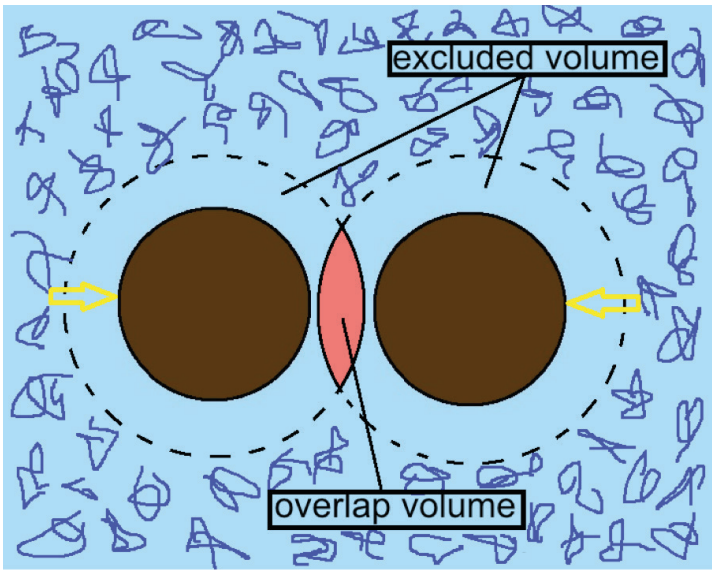

Figure 2.1 *A schematic illustrating the depletion flocculation mechanism at the particle scale. The excluded volume, the overlap volume, and the direction of the osmotic pressure (yellow arrows) arising from the polymer (blue curves) are defined.*

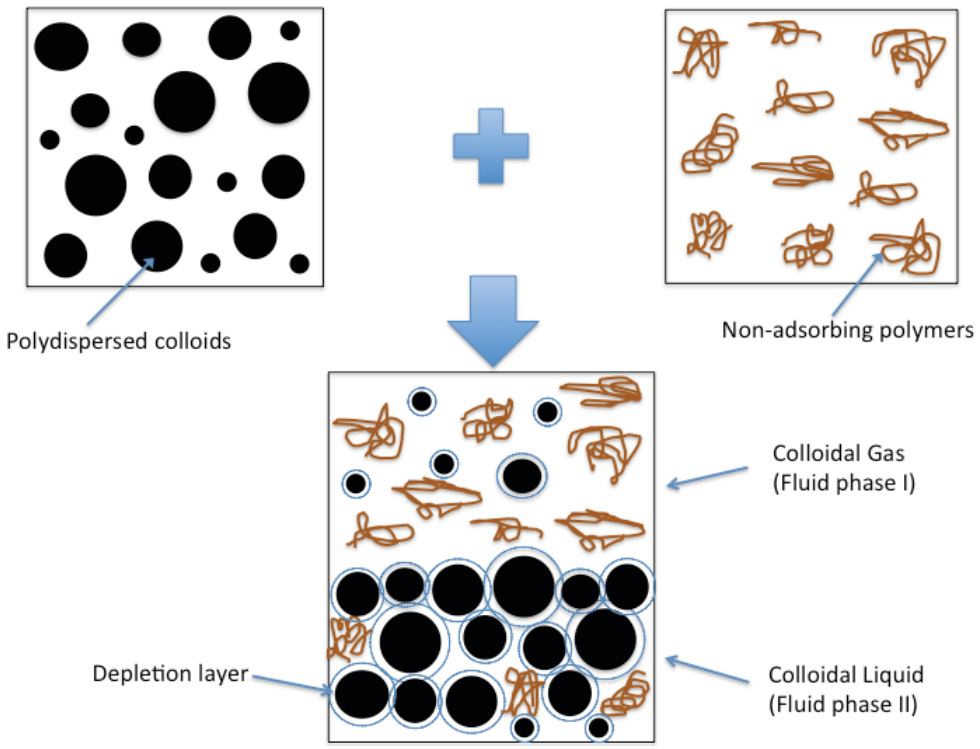

Figure 2.2 *A schematic illustrating the depletion flocculation mechanism at the macroscopic scale showing how a mixture of a polydispersed colloid in a solvent + a non-adsorbing polymer in a solvent separate into a polymer rich phase (phase I, G) and colloid rich phase (phase II, L).*

According to the Fleer–Tuinier model, the depletion thickness around a sphere (more formally the range of the depletion interaction), δ, is a function of colloid size, polymer volume fraction in the mixture, and the polymer-size to particle-radius ratio:

$$\delta = R_s 0.865\{q_R^{-2} + c_1 Y^{2\kappa}\}^{-0.44} \qquad (2.1)$$

where the terms appearing in equation (2.1) are expressed as:

$$Y = \left(\frac{\varphi}{\varphi_{ov}}\right) q_R^{-1/\kappa} \qquad (2.2)$$

$$\varphi_{ov} = \frac{3\,M_w}{4\,\pi\,R_g^3\,N_A\,\rho_{polystyrene}} \tag{2.3}$$

$$R_g = 0.012\,M_w^{0.595} \tag{2.4}$$

$$q_R = {R_g}\Big/{R_s} \tag{2.5}$$

and the symbols comprise: c_1=3.95, κ = 0.77, M_w is polymer molar mass, N_A is Avogadro's number, $\rho_{polystyrene}$ is polystyrene density, φ is the polymer volume fraction in the free volume not occupied by the particles and the depletion layer surrounding them, and φ_{ov} is the particle-free overlap volume fraction of polymer.

The chemical potential (μ) of particles in dispersions and their contributions to pressure times particle volume (pv) include both hard sphere and polymer effects:

$$\mu = \mu^0 + \mu^p \tag{2.6.a}$$

$$pv = (pv)^0 + (pv)^p \tag{2.6.b}$$

where μ^0 is the chemical potential of particles if assumed to be hard spheres in a solvent without polymers, μ^p is the polymer contribution to particle chemical potential, ν is particle volume, $(pv)^0$ is the polymer independent hard sphere contribution to pressure times particle volume, and $(pv)^p$ is the polymer contribution to pressure times particle volume. Hard sphere contributions to chemical potential and pressure times particle volume are well represented by accurate expressions reported by Carnahan and Starling:[7]

$$\mu^0 = \ln\eta + 8f + 7f^2 + 2f^3 \tag{2.7}$$

$$(pv)^0 = \eta + 4f^2 + 2f^3 \qquad (2.8)$$

where η is the colloidal particle volume fraction and f is:

$$f = \frac{\eta}{1-\eta} \qquad (2.9)$$

The polymer contributions to the chemical potential of particles and pressure times particle volume, were reported by Fleer–Tuinier[6] and are restated here:

$$\mu^p = \int_0^Y [\beta - (1+f)\beta_1]\left[q_R^{-1/\kappa} + 3\kappa c_2 Y^{3\kappa-1}\right] dY \qquad (2.10.a)$$

$$(pv)^p = \int_0^Y [\beta - f\beta_1]\left[q_R^{-1/\kappa} + 3\kappa c_2 Y^{3\kappa-1}\right] dY \qquad (2.10.b)$$

where: c_2=1.62 and κ =0.77 for excluded volume chains in good solvents. β_1 is first derivative of β with respect to f and β is defined and obtained as:

$$\alpha = \frac{\phi}{\varphi} = (1-\eta)\beta \qquad (2.11)$$

$$\beta = e^{-Q} \quad , \quad Q = Af + Bf^2 + Cf^3 \qquad (2.12)$$

$$A = (1+q)^3 - 1\,, \quad B = 3q^2\left(q + {}^3/_2\right), \quad C = 3q^3 \qquad (2.13)$$

where $\phi = \alpha\varphi$ is the polymer volume fraction, $q = \delta/R_s$, and α is the free volume fraction for polymers, defined within the model. Direct application of the Fleer–Tuinier model, comprising equations (2.1)-(2.13), valid for the behaviour of monodispersed hard sphere colloidal particles and monodispersed polymers in good solvents, to asphaltene + polystyrene + toluene mixtures yields at best only qualitative agreement with the observed phase behaviours, [6, 8, 9] as illustrated in Figure 2.3. By manipulating the assigned mean particle size for the asphaltene particles, the location of the critical point on the two-phase to one-phase boundary can be approximated but the two-phase envelope is poorly represented, particularly for the saturated polymer-rich phase composition. As polystyrene has a narrow size distribution and variation of polymer mean molar mass from 393,000 to 700,000 g/mole has little impact on the predicted critical points and phase boundaries, Figure 2.3.a vs Figure 2.3.b, it would appear that the representation of the asphaltenes is the principal weakness in the application of the model to this type of mixture, and the hence the best starting point for model modification.

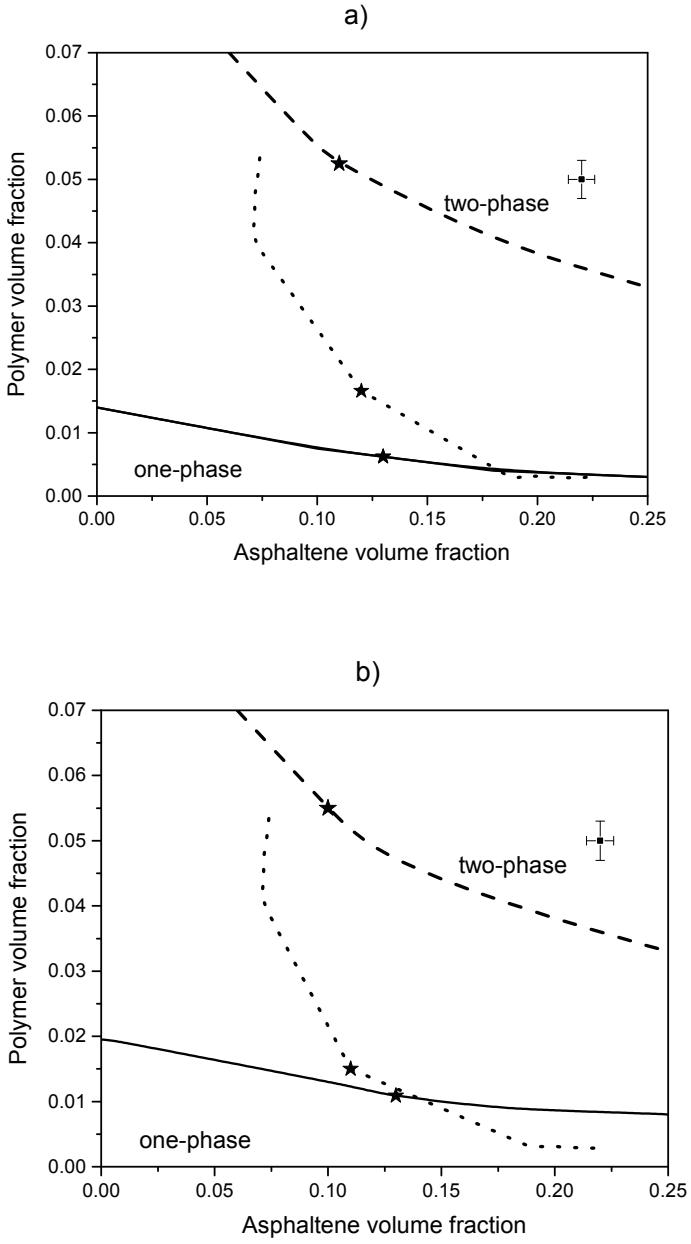

Figure 2.3 *A comparison between one-phase to two-phase boundaries predicted using the Fleer–Tuinier model and experimental phase diagrams (dotted curve) for mixtures of Maya asphaltenes + toluene + polystyrene for polystyrene molar masses: a) 393,000 g/mol and b) 700,000 g/mol, where asphaltene nanoparticle radii are set to 5.5 nm (dashed curve) and 22 nm (solid curve);* [6, 9] *(★): critical points.*

Asphaltenes, an ill-defined and self-aggregating petroleum fraction, present numerous challenges from the perspective of property measurement and modeling, whether in hydrocarbon resources or resource fractions from which they are partitioned physically or chemically, and in organic solvents once they are partitioned. In crude oils they comprise, in whole or in part, nanoaggregated domains that are filterable from a crude without addition of solvent.[10] Minimal partitioning occurs with a nominal pore size of 100 nm, while only a small fraction of aggregates pass through membranes with a nominal pore size of 5 nm. Chemical partitioning is performed by diluting an oil in a ratio of 40 g to 1 mL with an n-alkane at room temperature and then filtering the mixture using a filter with a nominal pore size of 500 nm or greater. The filter cake is treated further to eliminate inorganic or other matter, residual n-alkane, and to isolate the asphaltene fraction. There are numerous and well-established procedures for this chemical separation including ASTM D4055, IP 143, and ASTM D4124. The details of the thermophysical, chemical composition and other properties of the chemically separated asphaltenes vary with the method of partitioning, and even with modest variation of procedures within each method.[11] Irrespective of the method of separation, asphaltenes are a multiphase powder at room temperature where particles collectively if not individually comprise solid, glass, and liquid phases. [12-13]

Conventionally, asphaltenes have been deemed insoluble in alkanes and soluble in benzene and toluene on the basis of macroscopic filtration measurements. This simplistic definition is at odds with the increasing and diverse collection of experimental data highlighting the nanostructured nature of asphaltenes. From a solution thermodynamics perspective, dissolution of a solid solute into a liquid includes two parts, the enthalpy of transition to liquid for the solute and the enthalpy associated with homogeneous mixing at a molecular

level. Nikooyeh and Shaw[11, 14] showed that only a fraction of asphaltenes undergo dissolution, and asphaltene aggregation is observed even in toluene at ppm level mass fractions.[15] Vapor pressure osmometry, calorimetric, rheology, centrifugation, filtration, dynamic light scattering, and SAXS measurements have been performed to probe the fraction of asphaltenes remaining aggregated, aggregate mean size, size distribution, and shape.[11, 15-20] For example, in toluene, radii of gyration values range from 1.5 nm up to higher than 16 nm depending on asphaltene concentration.[15, 18-21] Currently, the application of diverse experimental measurements provides dissonant impressions as to the nature of asphaltenes, even when used to probe the same samples. [17] This diversity in apparent asphaltene properties has also been seen in physically separated asphaltenes. Zhao et al. [22] filtered Athabasca bitumen (19 %wt asphaltenes) and Maya crude oil (16 %wt asphaltenes) at 473 K. They found that the amount of asphaltene retained depended on the filter pore size. For Maya crude oil, 50 wt. % of the asphaltenes passed through a 20 nm ceramic filter and 10wt % passed through a 5 nm ceramic filter and none of the aggregates exceeded 100 nm. Ching et al.[23] worked with conventional crude oils containing up to 7.6 wt% asphaltenes and did not observe retentates using a 30 nm Teflon filter at 353 K. These and other prior results[24] suggest that the size of asphaltene colloidal particles in both crude oils and concentrated toluene solutions is bounded with nominal sizes ranging from 1 to 100 nm. Recently, Yarranton et al.[17] and Long et al.[25] showed that the size distribution of asphaltene aggregates is bimodal. These results are consistent with the nanofiltration results[22] and if free molecules are included, the size distribution of asphaltenes is trimodal as sketched in Figure 2.4. The literature on this topic is currently qualitative with a focus on mode identification. Simultaneous quantitation of the mass fractions of asphaltenes in these three modes and their

trends with composition, temperature and other intensive or extensive variables remain subjects for the future.

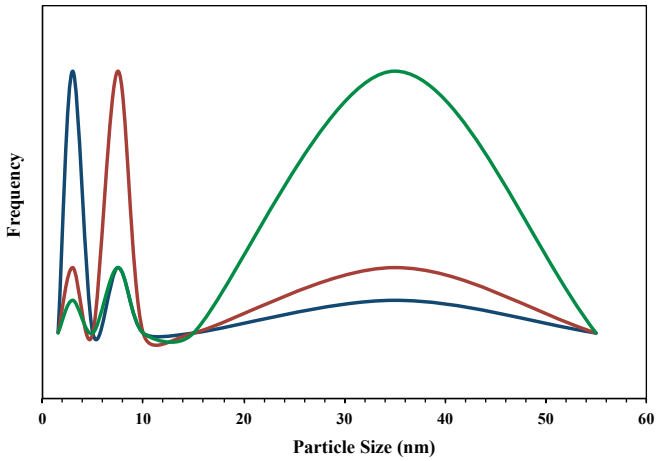

Figure 2.4 *Qualitative trimodal distributions of asphaltene size in toluene at low (blue), intermediate (red), and high (green) asphaltene volume fraction.*

While the nano particulate nature of asphaltenes is exploited industrially,[26-27] this aspect of their chemical and physical behavior is typically ignored in favour of simpler data treatments in the development of phase behavior models. Asphaltene behaviour models and experimental observations of their phase behaviour have become dissonant. For example, current asphaltene behaviour models treat asphaltenes as a conventional petroleum constituent, i.e.: as molecularly soluble species or molecular deposits (either solid or liquid). These models possess empirical [28-29] or molecular thermodynamic [30-31] bases and focus on describing the transition from "stable" nominally molecular to flocculated or aggregated and deposited asphaltenes. These models possess limited predictivity as they are based on incomplete or inappropriate chemistry and physics. Consequently, uncertainty regarding

reservoir and production system fouling, pipeline fouling, and refinery equipment fouling introduces technological risk as new hydrocarbon resources are exploited, and fouling in existing processes poses significant ongoing remediation costs.

In the current work, depletion flocculation induced phase behaviours arising in mixtures of polystyrene (a non-adsorbing polymer) + asphaltenes + toluene (a good solvent) are explored from a colloidal property perspective. Since asphaltenes aggregate in toluene, there are a minimum of two unknown asphaltene attributes that must be addressed: (1) the mass fraction of asphaltenes present in aggregates large enough to participate in the depletion flocculation phase behaviour mechanism, and (2) the global composition dependence of the mean asphaltene aggregate size. From the foregoing, it is clear that these attributes must be approximated, prior to their inclusion in a modified Fleer–Tuinier model.

2. Modification of the Fleer–Tuinier Model

The Fleer–Tuinier model cannot be used directly for polydispersed colloids with polydispersed polymers in solvents such as asphaltenes + polystyrene in toluene (Figure 2.3). In a prior work, Khammar and Shaw, [9] hypothesized that only a fraction of asphaltenes participated in the depletion flocculation mechanism and tested their hypothesis using a two step calculation. They first computed compositions of phases in equilibrium assuming that all of the asphaltenes participated in the phase separation mechanism. Inferred bimodal points were then used to calculate speeds of sound in each phase and the difference in the speed of sound between phases. The calculated speed of sound differences were then compared with measured speed of sound differences. A concentration independent fraction of asphaltene

colloidal particles participating in the phase separation mechanism, γ, was introduced to improve the agreement between calculated and experimental speed of sound differences. In their work, the total volume fraction of asphaltenes, η was subdivided into two fractions:

$$\eta=\eta^{*}+\eta^{'} \tag{2.14}$$

where:

$$\eta^{*}=\gamma\,\eta \tag{2.15}$$

$$\eta^{'}=(1-\gamma)\,\eta \tag{2.16}$$

η^{*} is the volume fraction of asphaltene colloidal particles that are large enough to cause phase separation, $\eta^{'}$: the volume fraction of asphaltenes that are too small to participate in the phase separation and γ: the fraction of asphaltene colloidal particles causing phase separation. The volume fractions of asphaltenes in the coexisting phases (I), (II) become:

$$\eta_{I}=\eta_{I}^{*}+\eta_{I}^{'}=\eta_{I}^{*}+(1-\gamma)\,\eta \tag{2.17}$$

$$\eta_{II}=\eta_{II}^{*}+\eta_{II}^{'}=\eta_{II}^{*}+(1-\gamma)\,\eta \tag{2.18}$$

because the volume fractions of asphaltenes that are too small to participate in the phase separation mechanism are expected to have the same values in both phases. Figure 2.5 shows a comparison between calculated and experimental speed of sound differences between the separated phases for different values of the fraction γ and indicates a preferred value of γ=0.63 for polystyrene with a Mw of 393,000 g/mol. While this modification provides quantitative estimates for speed of sound differences between phases, and underscores the importance of the details of asphaltene behaviour in mixture property calculation, this modification failed to reproduce experimental two-phase to single-phase phase boundaries. Clearly, both the polydispersity and the mean size of asphaltene aggregates require variation.

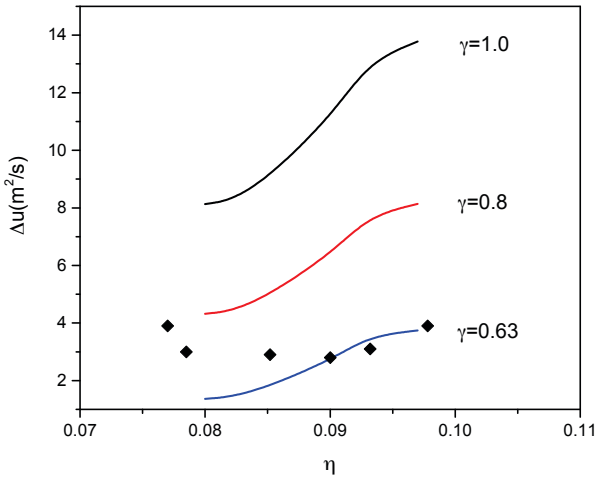

Figure 2.5 *Calculated (curves) and experimental (points) speed of sound difference values between colloid rich and polymer rich phases as a function of global asphaltene volume fraction in a mixture of asphaltene + polystyrene (Mw=393,000 g/mol) + toluene.*[8, 9] *γ is a parameter.*

Paricaud,[32] and Fasolo and Sollich[33] addressed particle polydispersity effects with a complex mathematical treatment that does not consider variation of the size distribution of particles with composition. A simpler treatment of particle polydispersity that builds on the work of Khammar and Shaw[9] is adopted in the present work, because details of the size distribution of asphaltenes and their dependence on global composition are unknown and not readily measured. The variation of the average size of asphaltene particles with global composition is modeled using an empirical correlation and asphaltene polydispersity is accommodated by allowing the fraction of asphaltenes participating in the depletion flocculation mechanism (γ)

to vary with composition. With these modifications, the free volume fraction for polymers in the Fleer–Tuinier model, defined in equation (2.11), is replaced with:

$$\alpha' = h(\eta) * \alpha \tag{2.19}$$

where

$$h(\eta) = (\frac{Z}{Rs(\eta)})^3 \tag{2.20}$$

Z, an unknown constant, is the smallest particle size participating in phase separation, $R_s(\eta)$ is the average asphaltene particle size function, $h(\eta)$ is a cubic function of particle size because it is a modifying factor for free volume fraction which changes with the third power of particle size. Both $h(\eta)$ and $R_s(\eta)$ are functions of asphaltene volume fraction (η). The modified asphaltene volume fraction, appearing in the modified Fleer–Tuinier model is:

$$\eta_{modified} = (\eta_{FT} / \gamma) \tag{2.21}$$

where η_{FT} is the asphaltene volume fraction that participates in phase separation obtained from Fleer–Tuinier model and $\eta_{modified}$ is total asphaltene volume fraction.

Values for the coefficient Z, and functions for R_s and γ, are obtained by fitting the modified Fleer–Tuinier model to available phase boundary and phase composition data.[8-9] The possible ranges of values are constrained: by natural physical limits for volume fractions ($0 < \alpha' < 1$, $0 < \gamma < 1$), the minimum mean size for asphaltene aggregates $R_s > \sim 1.5$ nm, by requiring the model to conform with an experimentally available tie line, and by requiring that the fitted critical point and adjacent tie lines conform with experimental values obtained from speed of sound data.[8-9, 34]

3. Model Validation

3.1 Relative Phase Volumes

In addition to the data noted above, the experimental data sets[8-9, 35] include phase volume fractions for the colloid gas and colloid liquid phases, in the two-phase region. These data are not included in the regression and are used to test the over all quality of the modified Fleer–Tuinier model—a combined measure of the quality of tie line and two phase region boundary prediction. The loci of global compositions where the volume fractions of the polymer rich phase (L1) and the asphaltene-rich phase (L2) are equal intersects the two-phase boundary with the single phase region at the critical point. These loci were not forced to intersect the critical point computed using classical volumetric derivative properties obtained using the modified Fleer–Tuinier model and they provide a second and sensitive measure of model quality particularly in the critical region.

3.2 Enthalpy of Solution Measurements for Maya Asphaltenes in Toluene

There are no direct measures of the size of asphaltenes or the fraction participating in depletion flocculation. Enthalpies of solution measurements for asphaltenes in toluene include a combination of phase change (positive enthalpy), dissolution (positive/negative enthalpy) and sorption of solvent on particle surfaces (negative enthalpy). Aggregation enthalpies are negligible compared to these phenomena. Differential enthalpy of solution measurements obtained by adding a small amount of asphaltene to a solvent already containing asphaltenes are sensitive to and should correlate with changes in the fraction of asphaltene that are large enough to participate in the depletion flocculation mechanism because these measurements are sensitive to the balance between sorption and dissolution

processes at the composition of the measurements. The differential enthalpy of solution measurements, performed in this work with Maya pentane asphaltenes, make use of the same equipment and experimental protocols used by Nikooyeh and Shaw.[11] The differential enthalpy of solution values obtained are compared with computed values for the change in the fraction of asphaltenes large enough to participate in the depletion flocculation mechanism ($d\gamma/d\eta$) at the same composition using a linear model:

$$H = (1-\gamma)H_1 + \gamma H_2 \qquad (2.22)$$

where H, H_1, and H_2 are enthalpy of solution of asphaltenes in toluene, the enthalpy at $\gamma = 0$, and the enthalpy at $\gamma = 1$ respectively. H_1 includes phase change and dissolution. H_2 reflects sorption of solvent only. Both H_1 and H_2 can vary with global composition. As the calorimetric measurements are performed on a mass basis, differentiating equation (2.22) with respect to asphaltene volume fraction gives:

$$\left(\frac{dH}{d\omega}\right)\left(\frac{d\omega}{d\eta}\right) = (1-\gamma)\left(\frac{dH_1}{d\omega}\right)\left(\frac{d\omega}{d\eta}\right) + \gamma\left(\frac{dH_2}{d\omega}\right)\left(\frac{d\omega}{d\eta}\right) + \left(\frac{d\gamma}{d\eta}\right)(H_2 - H_1) \qquad (2.23)$$

where ω is the mass fraction of asphaltenes. Rearranging equation (2.23), one obtains:

$$\left(\frac{dH}{d\omega}\right) = \left(\frac{dH_1}{d\omega}\right) + \gamma\left(\frac{dH_2}{d\omega} - \frac{dH_1}{d\omega}\right) + \left(\frac{d\gamma}{d\eta}\right)\frac{(H_2 - H_1)}{\left(\frac{d\omega}{d\eta}\right)} \qquad (2.24)$$

By neglecting the difference term $\left(\frac{dH_2}{d\omega} - \frac{dH_1}{d\omega}\right)$, equation (2.24) is well approximated as:

$$\left(\frac{dH}{d\omega}\right) = \left(\frac{dH_1}{d\omega}\right) + \left(\frac{d\gamma}{d\eta}\right)\frac{(H_2 - H_1)}{\left(\frac{d\omega}{d\eta}\right)} \qquad (2.25)$$

Mass fraction and volume fraction are defined interchangeably as:

$$\omega = \frac{\rho_{asph}\,\eta}{\rho_{asph}\,\eta + (1-\eta)\rho_{tol}} \qquad (2.26)$$

$$\eta = \frac{\frac{\omega}{\rho_{asph}}}{\frac{\omega}{\rho_{asph}} + \frac{1-\omega}{\rho_{tol}}} \qquad (2.27)$$

where ρ_{asph} (1.18 g/cm^3) and ρ_{tol} (0.86 g/cm^3) are asphaltene density, and toluene density respectively. The derivative:

$$\left(\frac{d\omega}{d\eta}\right) = \left(\frac{\rho_{asph}}{\rho_{tol}}\right)\left(\frac{1}{\eta^2\left(\frac{1}{\eta} + \frac{\rho_{asph}-\rho_{tol}}{\rho_{tol}}\right)^2}\right) \qquad (2.28)$$

is readily substituted into equation (2.25) :

$$\left(\frac{dH}{d\omega}\right) = \left(\frac{dH_1}{d\omega}\right) + \left(\frac{d\gamma}{d\eta}\right)(H_2 - H_1)\,\eta^2\left(\frac{1}{\eta} + \frac{\rho_{asph}-\rho_{tol}}{\rho_{tol}}\right)^2\left(\frac{\rho_{tol}}{\rho_{asph}}\right) \quad (2.29)$$

Given the disparity between the mean molar mass of asphaltenes, which is at least an order of magnitude larger than the molar mass of toluene, the $\left(\frac{dH_1}{d\omega}\right)$ term in equation (2.29) may be treated as a constant. The difference term ($H_2 - H_1$) is also not expected to vary greatly with composition relative to measurement uncertainty and the variation of γ. Thus, a linear relationship between $\left(\frac{dH}{d\omega}\right)$ and $\left(\frac{d\gamma}{d\eta}\right)\eta^2\left(\frac{1}{\eta} + \frac{\rho_{asph}-\rho_{tol}}{\rho_{tol}}\right)^2$ values would provide further independent, if indirect, experimental grounding, for the *γ(η)* correlation.

4. Results and Discussion

4.1 Model Parameter Identification

The composition independent size parameter, Z = 5.1 nm, and the composition dependent parameters $R_s(\eta)$:

$$R_s(\eta) = -157.58\left(\frac{\eta}{1-\eta}\right)^3 + 109.6\left(\frac{\eta}{1-\eta}\right)^2 + 62.292\left(\frac{\eta}{1-\eta}\right) + 1.5 \quad (2.30)$$

and $\gamma(\eta)$:

$$\gamma(\eta) = 0.99\left(e^{0.001835\left(\frac{\eta}{1-\eta}\right)} - e^{-31.05\left(\frac{\eta}{1-\eta}\right)}\right) \quad (2.31)$$

were obtained by fitting the modified FT depletion flocculation model, to Maya asphaltene + toluene + polystyrene (393000 and 700000 g/mole) phase boundary data. Value ranges for $R_s(\eta)$ and $\gamma(\eta)$ are shown in Figures 2.6 and 2.7 respectively and conform to expectation. The correlated average aggregate size (Figure 2.6), fit within the two-phase region, merges with the cloud of experimental asphaltene aggregate size measurements at low asphaltene volume fraction (within the single phase region). At a volume fraction = 0.3, corresponding to a mass fraction of ~ 0.5, the regressed average aggregate size is ~ 24 nm. Thus, the range of values is well bounded and consistent with the range of experimental measurements. The fraction of asphaltenes large enough to participate in the depletion flocculation mechanism (Figure 2.7) trends to zero at low volume fraction, and approaches unity at high asphaltene volume fractions. Since asphaltene aggregate size is independent of the polymer molar mean molar mass, the same $R_s(\eta)$ and $\gamma(\eta)$ functions and the same Z value apply to both asphaltene + toluene + polystyrene mixtures.

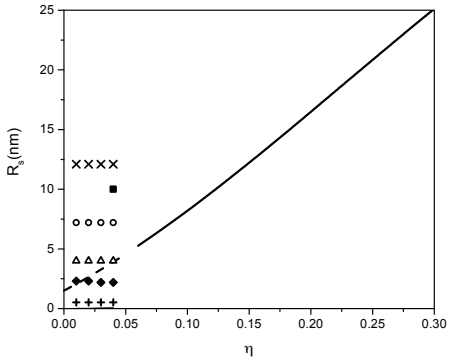

Figure 2.6 *Correlated average asphaltene particle size in toluene, $R_s(\eta)$, equation (2.30). The solid curve shows range of regressed values in the two-phase region and the dotted curve shows the extrapolation into the one-phase region. Experimental asphaltene sizes for diverse samples and based on a range of methods,[17] (×): H92H by DLS; (■): C-5 Maya asphaltenes by Acoustic Spectrometer; (O): H92H by SAXS; (Δ): H60L by SAXS; (◆): H92L by SAXS; (+): H92L by DLS.*

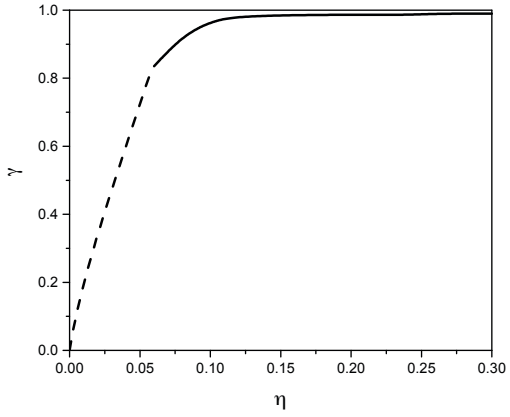

Figure 2.7 *Correlation for the fraction of asphaltenes large enough to participate in the depletion flocculation mechanism, γ, (2.31). The solid curve shows range of regressed values in the two-phase region and the dotted curve shows the extrapolation into the one-phase region.*

4.2 Computed Phase Diagrams for Maya Asphaltene + Toluene + Polystyrene Mixtures

Computed phase diagrams for Maya asphaltene + toluene + polystyrene mixtures, based on the modified Fleer–Tuinier model, along with experimental phase boundary measurements are shown for polystyrene Mw= 393,000 g/mole and Mw = 700,000 g/mole in Figures 2.8.a and 2.8.b respectively. The qualitative and quantitative outcomes are similar for both sets of calculations. The two-phase regions are identified to within the uncertainty of the experimental phase boundaries interpolated from adjacent measurements in the single and two phase regions, or inferred using the method of Bodnar and Oosterbaan[34] remote from the critical points for both phase diagrams. While the overall fit to the data is better for the larger polymer, Figure 2.8.b vs Figure 2.8.a, the fit is satisfactory for both cases, particularly given the magnitude of the phase boundary measurement uncertainty—indicated as an inset in the phase diagrams.

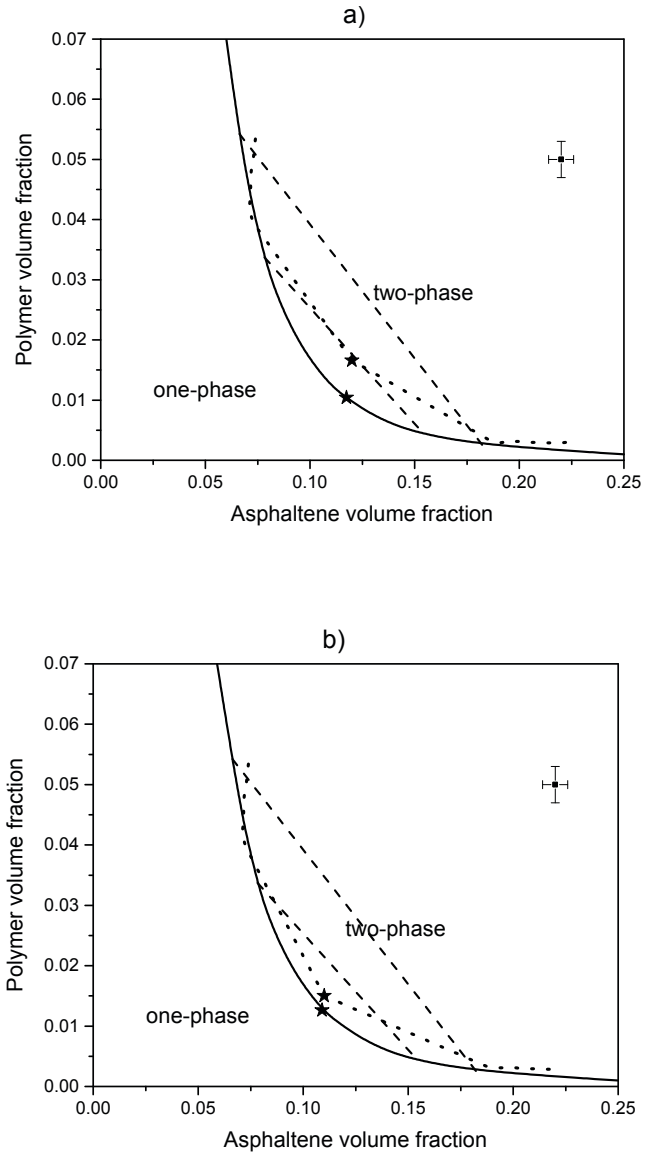

Figure 2.8 *A comparison between one-phase to two-phase boundaries predicted using the modified Fleer–Tuinier model (solid curves) and experimental phase diagrams (dotted curves) for mixtures of asphaltenes + toluene + polystyrene for polystyrene molar masses: a) 393,000 g/mol and b) 700,000 g/mol, (★): critical points; (dashed lines): computed tie lines.*

4.3 Model Parameter Validation

4.3.1 Model Parameter Validation using Volume Fractions of Phases

Computed volume fractions for the polymer-rich phase are compared with measured volume fractions of the polymer-rich phase. Parity plots are shown in Figure 2.9. At volume fractions exceeding ~ 0.4, the volume fraction of the polymer-rich phase is well represented by the model. At low volume fractions, the volume fraction is over-predicted by the model. This reflects the high relative deviation of the polymer volume fraction in the asphaltene-rich phase, even though the absolute deviation is small.

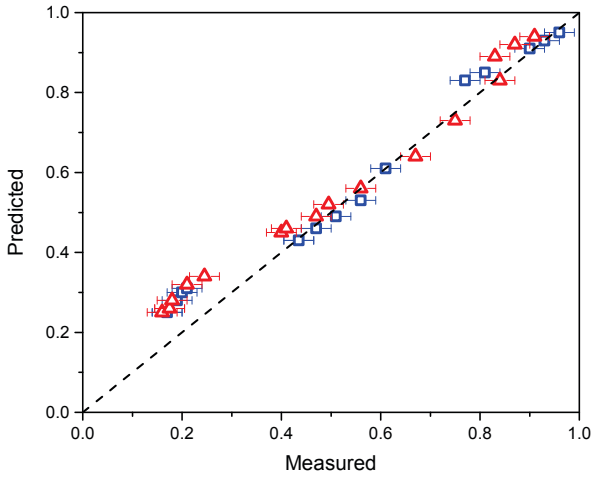

Figure 2.9 *Parity plots for measured*[8-9, 35] *and predicted (modified Fleer–Tuinier model) polymer-rich phase volume fractions for Maya asphaltenes + polystyrene [Mw=393,000 g/mol (red triangles) and Mw=700,000 g/mol (blue squares)] + toluene mixtures.*

4.3.2 Model Parameter Validation Using Differential Enthalpy of Solution Data for Maya Asphaltenes in Toluene

For mixtures of Maya asphaltenes + toluene, enthalpies of solution are dominated by phase change and dissolution (net positive enthalpy of solution) at low asphaltene mass fraction. With increasing asphaltene mass fraction, the importance of phase change and dissolution diminishes in favour of solvent sorption and at high mass fraction the enthalpies of solution are dominated by sorption (negative enthalpy of solution). Consequently, at low asphaltene volume fraction, where the fraction of large asphaltene aggregates is low but is changing rapidly with volume fraction, the differential enthalpy of solution is positive. At high asphaltene volume fraction, where $d\gamma/d\eta$ approaches zero, the differential enthalpy of solution is also expected to approach a negative asymptotic value. Thus $d\gamma/d\eta$ and $\left(\frac{dH}{d\omega}\right)$ are closely related, and to a first approximation, experimental differential enthalpy of solution $\left(\frac{dH}{d\omega}\right)$ values and computed $\left(\frac{d\gamma}{d\eta}\right)\eta^2\left(\frac{1}{\eta}+\frac{\rho_{asph}-\rho_{tol}}{\rho_{tol}}\right)^2$ values, both reported in Table 2.1, should be linearly related, as outlined in section 3.2. The anticipated linearity is demonstrated in Figure 2.10, within the uncertainty of the experimental measurements. This outcome provides exogenous and independent support for the modified Fleer–Tuinier model and for the correlation of γ, in particular, both within the two-phase region and for the extrapolation of the correlation into the single-phase region.

Table 2.1 *Differential enthalpy of solution* $\left(\frac{dH}{d\omega}\right)$ *measurements for Maya asphaltenes in toluene and the corresponding* $\left(\frac{d\gamma}{d\eta}\right)\eta^2\left(\frac{1}{\eta}+\frac{\rho_{asph}-\rho_{tol}}{\rho_{tol}}\right)^2$ *values.*

ω	η	$\left(\frac{dH}{d\omega}\right)$ (J/g)	$\left(\frac{d\gamma}{d\eta}\right)\eta^2\left(\frac{1}{\eta}+\frac{\rho_{asph}-\rho_{tol}}{\rho_{tol}}\right)^2$
0.01	0.008	2.5+/–1	24.1
0.04	0.0313	–0.1+/–1	12.3
0.08	0.0632	–2.1+/–1	4.5
0.12	0.0875	–4.3+/–1	2.0
0.13	0.099	–4.6+/–1	1.1

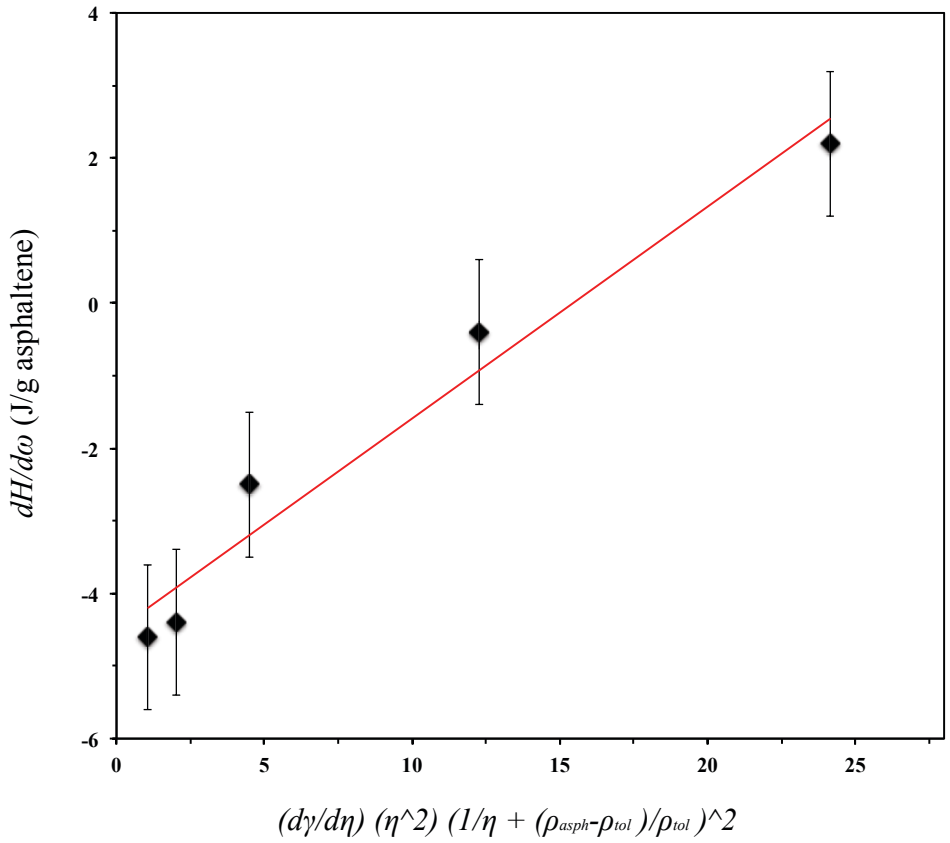

Figure 2.10 *Differential enthalpy of solution values for Maya asphaltenes in toluene at 298 K* $\left(\frac{dH}{d\omega}\right)$ *vs computed* $\left(\frac{d\gamma}{d\eta}\right)\eta^2\left(\frac{1}{\eta}+\frac{\rho_{asph}-\rho_{tol}}{\rho_{tol}}\right)^2$ *values.*

5. Conclusions

In this work, the Fleer–Tuinier model for describing the phase behaviour of mixtures comprising monodispersed particles + non adsorbing polymer + good solvent was modified to accommodate the variation of the mean particle size and the fraction of particles large enough to participate in the depletion flocculation mechanism as a function of particle volume fraction on a polymer free basis. Two sets of experimental phase behaviour data for Maya asphaltenes + polystyrene (Mw = 393,000 and 700,000 g/mole) + toluene were

simulated quantitatively using this modified Fleer–Tuinier model. The phase boundaries, tie lines and critical points for both mixtures were all well represented and the model was further validated, as a whole, against relative phase volume data (not used for regression), and the change in the fraction of particles large enough to participate in the depletion flocculation mechanism with composition was found to be consistent with differential enthalpy of solution results for Maya asphaltenes. Generalization of this promising phase behaviour simulation framework with respect to temperature and asphaltene source, and generalization and simplification of the model input parameters comprise topics for future work.

Acknowledgements

The authors thank Amin Pourmohammadbagher for assistance with calorimetric measurements and Prof. Janet Elliott for helpful discussions, and gratefully acknowledge financial support from the sponsors of the NSERC Industrial Research Chair in Petroleum Thermodynamics: the Natural Sciences and Engineering Research Council of Canada (NSERC), Alberta Innovates Energy and Environment Solutions, British Petroleum, ConocoPhillips Canada Resources Corp., Nexen Energy ULC, Shell Canada Ltd., Total E&P Canada Ltd., Virtual Materials Group.

Glossary:

f $\frac{\eta}{1-\eta}$

H enthalpy of solution

H_1 enthalpy of phase change + dissolution

H_2 enthalpy of sorption

M_w polystyrene mean molar mass

p pressure

$(pv)^0$ hard sphere contribution to pressure times particle volume

$(pv)^p$ polymer contribution to pressure times particle volume

q size ratio δ/R_s

q_R size ratio R_g/R_s

R_g radius of gyration of polymer

R_s colloidal particle radius, asphaltene radius

y normalized particle-free polymer volume fraction φ/φ_{ov}

Y $yq_R^{-1/k}$

Z smallest particle size participating in the phase separation during depletion flocculation

α free volume fraction

γ the fraction of asphaltene colloidal particles causing phase separation

δ depletion thickness around a sphere; range of the depletion interaction

η colloid volume fraction, asphaltene volume fraction

η^* volume fraction of participating asphaltenes

η' volume fraction of non-participating asphaltenes

κ De Gennes exponent in the Fleer–Tuinier model

μ colloid chemical potential

μ^0 hard sphere contribution to colloid chemical potential

μ^p polymer contribution to colloid chemical potential

v colloid volume

$\rho_{asph.}$ asphaltene density

$\rho_{poly.}$ polystyrene density

$\rho_{tol.}$ toluene density

φ particle-free volume fraction of polymer

φ_{ov} particle-free overlap volume fraction of polymer

ϕ polymer volume fraction, $\alpha\,\varphi$

ω weight fraction of asphaltene

REFRENCES:

(1) Lima, A.F.; Mansur, C.R.E.; Lucas, E.F.; Gonzalez, G. Polycardanol or Sulfonated Polystyrene as Flocculants for Asphaltene Dispersions. Energy Fuels, 2010, 24, 2369-2375.

(2) Myakonkaya, O.; Eastoe, J. Low Energy Methods of Phase Separation in Colloidal Dispersions and Microemulsions. Adv. Colloid Interface Sci., 2009, 149, 39-46.

(3) Poon, W.C.K. The Physics of a Model Colloid-Polymer Mixture. J. Phys. Condens. Matter, 2002,14, 859-880.

(4) Lekkerkerker, H.N.W.; Tuinier, R. Colloids and the Depletion Interaction, Springer, 2011, New York.

(5) Lekkerkerker, H.N.W.; Poon, W.C.K.; Pusey, P.N.; Stroobants, A.; Warren, P.B. Phase Behaviour of Colloid + Polymer Mixtures. Europhys. Lett., 1992, 20, 559-564.

(6) Fleer, G.J.; Tuinier, R. Analytical Phase Diagrams for Colloids and Non-adsorbing polymer. Adv. Colloid Interface Sci., 2008, 143, 1-47.

(7) Carnahan, N.F.; Starling, K.E. Equation of State for Nonattracting Rigid Spheres, J Chem Phys, 1969, 51, 635-636.

(8) Khammar, M. The Phase Behaviour of Asphaltene + Polystyrene + Toluene Mixtures at 293 K. PhD Thesis, University of Alberta, April 2011.

(9) Khammar, M.; Shaw, J.M.; Estimation of Phase Composition and Size of Asphaltene Colloidal Particles in Mixtures of Asphaltene + Polystyrene + Toluene at 293K and Atmospheric Pressure, Fluid Phase Equilib., 2012, 332,105-119.

(10) Zhao, B.; Shaw, J.M. Composition and Size Distribution of Coherent Nanostructures in Athabasca Bitumen and Maya Crude Oil. Energy Fuels, 2007, 21 (5), 2795–2804.

(11) Nikooyeh, K.; Shaw, J.M. On Enthalpies of Solution of Athabasca Pentane Asphaltenes and Asphaltene Fractions. Energy Fuels, 2013, 27(1), 66-74.

(12) Bagheri, S.R.; Bazyleva, A.; Gray, M.R.; McCaffrey, W.C.; Shaw, J.M. Observation of Liquid Crystals in Heavy Petroleum Fractions. Energy Fuels, 2010, 24 (8), 4327–4332.

(13) Bazyleva, A.; Fulem, M.; Becerra, M.; Zhao, B.; Shaw, J.M. Phase Behaviour of Athabasca Bitumen. J. Chem. Eng. Data, 2011, 56 (7), 3242–3253.

(14) Zhang, Y.; Takanohashi, T.; Shishido, T.; Sato, S.; Saito, I. Estimating the Interaction Energy of Asphaltene Aggregates with Aromatic Solvents. Energy Fuels, 2005, 19(3), 1023-1028.

(15) Mostowfi, F.; Indo, K.; Mullins, O.C.; McFarlane, R. Asphaltene Nanoaggregates Studied by Centrifugation. Energy Fuels, 2009, 23, 1194-1200.

(16) Yarranton, H.W. Investigation of Asphaltene Association with Vapor Pressure Osmometry and Interfacial Tension Measurements. Ind. Eng. Chem. Res., 2000, 39(8), 2916-2924.

(17) Yarrranton, H.W.; Ortiz, P.D.; Barrera, D.M.; Stasik, E.N.; Barre, L.; Frot, D.; Eyssautier, J.; Zeng, H.; Xu, G.; Dechaine, G.; Becerra, M.; Shaw, J.M.; McKenna, A.M.; Mapolelo, M.M.; Bohne, C.; Yang, Z.; Oake, J. On the Size Distribution of Self-Associated Asphaltenes. Energy Fuels, 2013, 27(9), 5083-5106.

(18) Espinat, D.; Fenistein, D.; Barre, L.; Frot, D.; Briolant, Y. Effects of Temperature and Pressure on Asphaltenes Agglomeration in Toluene. A Light, X-ray, and Neutron Scattering Investigation. Energy Fuels, 2004, 18, 1243-1249.

(19) Barre, L.; Simon, S.; Palermo, T. Solution Properties of Asphaltenes. Langmuir, 2008, 24, 3709-3717.

(20) Sheu, E. Y. Small Angle Scattering and Asphaltenes. J. Phys.: Condens. Matter, 2006, 18, 2485-2498.

(21) McKenna, A.M.; Blakney, G.T.; Xian, F.; Glaser, P.B.; Rodgers, R.P.; Marshall, A.G. Heavy Petroleum Composition 2. Progression of the Boduszynski Model to the Limit of Distillation by Ultrahigh Resolution FT-ICR Mass Spectrometry. Energy Fuels, 2010, 24, 2939–2946.

(22) Zhao, B.; Shaw, J.M. Composition and Size Distribution of Coherent Nanostructures in Athabasca Bitumen and Maya Crude Oil. Energy Fuels, 2007, 21, 2795-2804.

(23) Ching, M.J.T.M.; Pomerantz, A.E.; Andrews, A.B.; Dryden, P.; Schroeder, R.; Mullins, O.C.; Harrison, C. On the Nanofiltration of Asphaltene Solutions, Crude Oils, and Emulsions. Energy Fuels, 2010, 24, 5028-5037.

(24) Akbarzadeh, K.; Hammami, A.; Kharrat, A.; Zhang, D.; Allenson, S.; Creek, J.; Kabir, S.; Jamaluddin, A.; Marshal, A.G.; Rodgers, R.P.; Mullins, O.C.; Solbakken, T. Asphaltenes-Problematic but Rich in Potential, Oilfield Review, Schlumberger, 2007.

(25) Long, B.; Chadakowski, M.; Shaw, J.M. Impact of Liquid-Vapor to Liquid-Liquid-Vapor Phase Transitions on Asphaltene-Rich Nanoaggregate Behavior in Athabasca Vacuum Residue + Pentane Mixtures, Energy Fuels, 2013, 27(4), 1779-1790.

(26) Lucas, E.F.; Mansur, C.R.E.; Spinelli, L.; Queiros, Y.G.C. Polymer Science Applied to Petroleum Production. Pure Appl. Chem., 2009, 81, 473-494.

(27) Hashmi, S.M.; Quintiliano, L.A.; Firoozabadi, A. Polymeric Dispersants Delay Sedimentation in Colloidal Asphaltene Suspensions. Langmuir, 2010, 26, 8021-8029.

(28) deBoer, R.B.; Leerlooyer, K.; Eigner, M.R.P.; Bergen, A.R.D. Screening of Crude Oils for Asphaltene Precipitation, SPE Prod. Facil., 10(1), 1995, 55-61.

(29) Likhatsky, V.V.; Syunyaev, R.Z. New Colloidal Stability Index for Crude Oils Based on Polarity of Crude Oil Components, Energy Fuels, 24, 2010, 6483–6488.

(30) Panuganti, S.R.; Vargas, F.M.; Gonzalez, D.L.; Kurup, A.S.; Chapman, W.G. PC-SAFT Characterization of Crude Oils and Modeling of Asphaltene Phase Behaviour, Fuel, 2012, 93, 658-669.

(31) Ting, P.D.; Gonzalez, D.; Hiraski, G.; Chapman, W.G. Applications of the SAFT Equation of State to Asphaltene Phase Behaviour. Asphaltenes, Heavy Oils and Petroleomics, 2007, 301-327.

(32) Paricaud, P. Phase Equilibria in Polydisperse Nonadditive Hard-sphere Systems. Phys. Rev. E, 2008, 78, 021202.

(33) Fasolo, M.; Sollich, P. Effects of Polymer Polydispersity on the Phase behaviour of Colloid-Polymer Mixtures. J. Phys. Condens. Matter, 2005, 17, 797-812.

(34) Bodnar, I.; Oosterbaan, W. Indirect Determination of the Composition of the Coexisting Phases in a Demixed Colloid Polymer Mixture. J. Chem. Phys., 1997, 106, 7777-7780.

(35) Khammar, M.; Shaw, J.M. Liquid–Liquid Phase Equilibria in Asphaltene + Polystyrene + Toluene Mixtures at 293 K. Energy Fuels, 2012, 26 (2), 1075–1088.

Chapter 3: Support for an Asphaltene Nanoparticle Property Model based on Consistency with the Ostwald–Freundlich Equation

ABSTRACT: In chapter 2, the Fleer–Tuinier model was modified for the description of depletion flocculation driven phase behavior of monodispersed hard spheres + non-adsorbing polymer + good solvent, by incorporating empirical correlations for the variation of mean particle size and the fraction of the particle component participating in the depletion flocculation mechanism—the insoluble fraction to a first approximation. Quantitative fits to measured phase diagrams for Maya and Athabasca asphaltenes (nano-aggregating petroleum fractions) + polystyrene (non-adsorbing polymer) + toluene (good solvent) were obtained. According to the Ostwald–Freundlich equation, the solubility of nanoscale particles increases with decreasing particle size. In this work, the empirical functions for asphaltene mean aggregate size and solubility in toluene, reported previously, are shown to be consistent with the Ostwald–Freundlich equation. The importance of this result is discussed with respect to modeling solution behaviors of asphaltenes, and the broader development of depletion flocculation models for applications where partially soluble and aggregating colloids arise are discussed.

Key words: Size, Asphaltene, Solubility, Nanoparticle, Colloid, Thermodynamics

1. Introduction

Asphaltenes are a poorly defined self-aggregating component of crude oil. In the absence of comprehensive knowledge of *in situ* asphaltene properties, from their solubility in solvents, to their colloidality, to their mean particle size, and to the variation of these properties with composition, empirical approaches are required to model their solution behaviors. In the development of a phase behavior model for asphaltenes + polystyrene + toluene mixtures, in chapter 2 it was shown that it was necessary to modify the general Fleer–Tuinier model [1-2] describing the phase behavior of mixtures comprising non-adsorbing monodispersed polymers + monodispersed non-interacting hard sphere colloidal particles + good solvents to accommodate the impact of composition variations on asphaltene aggregate average size, and on the fraction of asphaltenes participating in the depletion flocculation mechanism. This mechanism arising from the addition of non-sorbing polymers to colloidal suspensions is one way to cause them to split into two phases (one rich in colloid, referred to as a colloid liquid, and the other rich in polymer, referred to as a colloid gas) over broad ranges of composition.[3-5] Other phase behaviors are also possible. The mechanism, leading to phase separation, comprises four steps:

1. Formation of a polymer free layer around individual colloidal particles

2. Development of an osmotic pressure, at the boundary of the polymer free zone as a consequence of this depletion

3. Formation of largely polymer free but solvent rich flocks as the polymer free layers of particles overlap

4. Separation of the fluid into bulk phases as flocks combine.

In the Fleer–Tuinier model, the depletion layer thickness around a sphere (the range of the depletion interaction), δ, is a function of both the polymer volume fraction, φ, and the ratio, $q_R = R_g/R_s$, of the radius of gyration R_g of the polymer to the particle radius R_s:

$$q = \frac{\delta}{R_s} = 0.865\{q_R^{-2} + c_1 Y^{2\kappa}\}^{-0.44} \quad (3.1)$$

$$Y = \left(\frac{\varphi}{\varphi_{ov}}\right) q_R^{-1/\kappa} \quad (3.2)$$

$$\varphi_{ov} = \frac{3\, M_w}{4\,\pi\, R_g^3\, N_A\, \rho_{polystyrene}} \quad (3.3)$$

$$R_g = 0.012\, M_w^{0.595} \quad (3.4)$$

$$q_R = {R_g}/{R_s} \quad (3.5)$$

where c_1=3.95, κ = 0.77, M_w is polymer mean molar mass, N_A is Avogadro's number, $\rho_{polystyrene}$ is polystyrene density, and φ_{ov} is the particle-free volume fraction of polymer.

The chemical potential of particles (μ) and the pressure times particle volume (pv) have a hard sphere contribution and a polymer contribution:

$$\mu = \mu^0 + \mu^p \quad (3.6.a)$$

$$pv = (pv)^0 + (pv)^p \quad (3.6.b)$$

where μ^0 is the chemical potential of particles if they are assumed to be hard spheres in a solvent without polymers, μ^p is the polymer contribution to particle chemical potential, ν is

particle volume, $(pv)^0$ is the hard sphere part of pressure times the particle volume without considering polymers, and $(pv)^p$ is the polymer contribution to pressure times particle volume. In this work all pv and μ terms have been normalized by kT (the thermal energy) to be dimensionless, where k is Boltzmann constant and T is temperature. The boundary curve between the one-phase and two-phase regions is calculated assuming equalities of chemical potentials and pressures times volumes for components in coexisting phases, and then solving them for the compositions.

For a dispersion of hard spheres in a fluid phase:[6]

$$\mu^0 = \ln\eta + 8f + 7f^2 + 2f^3 \qquad (3.7)$$

$$(pv)^0 = \eta + 4f^2 + 2f^3 \qquad (3.8)$$

where η is the colloidal particles volume fraction and f is:

$$f = \frac{\eta}{1-\eta} \qquad (3.9)$$

The polymer contribution to the chemical potential of particles and the pressure times volume are:[2]

$$\mu^p = \int_0^Y [\beta - (1+f)\beta_1]\left[q_R^{-1/\kappa} + 3\kappa c_2 Y^{3\kappa-1}\right] dY \qquad (3.10.a)$$

$$(pv)^p = \int_0^Y [\beta - f\beta_1]\left[q_R^{-1/\kappa} + 3\kappa c_2 Y^{3\kappa-1}\right] dY \qquad (3.10.b)$$

where: c_2=1.62 and κ =0.77 for excluded volume chains in good solvent. β_1 is the first derivative of β with respect to f and β is defined as:

$$\alpha = \frac{\phi}{\varphi} = (1-\eta)\beta \tag{3.11}$$

$$\beta = e^{-Q} \quad , \quad Q = Af + Bf^2 + Cf^3 \tag{3.12}$$

$$A = (1+q)^3 - 1\,, \quad B = 3q^2\left(q + {}^3\!/_2\right), \quad C = 3q^3 \tag{3.13}$$

where $\phi = \alpha\varphi$ is polymer volume fraction, $q = \delta/R_s$ is the depletion layer thickness to particle radius ratio, and α is the free volume fraction of polymer.

The modifications introduced in chapter 2 and then applied to an additional case where asphaltene type was varied[7] comprise correlations for property parameters $R_s(\eta)$ and $\gamma(\eta)$. Both of these parameters are composition dependent. The parameter $R_s(\eta)$ is the mean size of asphaltene colloids in toluene and the parameter $\gamma(\eta)$ is the mass fraction of asphaltenes that is colloidal in toluene. The remainder of asphaltenes is defined as soluble within the Ostwald–Freundlich interpretive framework. Z is a threshold mean particle size. With these modifications, α appearing in the Fleer–Tuinier model is replaced with α':

$$\alpha' = h(\eta) * \alpha \tag{3.14}$$

$$h(\eta) = \left(\frac{Z}{R_s(\eta)}\right)^3 \tag{3.15}$$

where α' is the modified free volume fraction for polymer chains. The colloid volume fraction along a phase boundary obtained from the Fleer–Tuinier model, $\eta_{FT,}$ is replaced with $\eta^{'}$ when preparing phase diagrams because asphaltenes are partially soluble in toluene:

$$\eta = (\eta_{FT}/\gamma) \tag{3.16}$$

The fitted correlations for Maya asphaltenes in toluene are: [1]

$$R_s(\eta) = -157.58\left(\frac{\eta}{1-\eta}\right)^3 + 109.6\left(\frac{\eta}{1-\eta}\right)^2 + 62.292\left(\frac{\eta}{1-\eta}\right) + 1.2 \tag{3.17.a}$$

$$Z = 5.1\ nm \tag{3.17.b}$$

$$\gamma(\eta) = 0.99\left(e^{0.001835\left(\frac{\eta}{1-\eta}\right)} - e^{-31.05\left(\frac{\eta}{1-\eta}\right)}\right) \tag{3.17.c}$$

The fitted correlations for Athabasca asphaltenes (data acquisition for Athabasca asphaltene mixture in chapter 4) in toluene are:[7]

$$R_s(\eta) = 26.86\left(\frac{\eta}{1-\eta}\right)^3 - 40.7\left(\frac{\eta}{1-\eta}\right)^2 + 21.07\left(\frac{\eta}{1-\eta}\right) + 1.9 \tag{3.18.a}$$

$$Z = 4\ nm \tag{3.18.b}$$

$$\gamma(\eta) = 0.73\left(e^{-0.001216\left(\frac{\eta}{1-\eta}\right)} - e^{-16.65\left(\frac{\eta}{1-\eta}\right)}\right) \tag{3.18.c}$$

The importance of these additions to the Fleer–Tuinier model is illustrated in Figure 3.1 where the performances of the Fleer–Tuinier model (Figure 3.1.a) and the modified Fleer–Tuinier model (Figure 3.1.b) vis-à-vis the measured phase diagram for Maya asphaltenes + toluene + polystyrene (Mw= 393,000 g/mol) at 298K are depicted. The phase behavior of the mixture is not represented by the Fleer–Tuinier model without modification.

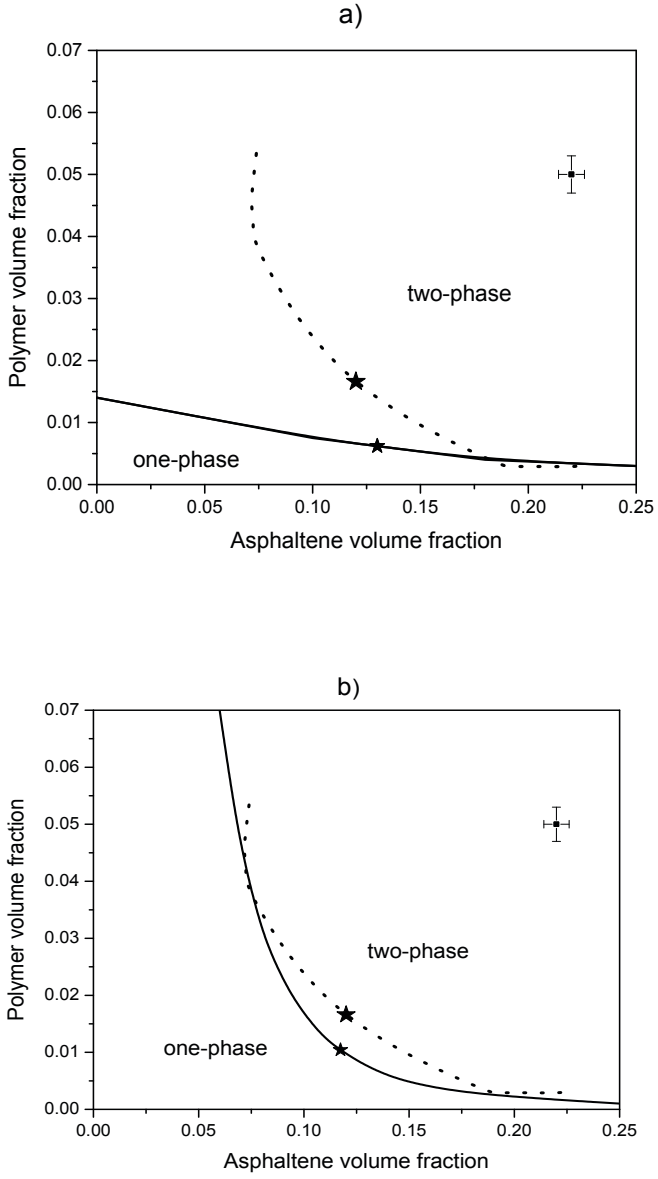

Figure 3.1 *Experimental and predicted phase diagrams for Maya asphaltenes + toluene + polystyrene (Mw =393,000 g/mole) at 298 K: a) Fleer–Tuinier predicted phase diagram with a=23nm and b) the modified Fleer–Tuinier model where Z = 5.1 nm and $R_s(\eta)$ and $\gamma(\eta)$ are defined by equations (3.17.a) and (3.17.c). Solid curves show predicted boundaries between the two-phase and one-phase regions and the dashed curves show the experimental boundaries. The stars (★) show critical points.*

The functional forms of equations (3.17.a,c) and (3.18.a,c) were selected for their simplicity and for the quality of their joint fit to experimental phase boundary data. It is unclear whether these functions are unique or if they link appropriately to underlying thermodynamic phenomena. For example, values of γ should reflect asymptotes in the enthalpy of solution for asphaltenes in toluene, at infinite dilution and at high volume fraction, and $d\gamma/d\eta$ values should be linearly correlated with differential enthalpies of solution of asphaltenes in toluene at the same composition. These provide independent, if approximate, checks on the basic form of the correlation for γ, that appear to be met.[1, 7] As part of the ongoing development of models for asphaltene behaviors in solution and other applications where particle size and solubility are functions of composition, conformance tests with behaviors anticipated by the well-known Ostwald–Freundlich nanoscopic solubility effect provide an opportunity to evaluate the empirical relationships for $R_s(\eta)$ and $\gamma(\eta)$ jointly at a more fundamental thermodynamic level.

The Ostwald–Freundlich equation describes the solubility dependence of a spherical solid particle in a liquid solution on the curvature of the solid–solution interface:[8-10]

$$x_k = x_k^{\infty} exp\left(\frac{2\, v_k^S \sigma^{SD}}{R_u T R_s}\right) \qquad (3.19)$$

where x ,v, σ, R_u, R_s and T, are the mole fraction, molar volume, interfacial tension, universal gas constant, solid radius and temperature, respectively, and superscripts k, S, SD and ∞ indicate the solute, the solid phase, the solid–drop interface and flat interface, respectively.

The Ostwald–Freundlich equation arises from combining phase equilibrium (chemical potential equality) with the Laplace equation that relates the pressure difference across a

curved surface to the interfacial tension and radius of curvature. The Ostwald–Freundlich equation is the solubility analog of the Kelvin equation describing the change in vapour pressure with liquid–vapor interface curvature, or the Gibbs–Thompson equation describing the change in freezing point with solid–liquid interface curvature. For large solid particles (low interface curvature) the Ostwald–Freundlich equation has no effect and solubility of large solid particles is a thermodynamic property. However for nanometer scale solid particles, the Laplace pressure becomes important and particle solubility is influenced by particle size. The Ostwald–Freundlich effect is well-known to enhance the solubility of nano particulate pharmaceutics,[11-12] to contribute to the physics of soluble nanoparticle–liquid solution complexes in atmospheric phenomena,[13-14] and to control the kinetics of nanoparticle nucleation and dissolution,[15-16] Eslami and Elliott present a more general form of the Ostwald–Freundlich equation and show that this equation plays an important role in the equilibrium behavior and thermodynamic stability of nanodrop concentrating processes.[17]

The Ostwald–Freundlich equation provides a clear relationship between solute particle size and solute solubility. It is an open question whether equations (3.17.a) and (3.18.a), intended to define the mean particle size, and equations (3.17.c) and (3.18.c), intended to define fractional insolubility, conform to this underlying thermodynamic phenomenon. In this work, an Ostwald–Freundlich framework is derived, and the above equations are tested. As many required physical properties of asphaltenes are unknown, uncertainty is addressed explicitly in the evaluation.

2. Development of an Asphaltene Specific Ostwald–Freundlich Test Equation

Rearranging the Ostwald–Freundlich Equation, equation (3.19) yields:

$$ln(x_k) = L\frac{1}{R_s} + J \tag{3.20}$$

where $L = \frac{2\, v_k^S \sigma^{SD}}{R_u T}$ and $J = ln(x_k^{\infty})$. Equation (3.20) shows that the Ostwald–Freundlich equation implies that $ln(x_k)$ versus $\frac{1}{R_s}$ should be linear. In order to see whether the functional form of the parameters resulting from fitting the empirically modified Fleer–Tuinier model can be explained by the Ostwald–Freundlich effect, variables appearing in the empirically modified Fleer–Tuinier model must be converted to Ostwald–Freundlich equation parameters. More specifically, the colloidal asphaltene mass fraction, γ, asphaltene volume fraction, η, and polymer volume fraction, ϕ, must be linked to the soluble asphaltene mole fraction, x_a^s.

These parameters can be expanded in terms of volume and mass contributions:

$$\gamma = \frac{m_a^c}{m_a^c + m_a^s} \tag{3.21}$$

$$\eta = \frac{V_a^c + V_a^s}{V_a^c + V_a^s + V_t + V_p} \tag{3.22}$$

$$\phi = \frac{V_p}{V_a^c + V_a^s + V_t + V_p} \tag{3.23}$$

$$x_a^s = \frac{n_a^s}{n_a^s + n_t + n_p} \tag{3.24}$$

where *V*, *m* and *n* are volume, mass and number of moles and subscripts *a, t* and *p* denote asphaltene, toluene and polymer and superscripts *c* and *s* stand for the colloidal and soluble portions of asphaltenes.

By making use of the relationships of *m, n* and *V* with density, ρ, and molar mass, *M*:

$$n = \frac{m}{M} \tag{3.25}$$

$$\rho = \frac{m}{V} \tag{3.26}$$

equation (3.21) can be re-arranged to provide an expression for n_a^s:

$$n_a^s = \frac{n_a^c(1-\gamma)}{\gamma} \tag{3.27}$$

An expression for n_p is obtained by rearranging equation (3.23) and substituting it into equations (3.25) – (3.27):

$$n_p = \frac{\rho_p \phi}{M_p(1-\phi)}\left(M_t \frac{n_t}{\rho_t} + M_a n_a^c \left(\frac{1}{\rho_a^c} + \frac{(1-\gamma)}{\gamma \rho_a^s}\right)\right) \tag{3.28}$$

An expression for n_t is obtained by substituting equations (3.25) – (3.28) into equation (3.22) and rearranging:

$$n_t = \frac{\rho_t}{M_t}\left(M_a n_a^c \left(\frac{1}{\rho_a^c} + \frac{(1-\gamma)}{\gamma \rho_a^s}\right)\left(\frac{(1-\phi-\eta)}{\eta}\right)\right) \tag{3.29}$$

Finally, the test equation is obtained by substituting equations (3.27) – (3.29) into equation (3.24):

$$x_a^s = \frac{\dfrac{(1-\gamma)}{\gamma}}{\dfrac{(1-\gamma)}{\gamma} + \left(M_a \left(\dfrac{1}{\rho_a^c} + \dfrac{(1-\gamma)}{\gamma \rho_a^s}\right)\left(\dfrac{\rho_t}{M_t}\dfrac{(1-\phi-\eta)}{\eta} + \dfrac{\rho_p}{M_p}\dfrac{\phi}{\eta}\right)\right)} \tag{3.30}$$

Equation (3.30) gives the mole fraction of soluble asphaltenes in terms of model variables and the physical properties of the mixture. There are a large number of properties and parameters appearing in equation (3.30). Their values and uncertainties are listed in Table 3.1. Given the uncertainty of the molar mass and density of asphaltenes, the impact of polymer volume fraction, ϕ, variation on asphaltene solubility is neglected. By substituting

these values into equation (3.30) a plot of $ln(x_a^s)$ versus $\frac{1}{R_s}$ can be prepared. If a linear relationship is obtained, then the correlations for R_s and γ in the modified Fleer–Tuinier model conform to the Ostwald–Freundlich equation.

Table 3.1 *Parameter values used in equation (3.30).*

Parameter	**Value +/– uncertainty**
$\rho_a^c \approx \rho_a^s$ (g/cm^3)	1.18+/– 0.02
ρ_p(g/cm^3)	1.05
ρ_t(g/cm^3)	0.86
M_a (g/mol)	2000+/–1000
M_p(g/mol)	393,000
M_t(g/mol)	92.14
Maya asphaltenes	R_s (nm) Equation (3.17.a) +/– 0.5 γ Equation (3.17.c) +/– 0.03
Athabasca asphaltenes	R_s (nm) Equation (3.18.a) +/– 0.5 γ Equation (3.18.c) +/– 0.03
ϕ	0

3. Results and Discussion

The test equation, equation (3.30), was applied to Maya and Athabasca asphaltenes using the parameters, equations and uncertainties noted in Table 3.1. The results of the preliminary tests for linearity are summarized in Figure 3.2.a. The uncertainties shown in the figure

reflect the lower and upper values for x_a^s and R_s according to Table 3.1. The empirical correlations defined in chapter 2 underlying the relationship between x_a^s and R_s for both asphaltenes can be treated as linear at higher than a certain size (~ 2.9 nm) within the uncertainty of the parameters in the two-phase region where the parameters were fit to the two-phase to one-phase boundaries (Figure 3.2.a). The asphaltene property relationships conform with the Ostwald–Freundlich equation within a certain volume fraction. The R^2 values for the Maya and Athabasca asphaltene property correlations in this region are 0.99 and 0.94 respectively and the lines fit within the uncertainties of the values. Extrapolation of these fitted lines to large particles yields (x_k^∞) values that are equivalent to 100 - 300 ppm and 30 - 100 ppm on a mass basis for Athabasca and Maya asphaltenes in toluene. These values are consistent with reported limiting compositions for asphaltene aggregate formation in toluene > 50 ppm.[18]

Care must be taken in the extrapolation of the fitted lines to small particles because the solubility of small particles, according to the Ostwald–Freundlich equation, exceeds the mole fraction of asphaltenes in the mixture. For example, asphaltene mole fractions of 0.0001, 0.001 and 0.01 correspond to volume fractions of 0.0016 +/- 0.0008, 0.016+/- 0.008, 0.14+/- 0.06, respectively. In order to maintain solid–liquid equilibrium, the corresponding (R_s, η) pairs for Athabasca asphaltenes are (6 nm, > 0.4), (3.1 nm, 0.07) and (2.7 nm, 0.04). Unless the size distribution is quite broad, according to Figure 3.2 Athabasca asphaltenes become fully soluble below ~ 2.9 nm or a volume fraction of ~ 0.05. For Maya asphaltenes, the corresponding (R_s, η) pairs are (3.9 nm, 0.04), (2.5 nm, 0.02) and (1.8 nm, 0.01) and Maya asphaltenes can be expected to be fully soluble below ~ 3 nm or a volume fraction of ~ 0.03. To be fully consistent with the Ostwald–Freundlich equation γ must go to zero, not at the

origin, as correlated in equations (3.17.c) and (3.18.c), but at a finite mean asphaltene aggregate size. This is readily accommodated because, in the one phase region adjacent to the origin, the functions for R_s, equations (3.17.a) and (3.18.a), and for γ, equations (3.17.c) and (3.18.c), are only constrained by the limiting values at the origin, where by definition the insoluble asphaltene fraction, γ, trends to zero (Figure 3.3) and R_s trends to the aggregate size observed experimentally at low mass fraction 1.5 nm (Figure 3.4). Thus equation (3.17.c) and (3.18.c) overestimate γ at low asphaltene volume fraction and the correlations diverge from the Ostwald–Freundlich equation. The Ostwald–Freundlich equation can be used to impose a needed and consistent constraint on γ. It suggests that γ trends to zero at $R_s \sim 3$ nm (Figure 3.5). Without affecting two-phase to one-phase boundary placement, equations (3.17.c) and (3.18.c) can be recast as:

$$\gamma(\eta) = 0.963\, e^{0.1082\left(\frac{\eta}{1-\eta}\right)} - 5.456\, e^{-60.98\left(\frac{\eta}{1-\eta}\right)} \qquad (3.31)$$

$$\gamma(\eta) = 0.683\, e^{0.2029\left(\frac{\eta}{1-\eta}\right)} - 5.909\, e^{-35.84\left(\frac{\eta}{1-\eta}\right)} \qquad (3.32)$$

Thus, the empirical correlations for asphaltene aggregate average size and asphaltene solubility appearing in the modified Fleer–Tuinier model are fully consistent with the Ostwald–Freundlich equation and with available asphaltene solubility data in toluene (Figure 3.2.b).

This outcome is not an obvious one. The Ostwald–Freundlich equation describes the relationship between the size of solid crystalline particles, and their solubility in a solvent. Hydrocarbon solids such as asphaltenes present complex phase behaviours including co-

existing liquid crystal, solid and glass phases. Asphaltenes also possess spatial inhomogeneities at the micro if not the nanoscale. [19-22] The outcome is however fortuitous because, even if the chemistry and physics underlying the Ostwald–Freundlich equation can be viewed as a primitive representation of the complexity of the phase behavior of asphaltenes, it clearly underpins correlations for R_s and γ for asphaltene + solvent mixtures in particular and for ill-defined nano aggregated mixtures more generally.

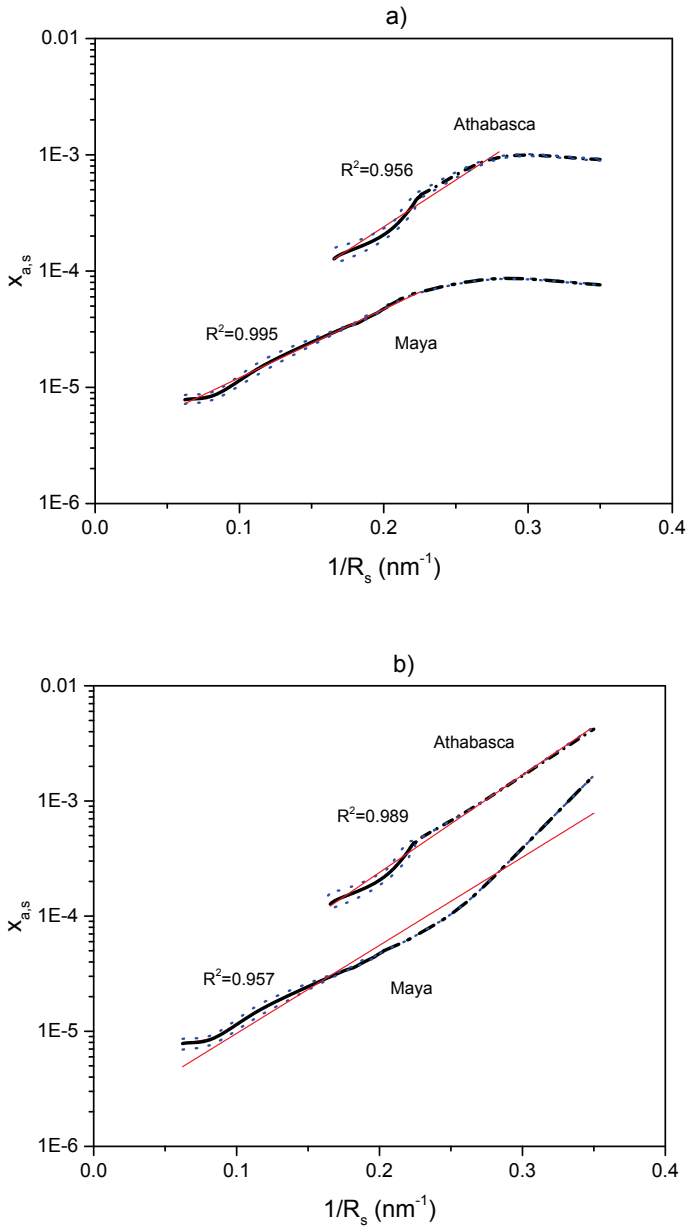

Figure 3.2 *Conformance check for empirical asphaltene property models, a) equations (3.17.a-c) and (3.18.a-c), b) equations (3.17.a, 3.31) and (3.18.a, 3.32) with the Ostwald–Freundlich equation for Maya and Athabasca asphaltenes Uncertainties (blue dotted curves); Linear fits (solid red lines).*

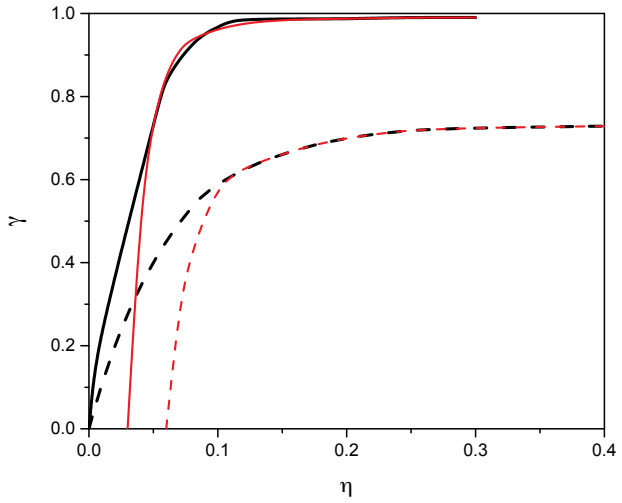

Figure 3.3 *γ, versus asphaltene volume fraction, η, for Maya asphaltenes (equation (3.17.c)) (solid curve) and Athabasca asphaltenes (equation (3.18.c)) (dashed curve) in toluene. The red curves show the γ functions constrained by Ostwald–Freundlich equation (equations (3.31) and (3.32)).*

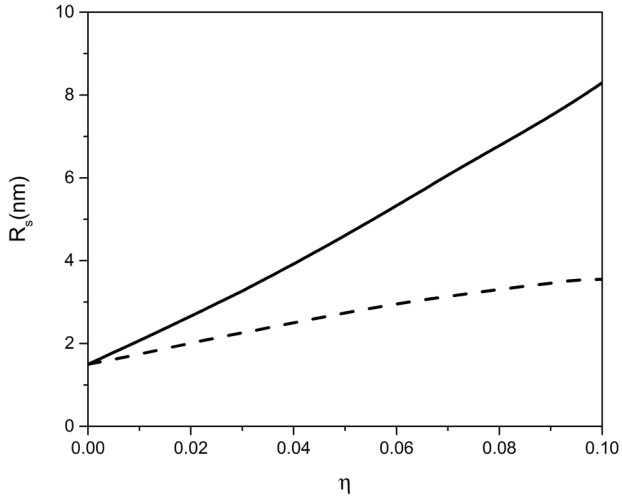

Figure 3.4 *R_s versus asphaltene volume fraction, η, for Maya asphaltenes (equation (3.17.a)) (solid curve) and Athabasca asphaltenes (equation (3.18.a)) (dashed) in toluene.*

From Figure 3.5, it appears that gamma is a function of R_s only with a maximum value dictated by the asphaltene.

$$\gamma(R_s, \gamma_{max}) = \gamma_{max}\, R_{s0}\, (0.33\, e^{0.001422 R_s} - 4.24\, e^{-0.8467 R_s}) \qquad (3.33)$$

where R_{s0} is the minimum R_s to be insoluble (~3 nm) and γ_{max} is the maximum colloidal fraction of asphaltene, 0.99 and 0.74 for Maya and Athabasca asphaltenes respectively.

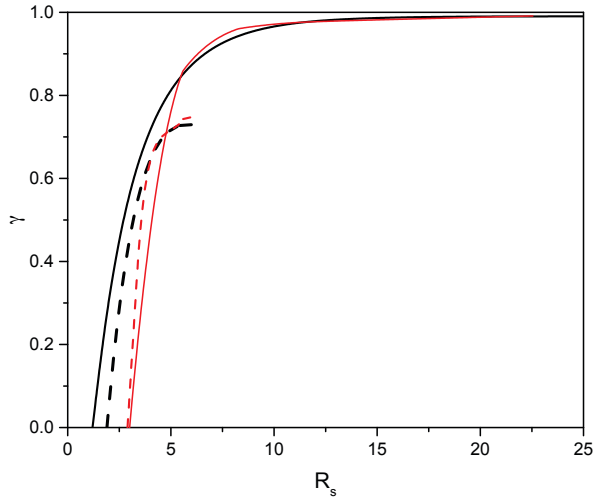

Figure 3.5 *γ versus R_s for Maya asphaltenes (solid curve) and Athabasca asphaltenes (dashed curve) in toluene. The red curves show the γ functions constrained by Ostwald–Freundlich equation.*

4. Conclusion

The property functions obtained for Maya asphaltenes in chapter 2 and for Athabasca asphaltenes previously[7] for asphaltenes in toluene were validated by comparison with the Ostwald–Freundlich equation. It was concluded that the functions for the size of asphaltene particles and their solubility in toluene are consistent with the Ostwald–Freundlich equation at volume fractions higher than 0.03 and 0.05 for Maya and Athabasca asphaltenes, respectively. From the Ostwald–Freundlich equation, one can say that asphaltene solubility in toluene should decrease with particle size. On the other hand, our property model predicted that asphaltenes tend to form more colloidal nanoparticles (larger γ) and increase their sizes with increasing concentration implying that the more and the larger particles, the less solubility. Herein, the obtained property functions were examined for consistency and restricted with the Ostwald–Freundlich equation at low volume fractions. From the restrictions enforced by the Ostwald–Freundlich equation, asphaltenes are treated as soluble in toluene if their average radius is less than 3 nm. This occurs at volume fractions less than 0.03 and 0.05 for Maya and Athabasca asphaltenes, respectively. By incorporating the Ostwald–Freundlich equation, which links the size of nanoparticles to their solubility in the parameterization of the modified Fleer–Tuinier model, the number of parameters that must be identified to model partially soluble particles by fitting experimental data will be minimized. The results are of importance from modeling and experimental points of view.

Acknowledgements

The authors gratefully acknowledge financial support from the sponsors of the NSERC Industrial Research Chair in Petroleum Thermodynamics: the Natural Sciences and Engineering Research Council of Canada (NSERC), Alberta Innovates Energy and Environment Solutions, BP Canada, ConocoPhillips Canada Resources Corp., Nexen Energy ULC, Shell Canada Ltd., Total E&P Canada Ltd., and the Virtual Materials Group. J.A.W Elliott holds a Canada Research Chair in Thermodynamics and gratefully acknowledges financial support from NSERC.

Glossary

f $\frac{\eta}{1-\eta}$

M_w polystyrene mean molar mass

p pressure

$(pv)^0$ hard sphere contribution to pressure times particle volume

$(pv)^p$ polymer contribution to pressure times particle volume

q size ratio δ/R_s

q_R size ratio R_g/R_s

m mass

M molar mass

m_a^c mass of colloidal asphaltene

m_a^s mass of soluble asphaltene

n_a^c number of colloidal asphaltene moles

n_a^s number of soluble asphaltene moles

n_p number of polymer moles

n_t number of toluene moles

R_g radius of gyration of polymer

R_s colloidal particle radius, asphaltene radius

R_u universal gas constant

T temperature

V volume

V_a^c volume of colloidal asphaltene

V_a^c volume of soluble asphaltene

V_p volume of polymer

V_t volume of toluene

x mole fraction

x_a^s soluble asphaltene mole fraction

x_k solute mole fraction

x_k^∞ solute mole fraction at flat interface

y normalized particle-free polymer volume fraction ϕ/ϕ_{ov}

Y $yq_R^{-1/k}$

Z smallest particle size participating in the phase separation during depletion flocculation

α free volume fraction for polymers

γ the fraction of asphaltene colloidal particles causing phase separation

δ depletion thickness around a sphere; range of the depletion interaction

η colloid volume fraction, asphaltene volume fraction

η_{FT} asphaltene volume fraction calculated by Fleer–Tuinier model

κ De Gennes exponent in the Fleer–Tuinier model

μ colloid chemical potential

μ^0 hard sphere contribution to colloid chemical potential

μ^p polymer contribution to colloid chemical potential

ν colloid volume

v_k^s solid solute molar volume

$\rho_{asph.}$ asphaltene density

$\rho_{poly.}$ polystyrene density

$\rho_{tol.}$ toluene density

σ^{SD} solid-drop interfacial tension

φ particle-free volume fraction of polymer

φ_{ov} particle-free overlap volume fraction of polymer

ϕ polymer volume fraction, $\alpha\ \varphi$

REFERENCES

(1) Pouralhosseini, S.S.; Shaw, J.M, Simulating Depletion Flocculation in Asphaltene + Toluene + Polystyrene Mixtures, Submitted to Fluid Phase Equilib. 2015.

(2) Fleer, G.J.; Tuinier, R. Analytical Phase Diagrams for Colloids and Non-adsorbing Polymer. Adv. Colloid Interface Sci. 2008, 143, 1-47.

(3) Lima, A.F.; Mansur, C. R. E.; Lucas, E. F.; Gonzalez, G. Polycardanol or Sulfonated Polystyrene as Flocculants for Asphaltene Dispersions. Energy Fuels 2010, 24, 2369-2375.

(4) Myakonkaya, O.; Eastoe, J. Low Energy Methods of Phase Separation in Colloidal Dispersions and Microemulsions. Adv. Colloid Interface Sci. 2009, 149, 39-46.

(5) Poon, W.C.K. The Physics of a Model Colloid-Polymer Mixture. J. Phys. Condens. Matter 2002,14, 859-880.

(6) Carnahan, N.F.; Starling, K.E. Equation of State for Nonattracting Rigid Spheres, J. Chem. Phys. 1969, 51, 635-636.

(7) Pouralhosseini, S.S.; Alizadehgiashi, M.; Shaw, J.M. On the Phase Behavior of Athabasca Asphaltene + Polystyrene + Toluene Mixtures at 298 K, Energy Fuels. 2015.

(8) Defay, R.; Prigogine, I. Surface Tension and Adsorption / R. Defay and I. Prigogine; London, England : Longmans, 1966; English ed: 1966.

(9) Ostwald, W. On the Assumed Isomerism of Red and Yellow Mercury Oxide and the Surface-Tension of Solid Bodies. ZeitschriFleer-Tuinier Fur Physikalische Chemie-Stochiometrie Und VerwandtschaFleer-Tuinierslehre, 1900, 34, 495-503.

(10) Freundlich, H. Kapillarchemie. Akademische VerlagsgessellschaFleer-Tuinier, 1909, Leipzig.

(11) Johnson, K.C. Comparison of Methods for Predicting Dissolution and the Theoretical Implications of Particle-Size-Dependent Solubility. J. Pharm. Sci. 2012, 101, 681-689.

(12) Letellier, P.; Mayaffre, A.; Turmine, M. Solubility of Nanoparticles: Nonextensive Thermodynamics Approach. J. Phys-Condens. Mat. 2007, 19, 436229.

(13) Shchekin, A.K.; Rusanov, A. I. Generalization of the Gibbs-Kelvin-Kohler and Ostwald–Freundlich Equations for a Liquid Film on a Soluble Nanoparticle. J. Chem. Phys. 2008, 129, 154116.

(14) Shchekin, A.K.; Shabaev, I.V.; Rusanov, A.I. Thermodynamics of Droplet Formation Around a Soluble Condensation Nucleus in the Atmosphere of a Solvent Vapor. J. Chem. Phys. 2008, 129, 214111.

(15) Ely, D.R.; Garcia, R.E.; Thommes, M. Ostwald-Freundlich Diffusion-limited Dissolution Kinetics of Nanoparticles. Powder Technol. 2014, 257, 120-123.

(16) Wamatsu, M. Nucleation and Growth by Diffusion under Ostwald-Freundlich Boundary Condition. J. Chem. Phys. 2014, 140, 064702.

(17) Eslami, F; Elliott, J.A.W. Role of Precipitating Solute Curvature on Microdrops and Nanodrops during Concentrating Processess; The Non-Ideal Ostwald–Freundlich Equation, J. Phys. Chem. B, 2014, 118, 14675-14686.

(18) McKenna, A.M.; Donald, L.J.: Fitzsimmons, J.E.; Juyal, P.; Spicer, V.; Standing, K.G.; Marshall, A.G.; Rodgers, R.P. Heavy Petroleum Composition. 3. Asphaltene Aggregation, Energy Fuels, 2013, 27 (3), 1246–1256.

(19) Bagheri, S.R.; Bazyleva, A.; Gray, M.R.; McCaffrey, W.C.; Shaw, J.M. Observation of Liquid Crystals in Heavy Petroleum Fractions, Energy Fuels, 2010, 24 (8), 4327–4332.

(20) Bazyleva, A.; Fulem, M.; Becerra, M.; Zhao, B.; Shaw, J.M., Phase Behavior of Athabasca Bitumen, J. Chem. Eng. Data, 2011, 56. (7), 3242-3253.

(21) Bagheri, S.R.; Masik, B.; Arboleda, P.; Wen, Q.; Michaelian, K.H.; Shaw, J.M. Physical Properties of Liquid Crystals in Athabasca Bitumen Fractions, Energy Fuels, 2012, 26(8), 4978-4987.

(22) Bazyleva, A.; Becerra, M.; Stratiychuk-Dear, D.: Shaw, J.M., Phase Behavior of Safaniya Vacuum Residue, Fluid Phase Equilib., 2014, 80, 28-38.

Chapter 4: On the Phase Behavior of Athabasca Asphaltene + Polystyrene + Toluene Mixtures at 298 K

ABSTRACT: Asphaltene aggregation and deposition are common concerns in reservoirs, and during production, transport and refining of petroleum fluids. Polymer addition provides one approach for the modification and control of asphaltene behavior. Asphaltene nanoaggregates are stable in toluene but when a non-adsorbing polymer like polystyrene is added two liquid phases, one enriched in asphaltenes and toluene and one enriched in toluene and polymer, are formed due to depletion flocculation. This phase separation mechanism impacts nanoaggregate but not molecular behaviours. In this work, an experimental phase diagram for Athabasca asphaltene + toluene + polystyrene mixtures including a two-phase critical point is presented, at 298 K. The compositions of phases and the critical point are compared with those arising in equivalent mixtures with Maya asphaltenes published previously. These experimental outcomes are also interpreted using a modified Fleer–Tuinier model and the possibility of the development of an asphaltene separation process based on the depletion flocculation mechanism is discussed.

Key words: Athabasca, Depletion, Flocculation, Asphaltenes, Phase Diagram

1. Introduction

Petroleum is a complex mixture of hydrocarbons that can be separated into saturates, resins, aromatics and asphaltenes, on the basis of filtration experiments (e.g.: ASTM D4055). The asphaltene fraction, nominally soluble in aromatic hydrocarbon liquids and nominally insoluble in alkane liquids, largely comprises sterically stabilized nanoaggregated materials even in toluene.[1-6] For example, asphaltenes are separable from toluene using ultracentrifugation, and as is the focus of the current work, by polymer addition,[7–10] that introduce phenomena that overcome the repulsive interactions among asphaltene colloidal particles[11]. Bridging flocculation based separation of asphaltene nanoaggregates from mixtures using polycardanol polymers and sulfunated polystyrene, that sorb on multiple nanoaggregates simultaneously in organic solvents, has been investigated, as has the use of non-sorbing polymers such as polystyrene that exploit the equally well established depletion flocculation mechanism to separate asphaltene aggregates from bulk fluids.[12-17]

Bridging flocculation is a readily visualized flocculation mechanism. Flocs form due to the sorption of multiple polymer molecules on two or more particle surfaces simultaneously, creating a web of bridges among them the particles. Depletion flocculation, exploited in the present work, requires more detailed treatment as it is less intuitive. If polymer molecules do not sorb on colloidal particle surfaces, this creates a thin polymer-free liquid layer around each particle. When polymer depleted layers surrounding adjacent particles interact, the particles are driven together due to osmotic pressure and their depleted layers combine. Multiple interactions among adjacent particles leads to the formation of large flocs, and as the process continues, separate colloid-rich and polymer-rich phases form.

There are two pertinent theories related to polymer–solvent phase behavior: Free volume theory[18] and Flory–Huggins theory.[19] Their application has led to the development of phenomenological modeling frameworks that are applicable to microgels in organic solvents,[20,21] to hard spheres + self-avoiding polymer chains[22,23] over restricted ranges of colloid diameter to polymer molecule radii of gyration (R_g), using a range of approaches including a two-component liquid-state integral theory[24]. The Fleer–Tuiner[25] model, based on free volume theory and valid for monodispersed hard sphere colloids and non-adsorbing polymers irrespective of their relative size, predicts the thickness of the depletion layer, and hence the phase behavior of mixtures, as a function of the ratio of the radius of gyration of the polymer to the radius of the colloidal particles and the polymer volume fraction in the mixture. This excellent general model was modified empirically for asphaltene + non-adsorbing polymer + toluene mixtures in chapter 2. In this modification, the mass fraction of asphaltenes present in aggregates large enough to participate in the depletion flocculation phase behavior mechanism, and the global composition dependence of the mean asphaltene aggregate size were included.[26] Empirical modification is required because the size of asphaltene molecules, and the size and mass fraction of aggregated asphaltenes much less their global composition dependence remain subjects of debate in the literature. For example, the reported mean molecular mass of asphaltenes ranges from approximately 700 Atomic Mass Unit (based on mass spectroscopy) to approximately 4000 AMU (based on vapor pressure osmometry).[27] Techniques such as vapor pressure osmometry tend to overestimate mean molecular mass due to aggregation, and mass spectroscopy tends to underestimate mean molecular mass.[28-30] The mean size and structure of asphaltenes aggregates in diverse non-precipitative environments have been studied using Small Angle X-ray Scattering

(SAXS), Small Angle Neutron Scattering (SANS), Dynamic Light Scattering (DLS) and nanofiltration, yielding nominal sizes in the range of 1 to 100 nm.[3,4,31-33] Again, different methods provide different means and size distributions. Espinat et al.[3] showed that pressure had no measurable impact on the microstructure of Safaniya vacuum residue asphaltenes in toluene but that mean aggregate size decreased with increasing temperature. By combining outcomes from the work of Zhao et al.,[31] Yarranton et al.,[32] and Long et al.[33] with other outcomes, one can infer that asphaltenes may be present in a molecular state, and aggregated states that range in size from a few tightly bound molecules, to two size ranges of larger structures ranging in size from ~1.5 nm to ~ 10 nm, and ~ 25 nm to less than 100 nm. The distribution of the asphaltene fraction among these diverse states is not known a priori, hence the need for empiricism.

In this work, a phase diagram for Athabasca pentane asphaltene + toluene + polystyrene mixtures at 298 K is prepared using an acoustic apparatus, operating procedures, and data interpretation methods described elsewhere in detail.[13-14, 34-35] Experimental and modeling outcomes for this mixture are also compared with outcomes for equivalent mixtures with Maya asphaltenes published previously.[13-14] The potential application of depletion flocculation as an asphaltene separation mechanism is also addressed.

2. Experimental

2.1 Materials

Athabasca Bitumen was provided by Syncrude Canada; toluene (99%) was obtained from Fisher Scientific. Polystyrene (M_w = 393400 g/mol, 1.05 g/cm^3) was purchased from Aldrich. Pentane asphaltenes were prepared from Athabasca bitumen according to ASTM D4055, as

has been done by others.[36-37] The asphaltenes were then mixed with toluene using a vortex mixer for 1 hour and were then sonicated for 2 hours. To interconvert mass and volume fractions, the density of asphaltenes was assumed to be 1.18 g/cm^3, and the measured density of toluene at 298 K is 0.86 g/cm^3.

2.2 Acoustic View Cell Apparatus and Experimental Procedure

The view cell apparatus, described in detail elsewhere[34] is depicted in Figure 4.1. In this work, samples are placed in a polybenzimidazole cell. Cell temperature is controlled using copper block immersion heaters/coolers attached to the cell lid. A mixture of ethylene glycol + water is circulated from a thermostat and through the blocks at a fixed temperature with an effective tolerance of ± 0.1 K. The sealed holder is placed inside an aluminum frame to which two sets of multi element acoustic probes are attached (inset) and coupled to the cell using acoustic gel. The probes are used in sender–receiver mode where the emitter probe is stimulated and the received signal is interpreted using a custom signal generation/interpretation software package (TomoView^{TM}, Olympus NDT) through a custom data transmission and acquisition interface (TomoScan Focus LT^{TM}, Olympus NDT). Liquid–liquid and liquid–vapour interfaces are identified from peaks in waveform amplitude and discontinuities in the time of flight data, or equivalently the speed of sound data, with elevation[13-14]. Sample opacity, illustrated in Figure 4.2.a, is not an impediment to liquid–liquid interface detection using acoustic measurements based on waveform amplitude peaks Figure 4.2.b, or speed of sound data, Figure 4.2.c.

Boundaries between single-phase and two-phase regions on the phase diagram were identified primarily using the method of Bodnar et al.[38] This method relies on the quality of relative phase volume fraction data obtained for three composition trajectories. Thus an

accurate relationship between volume and measured elevation must be available. A calibration curve for the view cell is shown in Figure 4.3. The uncertainty of interface elevations is +/- 0.3 mm. Further, it must be possible to add multiple aliquots of solvent, toluene in this case, to fixed starting mixtures of toluene + asphaltenes + polystyrene to create the trajectories, and to monitor the approach to a steady state volume distribution. Aliquots of toluene were added to prehomogenized samples within the cell using a syringe and stirred for 30 minutes. The stirrer was then removed and progress to a steady state volume distribution was monitored at 5-minute intervals for a minimum of one hour. If no phase boundary was identified after 1 hour then the sample was considered to comprise one bulk liquid phase. If two phases were present after one hour, the interface was tracked until no further interface movement could be detected, typically after 17 hours from the beginning of the experiment, and relative phase volumes were then recorded. Supplemental phase behavior measurements were performed adjacent to the phase boundary locations identified using the Bodnar et al.[38] method, in both the single-and two-phase regions to verify boundary placement.

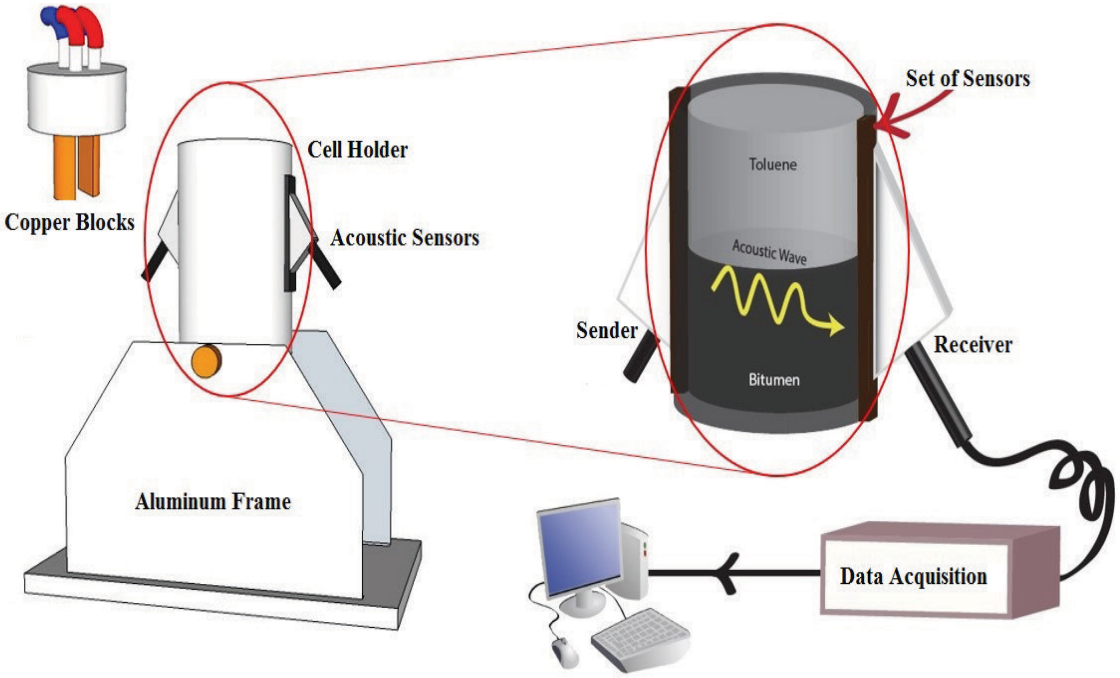

Figure 4.1 *Schematic of the acoustic view cell apparatus.*[35]

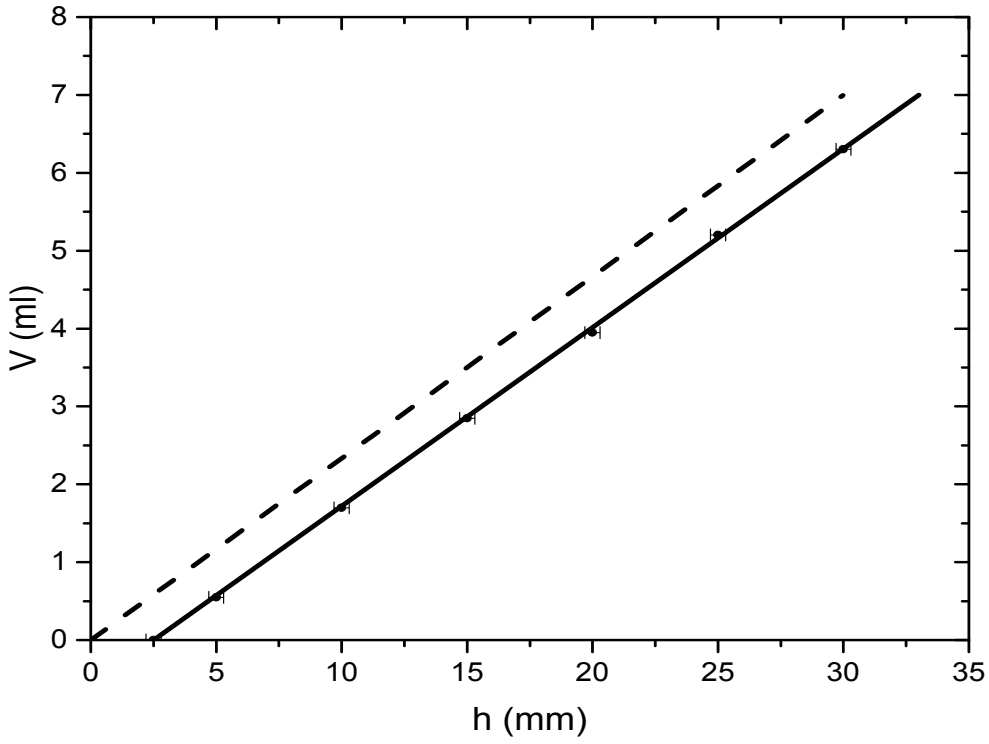

Figure 4.2 *Volume vs elevation calibration based on acoustic measurements of liquid-air interface, (solid line): apparent elevation measured acoustically; (dotted line): elevation from the bottom of the cell.*

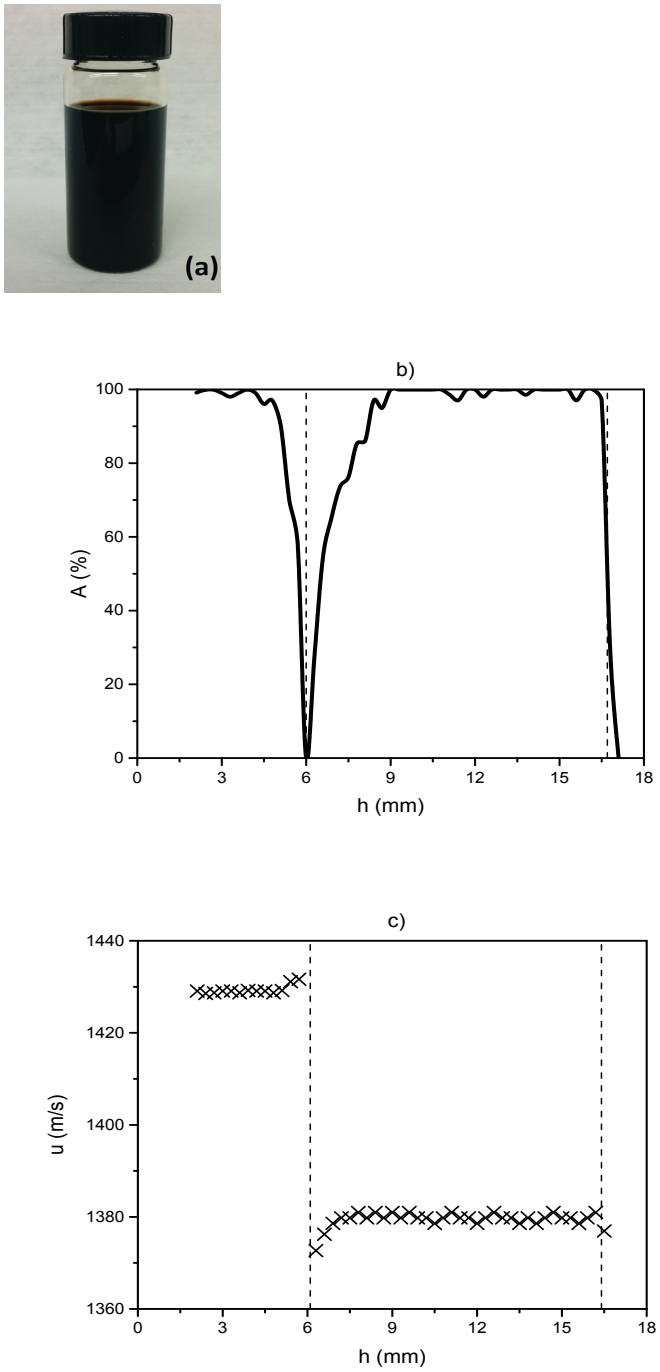

Figure 4.3 *Athabasca pentane asphaltenes (21.6 wt %) + toluene (66.3 wt %) + polystyrene (12.1 wt %) exhibiting liquid–liquid phase behavior: a) under visible light, b) based on acoustic waveform amplitude peaks, c) based on speed of sound values. The vertical dashed lines denote liquid–liquid and liquid–vapour interfaces.*

2.3 Determination of Phase Boundary Compositions Using the Bodnar et al.[38] Method

The Bodnar et al.[38] method makes use of phase volume fractions along trajectories p, q, and r, as illustrated in Figure 4.4, to construct tie lines and to identify the compositions of phases in equilibrium. This method has been applied previously to asphaltene + toluene + polystyrene mixtures.[13] The trajectories are constructed by selecting compositions remote from the origin and making phase volume measurements by adding aliquots of toluene, in this case, so that the trajectories trend to the origin. With reference to Figure 4.4, the upper phase volume fraction, R_p, at point P within the two-phase region is:

$$R_P = \frac{V_{II}}{V_{II}+V_I} = \frac{\eta_I-\eta_P}{\eta_I-\eta_{II}} = \frac{\phi_P-\phi_I}{\phi_{II}-\phi_I} \qquad (4.1)$$

and the polymer volume fraction at point P, ϕ_p, is:

$$\phi_P = \left(\frac{\eta_I\phi_{II}-\eta_{II}\phi_I}{\eta_I-\eta_{II}}\right) + \left(\frac{\phi_I-\phi_{II}}{\eta_I-\eta_{II}}\right)\eta_P = d + n\eta_P \qquad (4.2)$$

where V is volume, η is asphaltene volume fraction, ϕ is polymer volume fraction, subscripts I and II represent the asphaltene-rich phase and polymer-rich phase indices respectively, d is the intercept of the tie line with polymer volume fraction axis, and n is the tie line slope.

The phase compositions are calculated as:

$$\eta_I(P) = \eta_P + \frac{f_P^P \times l}{\sqrt{n^2+1}} \qquad (4.3.a)$$

$$\eta_{II}(P) = \eta_P - \frac{(1-f_P^P)\times l}{\sqrt{n^2+1}} \qquad (4.3.b)$$

$$\eta_I(q) = \eta_P \frac{C_p-n}{C_q-n} + \frac{f_q^Q \times l}{\sqrt{n^2+1}} \qquad (4.4.a)$$

$$\eta_{II}(q) = \eta_P \frac{C_p - n}{C_q - n} - \frac{(1 - f_q^Q) \times l}{\sqrt{n^2 + 1}} \qquad (4.4.b)$$

$$\eta_I(r) = \eta_P \frac{C_p - n}{C_q - n} + \frac{f_r^R \times l}{\sqrt{n^2 + 1}} \qquad (4.5.a)$$

$$\eta_{II}(r) = \eta_P \frac{C_p - n}{C_q - n} - \frac{(1 - f_r^R) \times l}{\sqrt{n^2 + 1}} \qquad (4.5.b)$$

where f_p^P, f_r^Q, and f_r^R are the volume fractions of the upper phase at point P along dilution line p, at point Q along dilution line q, and at point R along dilution line r respectively, l is the length of tie line, and c_p, c_q, and c_r are the slopes of the trajectories p, q and r respectively:

$$c_p = \frac{\phi^P}{\eta^P}, c_q = \frac{\phi^Q}{\eta^Q}, c_r = \frac{\phi^R}{\eta^R} \qquad (4.6)$$

An objective function:

$$Obj(n, l) = \sum_{x=p,q,r} \left[(n^2 + 1) \left(\eta_{I(x)} - \bar{\eta}_I \right) \right]^2 + \sum_{x=p,q,r} \left[(n^2 + 1) \left(\eta_{II(x)} - \bar{\eta}_{II} \right) \right]^2 \qquad (4.7)$$

is used to minimize the difference between average and individual asphaltene volume fractions and find the length (l) and slope (n) of tie lines *I-II*. As the fits to the three trajectories are imperfect, the extrapolated phase compositions possess uncertainty. It is for this reason that care is taken to minimize phase volume fraction and global composition uncertainties, and that phase volume measurements along the three trajectories in this work, Table 4.1, are supplemented by phase behavior measurements at compositions adjacent to the extrapolated phase boundaries, Table 4.2.

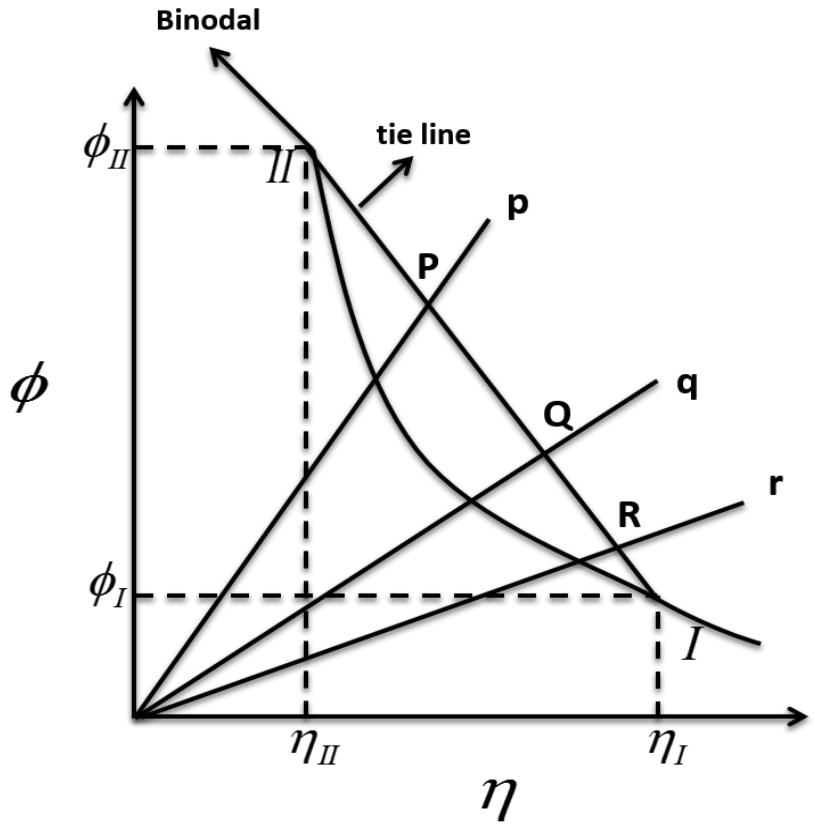

Figure 4.4 *An illustration of the Bodnar et al.* [38] *phase boundary construction method.*

Table 4.1 *Compositions and associated polymer-rich phase volume data (based on attenuation and speed of sound measurements) for trajectories p, q, and r.*

	Asphaltene volume fraction	Polystyrene volume fraction	Volume fraction of the polymer-rich phase (amplitude /speed of sound)
p	0.18	0.115	0.73
	0.17	0.109	0.73/0.72
	0.16	0.1024	0.75
	0.15	0.096	0.76
	0.12	0.077	0.86/0.87
	0.112	0.072	0.95
q	0.23	0.069	0.42
	0.22	0.066	0.43
	0.21	0.063	0.44
	0.2	0.06	0.46
	0.19	0.057	0.49/0.49
	0.18	0.054	0.54
r	0.27	0.043	0.18
	0.26	0.042	0.19
	0.25	0.04	0.19
	0.24	0.0384	0.19/0.2
	0.23	0.037	0.20

Table 4.2 *Additional composition points used to verify the phase boundary placement.*

Asphaltene volume fraction	Polystyrene volume fraction	Observed Phase Behaviour
0.05	0.090	L
0.075	0.086	L
0.10	0.064	L
0.10	0.130	LL
0.15	0.040	L
0.15	0.058	LL
0.16	0.048	LL
0.19	0.030	L
0.21	0.034	LL
0.25	0.02	L
0.33	0.035	LL
0.35	0.02	L

3. Depletion Flocculation Phase Behavior Model for Athabasca Pentane Asphaltenes + Toluene + Polystyrene Mixtures

3.1 Methodology

In a prior work, Pouralhosseini and Shaw[26] showed that it was necessary to modify the general Fleer–Tuinier model[25] describing the phase behaviour of mixtures comprising non-adsorbing polymers + monodispersed non-interacting hard sphere colloidal particles + good solvents to accommodate the impact of composition variation on asphaltene aggregate mean size, $R_s(\eta)$, and on the fraction of asphaltenes participating in the depletion flocculation

mechanism, $\gamma(\eta)$. Both of these parameters are composition dependent. A third parameter, Z, is a threshold mean particle size. With these modifications, the free volume fraction for polymer chains, α, appearing in the Fleer–Tuinier model is replaced with α':

$$\alpha' = h(\eta) * \alpha \tag{4.8}$$

where

$$h(\eta) = \left(\frac{Z}{Rs(\eta)}\right)^3 \tag{4.9}$$

$R_s(\eta)$ is the mean asphaltene particle size function. To prepare phase diagrams, the colloid volume fraction along a phase boundary obtained from the Fleer–Tuinier model, $\eta_{FT,}$ is replaced with η because only a fraction, γ, of the asphaltenes participate in the separation mechanism:

$$\eta = (\eta_{FT} / \gamma) \tag{4.10}$$

These parameters are obtained by fitting the modified Fleer–Tuinier depletion flocculation model to Athabasca asphaltene + toluene + polystyrene phase boundary data.

3.2 Model Parameter Validation

3.2.1 Predicted relative phase volumes

The predicted phase volume fractions in the two-phase region are compared with the measured values. The experimental phase volume data define the experimental phase boundaries but are not included directly in model parameter regression. A comparison between the two sets of values is used to evaluate the overall quality—a combined measure of the quality of tie line and two-phase region boundary prediction—of the fit of the modified Fleer–Tuinier model.

3.2.2 Enthalpy of Solution Measurements for Athabasca Asphaltenes in Toluene

There is no direct measurement of the asphaltene size or the fraction participating in the depletion flocculation mechanism. Differential enthalpy of solution measurements obtained by adding a small amount of asphaltene to a solvent already containing asphaltenes is sensitive to and should correlate with changes in the fraction of asphaltene that are large enough to participate in the depletion flocculation mechanism.[26] Differential enthalpies of solution measurements were previously performed for Athabasca asphaltenes in toluene at room temperature.[39] These measurements and supplemental ones performed as part of this work using the same equipment and following the same procedure[39] are compared with computed values for the change in the fraction of asphaltenes large enough to participate in the depletion flocculation mechanism with asphaltene volume fraction ($d\gamma/d\eta$) at the same composition:[26]

$$\left(\frac{dH}{d\omega}\right) = E + F\left(\frac{d\gamma}{d\eta}\right)\eta^2\left(\frac{1}{\eta} + \frac{\rho_{asph} - \rho_{tol}}{\rho_{tol}}\right)^2 \qquad (4.11)$$

where E and F are constants.

A linear relationship between $\left(\frac{dH}{d\omega}\right)$ and $\left(\frac{d\gamma}{d\eta}\right)\eta^2\left(\frac{1}{\eta} + \frac{\rho_{asph}-\rho_{tol}}{\rho_{tol}}\right)^2$ values provides independent but indirect experimental support for equation (4.10).

4. Results and Discussions

4.1 Phase Boundary Identification

The construction of the two-phase to one-phase boundary for Athabasca asphaltene + toluene + polystyrene mixtures at 298 K, based on the data in Tables 4.1 and 4.2, is presented in

Figure 4.5.a. Points on the constructed phase boundary obtained using the Bodnar et al. method[38] are shown in Figure 4.5.a along with the composition trajectories, the computed 50 vol. % curve (for each phase) that terminates at a liquid–liquid critical point on the phase boundary, and supplemental experimental points in the one-phase and two-phase regions. Trajectories p and q are trending toward a polymer-rich phase while trajectory r is tending toward an asphaltene-rich phase. The experimental phase diagram is shown as a smooth curve, without construction lines, in Figure 4.5.b, where it is compared with the corresponding phase diagram for Maya asphaltenes[13]. The phase diagrams are qualitatively similar. However, for the Athabasca asphaltenes there is significantly more polystyrene in the asphaltene-rich phase and more asphaltenes in the polymer-rich phase than arises in the Maya asphaltene case. The topologies of both of these phase diagrams are similar to the topology of the phase diagram for mixtures of silica particles sterically stabilized with stearyl alcohol + toluene + polystyrene.[40]

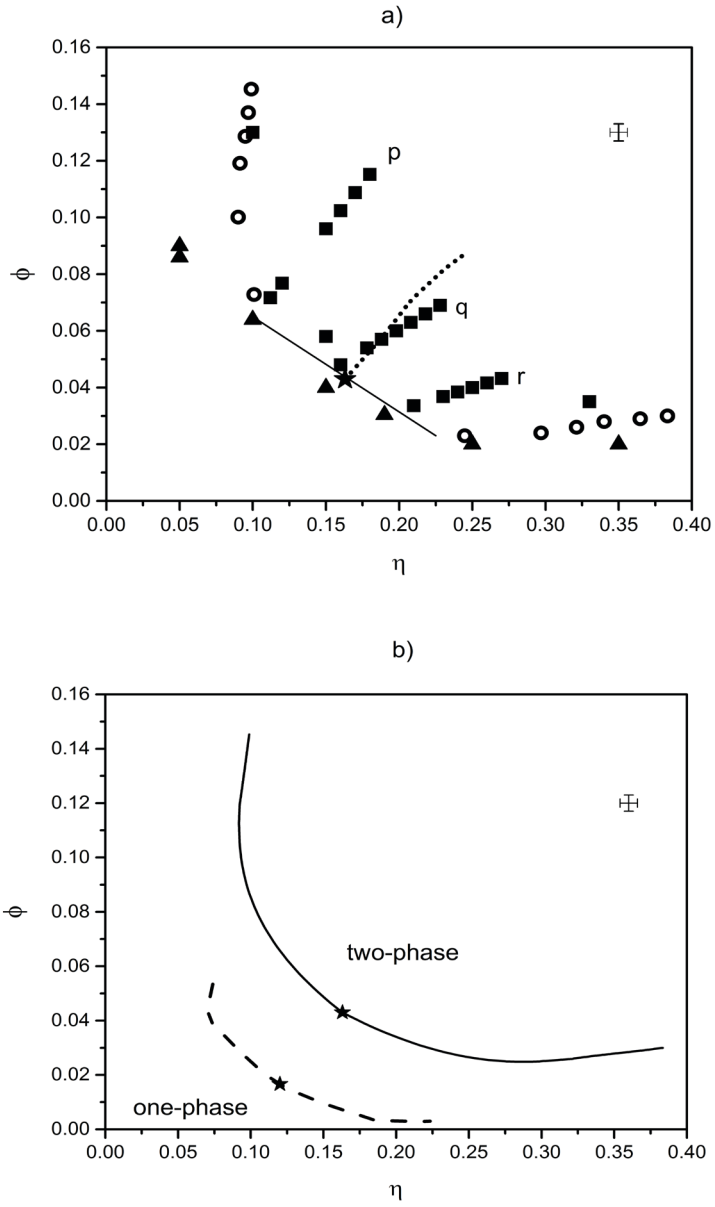

Figure 4.5 *One-phase to two-phase boundaries for asphaltene + polystyrene (Mw = 393,000 g/mol) + toluene mixtures: a) construction details for Athabasca asphaltene mixtures (square: two-phase; triangle: one-phase; dotted curve: 50% volume fraction; circle: binodal points), b) Experimental phase boundaries for Athabasca asphaltene (solid) and Maya asphaltene (dashed) curve + polystyrene (Mw = 393,000 g/mol) + toluene. Stars indicate critical points. Global composition uncertainty is inset.*

4.2 Fitted Property Model for Athabasca Asphaltenes

The composition independent mean size threshold for participation in the depletion flocculation mechanism, Z = 4 nm, and the composition dependent parameters, $R_s(\eta)$ (the mean asphaltene particle size) with the units of nm :

$$R_s(\eta) = 28.37\left(\frac{\eta}{1-\eta}\right)^3 - 40.7\left(\frac{\eta}{1-\eta}\right)^2 + 21.07\left(\frac{\eta}{1-\eta}\right) + 1.5 \qquad (4.12)$$

and γ (the fraction of asphaltenes participating in the depletion flocculation mechanism):

$$\gamma(R_s, \gamma_{max}) = \gamma_{max}\, R_{s0}\, (0.33\, e^{0.001422 R_s} - 4.24\, e^{-0.8467 R_s}) \qquad (4.13)$$

where R_{s0} is the minimum R_s to be insoluble (~3 nm) and γ_{max} is the maximum colloidal fraction of Athabasca asphaltene, 0.74, were obtained by fitting the modified Fleer–Tuinier depletion flocculation model to Athabasca asphaltene + toluene + polystyrene phase boundary data. The result is shown in Figure 4.6. Value ranges for γ and $R_s(\eta)$ are shown in Figures 4.7 and 4.8 respectively and conform to expectation. The fraction of Athabasca asphaltenes large enough to participate in the depletion flocculation mechanism (Figure 4.7) trends to zero at low volume fraction (~0.05), and approaches an asymptotic value (0.74) at high asphaltene volume fraction. The correlated average asphaltene aggregate size (Figure 4.8), falls within a narrow range and does not exceed 5 nm even at 0.4 volume fraction. Within the context of the regression, it would appear that the Athabasca asphaltenes are smaller in size than the Maya asphaltenes, and that a smaller fraction of the Athabasca asphaltenes participate in the depletion flocculation mechanism. The ranges of parameter values all fall within the range of expectation, and the regressed phase diagram, Figure 4.6, provides a near quantitative fit to the phase boundary data. At large asphaltene volume fraction, the modified model diverges from the experimental data because in the Fleer–

Tuinier model positive slopes for phase boundaries are precluded. Experimentally, in this work and elsewhere,[40-41] positive slopes at phase boundaries are observed.

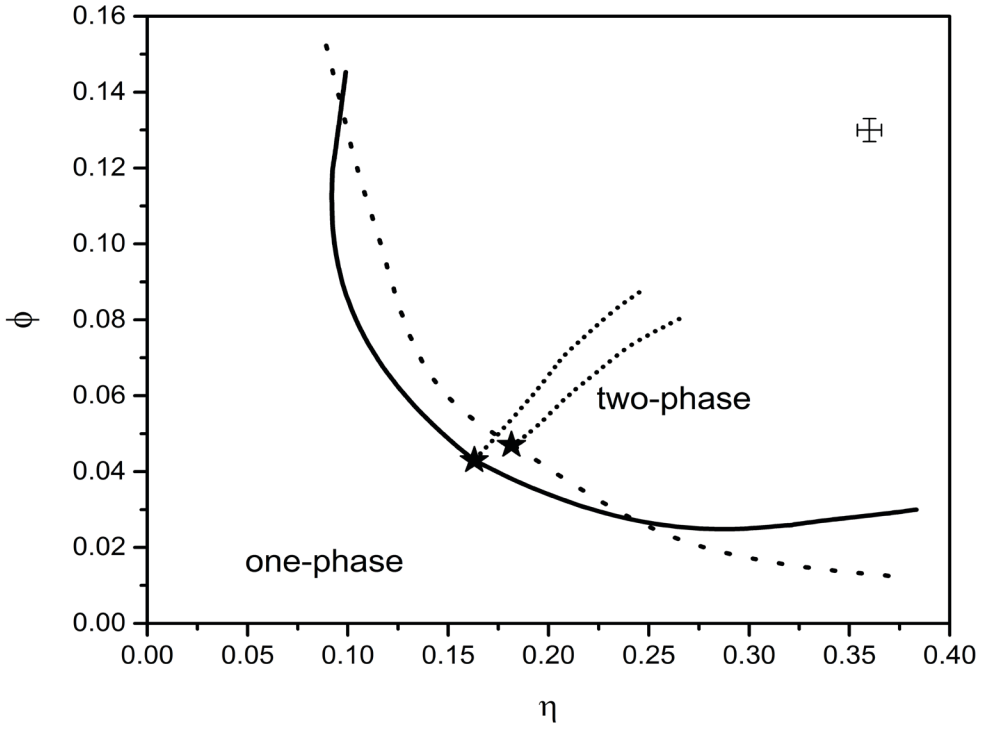

Figure 4.6 *Two-phase to one-phase boundary for Athabasca asphaltene + polystyrene (Mw = 393,000 g/mol) + toluene mixtures: modified Fleer–Tuinier phase behavior model (dashed), experimental boundary (solid) curves. The dotted lines are the 50% volume fraction loci and stars indicate critical points. The measured composition uncertainty is inset.*

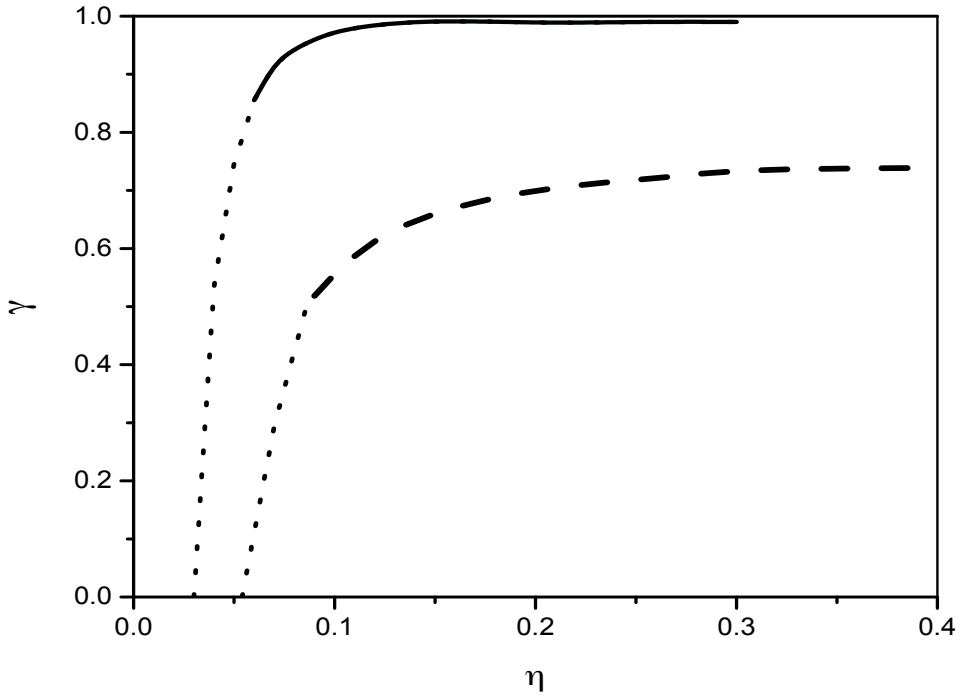

Figure 4.7 *The factions of Athabasca asphaltenes (dashed line) and Maya asphaltenes[26] (solid line) large enough to participate in the depletion flocculation mechanism in mixtures of toluene + polystyrene + asphaltene according to the regressions. The dotted parts of the curves show extrapolations of the model into the one-phase region.*

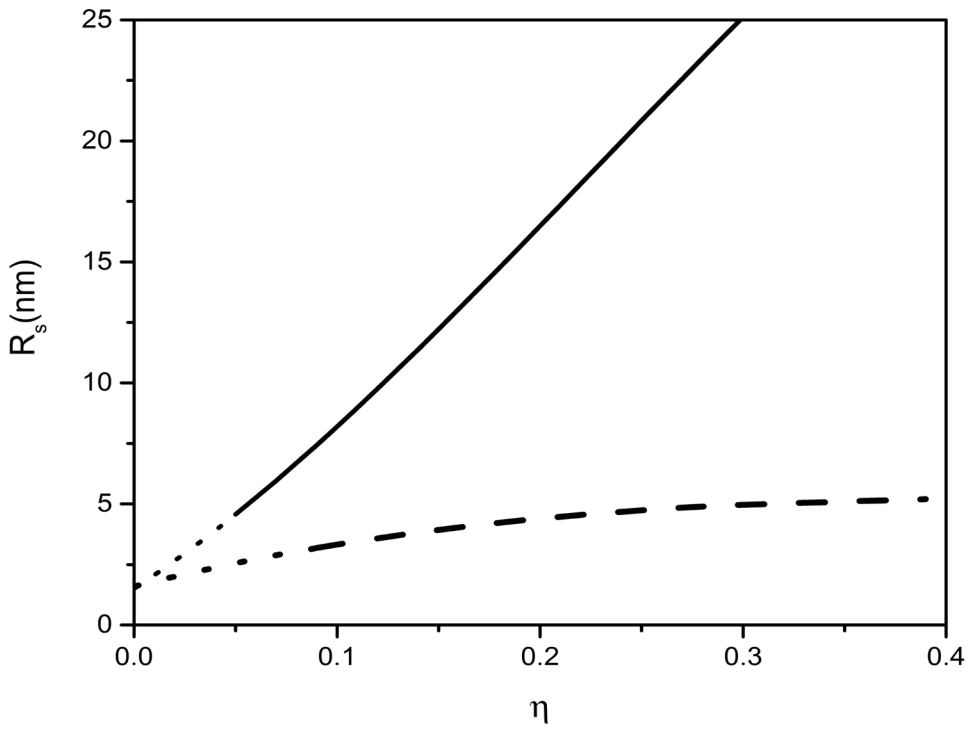

Figure 4.8 *The average particle size of Athabasca asphaltenes (dashed curve) and Maya asphaltenes[26] (solid curve) in mixtures of toluene + polystyrene + asphaltene according to the regressions. The dotted parts of the curves show extrapolations of the models into the one-phase region.*

4.3 Model Parameter Validation

4.3.1 Model Parameter Validation Using Polymer-Rich Phase Volume Fractions

A parity plot comparing predicted volume fractions for the polymer-rich phase with measured polymer-rich phase volume fractions is shown in Figure 4.9. The volume fraction of the polymer-rich phase is over predicted but the trend is well represented by the model. Despite the large relative error between the predicted volume fractions and the data, the absolute deviations are small, less than twice the measurement uncertainty, in most cases.

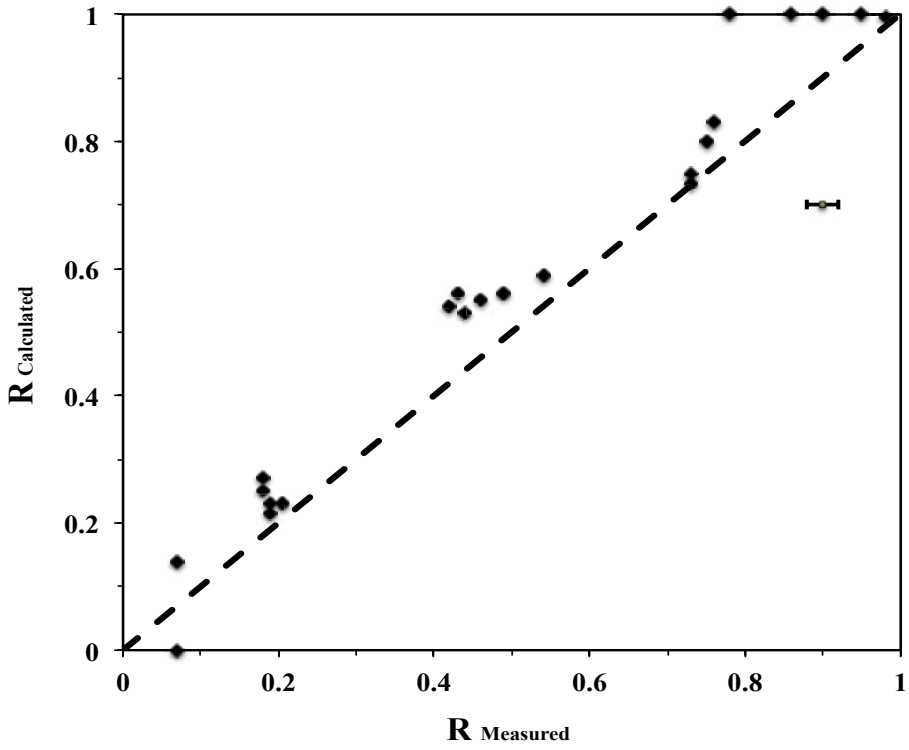

Figure 4.9 *Parity plot for polymer-rich phase volume fraction for mixtures of Athabasca asphaltenes + polystyrene (Mw=393,000 g/mol) + toluene. Calculated values are based on the modified Fleer–Tuinier model.*

4.3.2 Model Parameter Validation Using Differential Enthalpy of Solution Data for Athabasca Asphaltenes in Toluene

For mixtures of Athabasca asphaltene + toluene, at low asphaltene mass fractions enthalpies of solution are dominated by phase change and dissolution (net positive enthalpy of solution). With increasing mass fraction, the importance of phase change and dissolution diminishes in favour of solvent sorption and at high mass fraction the enthalpies of solution are dominated by sorption (negative enthalpy of solution). At low asphaltene volume fraction, where the fraction of asphaltenes remaining solid is low but changes rapidly with volume fraction, the differential enthalpy of solution is positive. At high asphaltene volume fraction, where $d\gamma/d\eta$

approaches zero, the differential enthalpy of solution is also expected to approach an unknown negative asymptotic value. In principle one would expect these two derivatives to be linearly related. The differential enthalpy of solution measurements and associated $\left(\frac{d\gamma}{d\eta}\right)\eta^2\left(\frac{1}{\eta}+\frac{\rho_{asph}-\rho_{tol}}{\rho_{tol}}\right)^2$ values are reported in Table 4.3. The two derivatives are linearly related, within the uncertainty of the experimental measurements, as shown in Figure 4.10. This outcome provides exogenous support for the parameter γ appearing in the modified Fleer–Tuinier model, equation (4.13). Data for Maya asphaltenes[26] are reproduced in Figure 4.10 and again underscore the property differences between the two asphaltenes.

Table 4.3 *Differential enthalpy of solution* $\left(\frac{dH}{d\omega}\right)$ *measurements for Athabasca asphaltenes in toluene*[39] *and the corresponding* $\left(\frac{d\gamma}{d\eta}\right)\eta^2\left(\frac{1}{\eta}+\frac{\rho_{asph}-\rho_{tol}}{\rho_{tol}}\right)^2$ *values.*

ω	η	$\left(\frac{dH}{d\omega}\right)$ (J/g)	$\left(\frac{d\gamma}{d\eta}\right)\eta^2\left(\frac{1}{\eta}+\frac{\rho_{asph}-\rho_{tol}}{\rho_{tol}}\right)^2$
0.002	0.001	6.5+/–1	12.1+/–0.3
0.010	0.007	5.2+/–1	11.1+/–0.3
0.013	0.009	5.0+/–1	10.2+/–0.3
0.11	0.081	–0.7+/–1	3.2+/–0.3
0.14	0.105	–2.3+/–1	2.4+/–0.3
0.15	0.11	–2.4+/–1	2.1+/–0.3

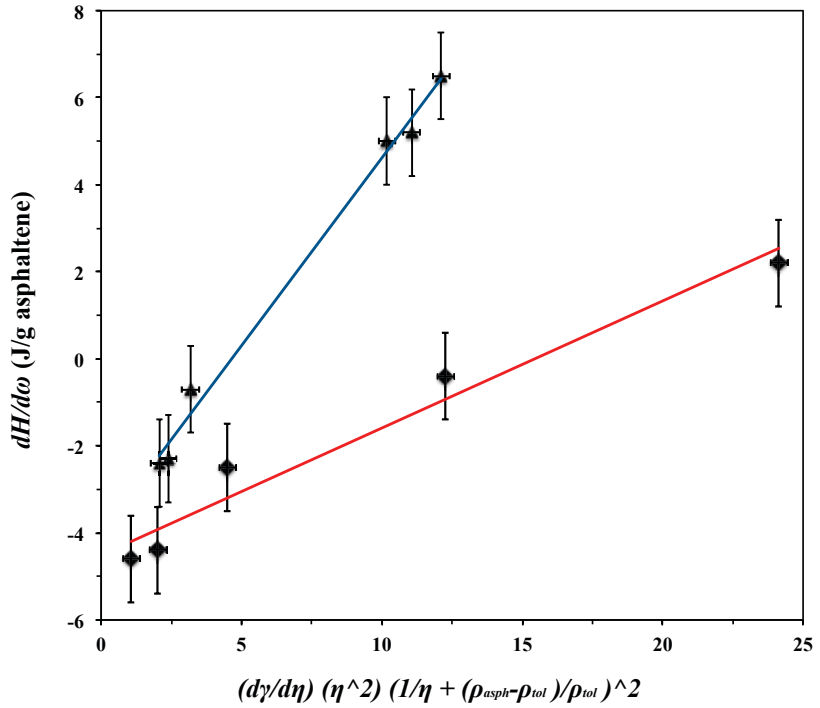

Figure 4.10 *Differential enthalpy of solution values* $\left(\frac{dH}{d\omega}\right)$ *for Athabasca asphaltenes (diamond) and for Maya asphaltenes (triangle) in toluene at 298 K vs* $\left(\frac{d\gamma}{d\eta}\right)\eta^2\left(\frac{1}{\eta}+\frac{\rho_{asph}-\rho_{tol}}{\rho_{tol}}\right)^2$.[26,39]

4.4 Depletion Flocculation and Asphaltene Separation

The large difference in the measured phase behaviours for Athabasca and Maya asphaltenes in toluene + polystyrene mixtures is indicative of the variability of all aspects of the colloidal properties of asphaltenes, and the sensitivity of this phase separation mechanism to this variability. For Maya asphaltenes, asphaltene-to-polystyrene ratios in the asphaltene-rich phase can exceed 20:1 at 298 K. For Athabasca asphaltenes the corresponding ratio is less than 8:1. From the fit of the modified Fleer–Tuinier model to the experimental phase boundaries this outcome appears to arise because Athabasca asphaltenes are smaller on average than Maya asphaltenes and a smaller mass fraction participates in the depletion flocculation mechanism. Clearly more knowledge is needed regarding the details and variability of asphaltene molecules and aggregate structures and the surface properties of asphaltene nanoaggregates, prior to the application of this aggregation mechanism in industrial processes. In addition to fundamental studies related to nanoparticle interactions, planned future work concerns whether phase diagrams for asphaltene + toluene + polystyrene are temperature dependent and whether depletion flocculation arises in whole asphaltene-rich crudes.

5. Conclusions

The phase behavior of Athabasca pentane asphaltenes + toluene + polystyrene (Mw = 393,000 g/mol) mixtures was explored. Polystyrene-rich and asphaltene-rich phases were identified, and were found to be present jointly or individually, in a pattern consistent with the depletion flocculation phase behavior mechanism. The two-phase to one-phase boundary including a liquid–liquid critical point was identified using the Bodnar et al. method. The

polymer-rich phase comprised approximately 9 vol % asphaltenes and the asphaltene-rich phase contained approximately 3 vol % polystyrene remote from the critical point. Comparable values for Maya asphaltenes, reported previously, are 6 vol % and less than 0.5 vol. % respectively. The difference in outcomes between Athabasca and Maya asphaltenes suggests that a larger mass fraction of Athabasca asphaltenes are present as molecules or as aggregates too small to participate in the depletion flocculation mechanism. In the absence of exogenous data on the distribution of asphaltenes among the molecular and various nanoaggregated states, it is not possible to generalize parameters for the prediction of phase boundaries for asphaltene + toluene + polystyrene mixtures. Further fundamental and applied research is warranted.

Acknowledgements

The authors thank Mildred Becerra for assistance with sample preparation, Marc Cassiede for assistance with acoustic measurements, and gratefully acknowledge financial support from the sponsors of the NSERC Industrial Research Chair in Petroleum Thermodynamics: Natural Sciences and Engineering Research Council of Canada (NSERC), Alberta Innovates, BP Canada, ConocoPhillips Canada Resources Corp., Nexen Energy ULC, Shell Canada Ltd., Total E&P Canada Ltd., Virtual Materials Group.

Glossary

A amplitude

c_p slope of dilution line p

c_q slope of dilution line q

c_r slope of dilution line r

d intercept of tie line

f_p^P volume fraction of upper phase at point P along dilution line p

f_q^Q volume fraction of upper phase at point Q along dilution line q

f_r^R volume fraction of upper phase at point R along dilution line r

h elevation

H enthalpy of solution

l length of tie line

M_w polystyrene mean molar mass

n slope of the tie line

R volume fraction of the upper phase

R_P volume fraction of the upper phase at point P

R_g radius of gyration of polymer

R_s colloidal particle radius, asphaltene radius

u speed of sound

V volume

Z smallest particle size attending phase separation during depletion flocculation

α free volume fraction

γ the fraction of asphaltene colloidal particles causing phase separation

η colloid volume fraction, asphaltene volume fraction

η_{FT} asphaltene volume fraction calculated by Fleer–Tuinier model

$\rho_{asph.}$ asphaltene density

$\rho_{poly.}$ polystyrene density

$\rho_{tol.}$ toluene density

φ particle-free volume fraction of polymer

ϕ polymer volume fraction, $\alpha\,\varphi$

ω weight fraction of asphaltene

REFERENCES

(1) Mehranfar, M.; Gaikwad, R.; Das, S.; Mitra, S.K.; Thundat, T. Effect of Temperature on Morphologies of Evaporation-Triggered Asphaltene Nanoaggregates. Langmuir 2014, 30(3), 800–804.

(2) Mostowfi, F.; Indo, K.; Mullins, O.C.; McFarlane, R. Asphaltene Nanoaggregates Studied by Centrifugation. Energy Fuels 2009, 23(3), 1194–1200.

(3) Espinat, D.; Fenistein, D.; Barré, L.; Frot, D.; Briolant, Y. Effects of Temperature and Pressure on Asphaltenes Agglomeration in Toluene. A Light, X-ray, and Neutron Scattering Investigation. Energy Fuels 2004,18(5), 1243–1249.

(4) Barré, L.; Simon, S.; Palermo, T. Solution Properties of Asphaltenes. Langmuir 2008, 24(8), 3709–3717.

(5) Lisitza, N.V.; Freed, D.E.; Sen, P.N.; Song, Y.Q. Study of Asphaltene Nanoaggregation by Nuclear Magnetic Resonance (NMR). Energy Fuels 2009, 23(3), 1189–1193.

(6) Andreatta, G.; Bostrom, N.; Mullins, O.C. High-Q Ultrasonic Determination of the Critical Nanoaggregate Concentration of Asphaltenes and the Critical Micelle Concentration of Standard Surfactants. Langmuir 2005, 21(7), 2728–2736.

(7) Branco, V.A.M.; Mansoori, G.A.; De Almeida Xavier, L.C.; Park, S.J.; Manafi, H. Asphaltene Flocculation and Collapse from Petroleum Fluids. J. Pet. Sci. Eng. 2001, 32(2–4), 217–230.

(8) Myakonkaya, O.; Eastoe, J. Low energy Methods of Phase Separation in Colloidal Dispersions and Microemulsions. Adv. Colloid Interface Sci. 2009, 149(1–2), 39–46.

(9) Gast, A.P.; Hall, C.K.; Russel, W.B. Polymer-Induced Phase Separations in Nonaqueous Colloidal Suspensions. J. Colloid Interface Sci. 1983, 96(1), 251–267.

(10) Mason, T.G. Osmotically Driven Shape-Dependent Colloidal Separations. Phys. Rev. E 2002, 66(6), 060402.

(11) Wang, S.; Liu, J.; Zhang, L.; Xu, Z.; Masliyah, J. Colloidal Interactions between Asphaltene Surfaces in Toluene. Energy Fuels 2009, 23(2), 862–869.

(12) Lima, A.F.; Mansur, C.R.E.; Lucas, E.F.; González, G. Polycardanol or Sulfonated Polystyrene as Flocculants for Asphaltene Dispersions. Energy Fuels 2010, 24(4), 2369–2375.

(13) Khammar, M.; Shaw, J.M. Estimation of Phase Composition and Size of Asphaltene Colloidal Particles in Mixtures of Asphaltene + Polystyrene + Toluene at 293 K and Atmospheric Pressure. Fluid Phase Equilib. 2012, 332, 105–119.

(14) Khammar, M.; Shaw, J.M. Liquid–Liquid Phase Equilibria in Asphaltene + Polystyrene + Toluene Mixtures at 293 K. Energy Fuels 2012, 26(2), 1075–1088.

(15) Asakura, S.; Oosawa, F. Interaction Between Particles Suspended in Solutions of Macromolecules. J. Polym Sci. 1958, 33(126), 183–192.

(16) Oosawa, F.; Asakura, S. Surface Tension of High-Polymer Solutions. J. Chem. Phys. 1954, 22(7), 1255–1255.

(17) Vrentas, J.S.; Duda, J.L. Diffusion in Polymer–Solvent Systems. I. Reexamination of the Free-Volume Theory. J Polym. Sci. Polym. Phys. Ed. 1977, 15(3), 403–416.

(18) Hsu, C.C.; Prausnitz, J.M. Thermodynamics of Polymer Compatibility in Ternary Systems. Macromolecules 1974, 7(3), 320–324.

(19) Sieglaff, C.L. Phase Separation in Mixed Polymer Solutions. J. Polym. Sci. 1959, 41(138), 319–326.

(20) Clarke, J.; Vincent, B. Stability of Non-aqueous Microgel Dispersions in the Presence of Free Polymer. J. Chem. Soc. Faraday Trans 1 Phy.s Chem. Condens. Phases 1981, 77(8), 1831.

(21) Saunders, B.R.; Vincent, B. Microgel Particles as Model colloids: Theory, Properties and Applications. Adv. Colloid Interface Sci. 1999, 80(1), 1–25.

(22) Bolhuis, P.G.; Meijer, E.J.; Louis, A.A. Colloid-Polymer Mixtures in the Protein Limit. Phys. Rev. Lett. 2003, 90(6), 068304.

(23) Pelissetto, A.; Hansen, J-P. An Effective Two-Component Description of Colloid−Polymer Phase Separation. Macromolecules 2006, 39(26), 9571–9580.

(24) Fuchs, M.; Schweizer, K.S. Structure of Colloid-polymer Suspensions. J. Phys. Condens. Matter. 2002, 14(12), R239, doi:10.1088/0953-8984/14/12/201.

(25) Fleer, G.J.; Tuinier, R. Analytical Phase Diagrams for Colloids and Non-adsorbing Polymer. Adv. Colloid Interface Sci. 2008, 143(1-2), 1–47.

(26) Pouralhosseini, S.S.; Shaw, J.M, Simulating Depletion Flocculation in Asphaltene + Toluene + Polystyrene Mixtures. (in preparation).

(27) Boduszynski Mieczyslaw, M. Asphaltenes in Petroleum Asphalts. Chemistry of Asphaltenes. Adv. Chem. 1981, 10.1021/ba-1981-0195.ch007.

(28) Groenzin, H.; Mullins, O.C. Molecular Size and Structure of Asphaltenes from Various Sources. Energy Fuels 2000,14(3), 677–684.

(29) Miller, J.T.; Fisher, R.B.; Thiyagarajan, P.; Winans, R.E.; Hunt, J.E. Subfractionation and Characterization of Mayan Asphaltene. Energy Fuels 1998, 12(6), 1290–1298.

(30) Andersen, S.I. Effect of Precipitation Temperature on the Composition of N-Heptane Asphaltenes. Fuel Sci. Technol. Int. 1994, 12(1), 51–74.

(31) Zhao, B.; Shaw, J.M. Composition and Size Distribution of Coherent Nanostructures in Athabasca Bitumen and Maya Crude Oil. Energy Fuels 2007, 21(5), 2795–2804.

(32) Yarrranton, H.W.; Ortiz, P.D.; Barrera, D.M.; Stasik, E.N.; Barre, L.; Frot, D.; Eyssautier, J.; Zeng, H.; Xu, G.; Dechaine, G.; Becerra, M.; Shaw, J.M.; McKenna, A.M.; Mapolelo, M.M.; Bohne, C.; Yang, Z.; Oake, J. On the Size Distribution of Self-Associated Asphaltenes. Energy Fuels 2013, 27(9), 5083–5106.

(33) Long, B.; Chadakowski, M.; Shaw, J. Impact of Liquid-Vapor to Liquid-Liquid-Vapor Phase Transitions on Asphaltene-Rich Nanoaggregate Behavior in Athabasca Vacuum Residue + Pentane Mixtures, Energy Fuels 2013, 27(4), 1779–1790.

(34) Khammar, M.; Shaw J.M. Phase Behaviour and Phase Separation Kinetics Measurement Using Acoustic Arrays. Rev Sci Instrum. 2011, 82(10), 104902.

(35) Alizadehgiashi, M.; Shaw J.M. Fickian and Non-Fickian Diffusion in Heavy Oil + Light Hydrocarbon Mixtures. Energy Fuels, 2015, 29(4), 2177–2189.

(36) Buenrostro-Gonzalez, E.; Lira-Galeana, C.; Gil-Villegas, A.; Wu, J. Asphaltene Precipitation in Crude oils: Theory and Experiments. AIChE J. 2004, 50(10), 2552–70.

(37) Fulem, M.; Becerra, M.; Hasan, M.D.A.; Zhao, B.; Shaw, J.M. Phase behaviour of Maya Crude Oil Based on Calorimetry and Rheometry. Fluid Phase Equilib. 2008, 272(1–2), 32–41.

(38) Bodnár, I.; Oosterbaan W.D. Indirect Determination of the Composition of the Coexisting Phases in a Demixed Colloid Polymer Mixture. J. Chem. Phys. 1997, 106(18), 7777–7780.

(39) Nikooyeh, K.; Shaw, J.M. On Enthalpies of Solution of Athabasca Pentane Asphaltenes and Asphaltene Fractions. Energy Fuels 2013, 27(1), 66-74.

(40) Hennequin, Y.; Evens, M.; Angulo, C.; Van Duijneveldt, J. Miscibility of small colloidal spheres with large polymers in good solvent. J. Chem. Phys., 2005, 123(5), 054906.

(41) Annunziata, O.; Ogun, O.; Benedek, G. Observation of liquid–liquid Phase Separation for Eye Lens Gamma S-crystallin. Proc. Natl. Acad. Sci. USA 2003, 100, 970–974.

Chapter 5: On the Temperature Independent Colloidal Phase Behavior of Maya Asphaltene + Toluene + Polystyrene Mixtures

ABSTRACT: Polystyrene, a non-adsorbing polymer, has been shown to cause Maya and Athabasca asphaltene + toluene mixtures to split into two stable liquid phases at room temperature. One phase is enriched in polystyrene and toluene. The other phase is enriched in asphaltene and toluene. The phase boundaries, tie lines and critical points for Maya asphaltene + toluene + polystyrene (M_w = 393,000 and 700,000 g/mol) and Athabasca asphaltene + toluene + polystyrene (M_w = 393,000 g/mol) have also been simulated at room temperature using a modified Fleer–Tuinier colloid phase behavior model. In this work, the temperature dependence of the depletion flocculation driven phase behavior is investigated for Maya asphaltene + toluene + polystyrene (M_w = 393,000 g/mol) mixtures both experimentally and theoretically. The coincidence of experimental two-phase to one-phase boundaries, including liquid–liquid critical points and tie lines at 248 K and 298 K illustrates the temperature independent nature of this phase behavior. This outcome is interpreted and predicted in terms of the known temperature dependence of the radius of gyration of polymer molecules, possible impacts of temperature variation on mean asphaltene aggregate size, and the relative importance of steric repulsion and depletion attraction effects in determining the phase behavior of asphaltene + toluene + polystyrene mixtures. Experimental and modeling outcomes are discussed.

Keywords: Temperature, Depletion, Flocculation, Asphaltenes, Phase Diagram

1. Introduction

Non-adsorbing polymer addition to colloidal solutions can cause phase separation by depletion flocculation.[1-3] This mechanism leads to the formation of a polymer-rich and colloid-depleted phase (colloid gas) and a colloid-rich and polymer-depleted phase (colloid liquid) because in the absence of adsorption, a polymer free volume, known as an excluded volume, develops in the fluid adjacent to particle surfaces. This results in an osmotic pressure difference between the bulk and locally depleted region, and when the excluded volumes of neighboring particles overlap, as illustrated in Figure 4.1, the excluded volume encompasses multiple particles. Following multiple particle–particle interactions bulk phases with contrasting compositions develop. Surface features such as ligands on particle surfaces create steric repulsive forces that further reduce the driving force for aggregation and increase the size of the polymer free volume. This increases the entropy of the colloidal solution and lowers the Helmholtz free energy of the colloidal solution relative to smooth hard spheres. Thus two forces are exerted on the adjacent particles shown in Figure 4.1: osmotic pressure, an attractive force due to the absence of non-adsorbing polymer in the fluid, shown in yellow, and a steric repulsive force due to ligands on particle surfaces shown in purple.

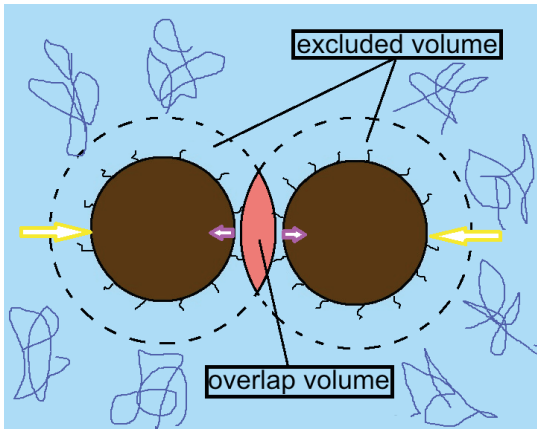

Figure 5.1 *Illustration of the depletion flocculation mechanism.*

The simplest model describing depletion flocculation induced phase behavior in colloids was proposed by Lekkerkerker et al.[4] and extended by Fleer and Tuinier to include all polymer size to particle radius ratios.[5] The Fleer–Tuinier model describes the phase behavior of mixtures of non-adsorbing monodispersed polymer + monodispersed hard sphere colloid particles + good solvents and does not include the repulsive effect noted above. The Fleer–Tuinier model, focuses on the relationship between the radius of gyration of the polymer (R_g) and the radius of the particles (R_s), their respective volume fractions (ϕ) and (η), and their impact on the depletion layer thickness (δ), and bulk phase behavior. Temperature is an implicit variable in the model. Temperature variation affects solvent density and hence volume fractions of a mixture prepared at a specific temperature. The radius of gyration of a polymer, in a good solvent, increases with increasing temperature. Temperature variation may also impact particle surface properties and density.

In the Fleer–Tuinier model, depletion thickness, δ, around a spherical particle with radius, R_s, is a function of both the polymer volume fraction in the mixture, φ, and q_R, the ratio of the particle radius and the polymer radius of gyration:

$$q = \frac{\delta}{R_s} = 0.865\{q_R^{-2} + c_1 Y^{2\kappa}\}^{-0.44} \tag{5.1}$$

$$Y = \left(\frac{\varphi}{\varphi_{ov}}\right) q_R^{-1/\kappa} \tag{5.2}$$

$$\varphi_{ov} = \frac{3\, M_w}{4\, \pi\, R_g^3\, N_A\, \rho_{polystyrene}} \tag{5.3}$$

$$R_g = 0.012\, M_w^{0.595} \tag{5.4}$$

$$q_R = {R_g}\Big/{R_s} \tag{5.5}$$

with c_1=3.95 and κ = 0.77 where M_w is polymer molecular weight, N_A is Avogadro's number, $\rho_{polystyrene}$ is polystyrene density, φ is the polymer volume fraction in the free volume not occupied by the particles and the depletion layer surrounding them and φ_{ov} is overlap volume fraction of polymer.

The chemical potential of particles (μ) and the pressure times the particle volume (pv) have a polymer contribution and a hard sphere contribution:

$$\mu = \mu^0 + \mu^p \quad (5.6.a)$$

$$pv = (pv)^0 + (pv)^p \quad (5.6.b)$$

where μ^0 is the chemical potential of particles if they are assumed to be hard spheres in a solvent without polymers, μ^p is the polymer contribution to particle chemical potential, v is particle volume, $(pv)^0$ is the hard sphere part of pressure times the particle volume without considering polymers, and $(pv)^p$ is the polymer contribution to pressure times particle volume. In this work, pv and μ terms were normalized by kT, the thermal energy, to be dimensionless where k is the Boltzmann constant and T is temperature. For a dispersion of hard spheres in a fluid, there are very precise expressions for μ^0 and $(pv)^0$: [6]

$$\mu^0 = \ln\eta + 8f + 7f^2 + 2f^3 \quad (5.7)$$

$$(pv)^0 = \eta + 4f^2 + 2f^3 \quad (5.8)$$

where η is the colloidal particle volume fraction and f is:

$$f = \frac{\eta}{1-\eta} \quad (5.9)$$

The polymer contribution to the chemical potential of particles and pressure times particle volume are obtained from:[5]

$$\mu^p = \int_0^Y [\beta - (1+f)\beta_1]\left[q_R^{-1/\kappa} + 3\kappa c_2 Y^{3\kappa-1}\right] dY \quad (5.10.a)$$

and

$$(pv)^p = \int_0^Y [\beta - f\beta_1]\left[q_R^{-1/\kappa} + 3\kappa c_2 Y^{3\kappa-1}\right] dY \qquad (5.10.b)$$

where: c_2=1.62 and κ =0.77 for the excluded volume of chains in good solvent. β_1 is the first derivative of β with respect to *f* and β is defined and obtained from:

$$\alpha = \frac{\phi}{\varphi} = (1-\eta)\beta \qquad (5.11)$$

$$\beta = e^{-Q} \quad , \quad Q = Af + Bf^2 + Cf^3 \qquad (5.12)$$

$$A = (1+q)^3 - 1\,, \quad B = 3q^2\left(q + {}^3/_2\right), \quad C = 3q^3 \qquad (5.13)$$

where $\phi = \alpha\varphi$ is polymer volume fraction, $q = \delta/R_s$, and α is the free volume fraction for the polymer.

The Fleer–Tuinier model, equations (5.1) to (5.13), does not describe the behavior of asphaltenes + toluene + polystyrene at 298 K, as illustrated in Figure 5.2.a, without modification because asphaltenes are polydispersed, and the mean size and the fraction that can participate in depletion flocculation both vary with global composition. While complex treatments for polydispersity exist[7-8], a simpler treatment of particle polydispersity that builds on the work of Khammar and Shaw was added to the Fleer–Tuinier model,[9-10] where the variation of the average size of asphaltene particles with global composition was modeled using an empirical correlation and asphaltene polydispersity was accommodated by allowing the fraction of asphaltenes participating in the depletion flocculation mechanism (γ) to vary with composition. These modifications impact equation (5.11):

$$\alpha' = H(\eta) * \alpha \qquad (5.14)$$

$$H(\eta) = \left(\frac{Z}{R_s(\eta)}\right)^3 \qquad (5.15)$$

where α' is the modified free volume fraction for polymer chains, $R_s(\eta)$ is the average asphaltene particle size function, and Z is the smallest particle size participating in phase separation. To prepare phase diagrams, the colloid volume fraction along a phase boundary obtained from the Fleer–Tuinier model, $\eta_{FT,}$ is replaced with η because only a fraction, γ, of the asphaltenes participate in the separation mechanism:

$$\eta = (\eta_{FT}/\gamma) \quad (5.16)$$

For Maya asphaltenes, $Z = 5.1\ nm,$ and the fitted correlations for $R_s(\eta),$ with the units of nm, and γ , dimensionless, at room temperature are obtained in chapter 2:[9]

$$R_s(\eta) = -157.58\left(\frac{\eta}{1-\eta}\right)^3 + 109.6\left(\frac{\eta}{1-\eta}\right)^2 + 62.292\left(\frac{\eta}{1-\eta}\right) + 1.5 \quad (5.17)$$

$$\gamma(R_s, \gamma_{max}) = \gamma_{max}\, R_{s0}\, (0.33\, e^{0.001422 R_s} - 4.24\, e^{-0.8467 R_s}) \quad (5.18)$$

where R_{s0} is the minimum R_s to be insoluble (~3 nm) and γ_{max} is the maximum colloidal fraction of Maya asphaltene, 0.99. With these modifications, the phase behaviour of Maya asphaltenes + toluene + polystyrene is well represented at 298 K, as illustrated in Figure 5.2.b.[9] However, this model is not explicit in temperature and the subject of this work is the development and validation of a robust model that includes the variation of asphaltene, polymer and solvent properties with temperature.

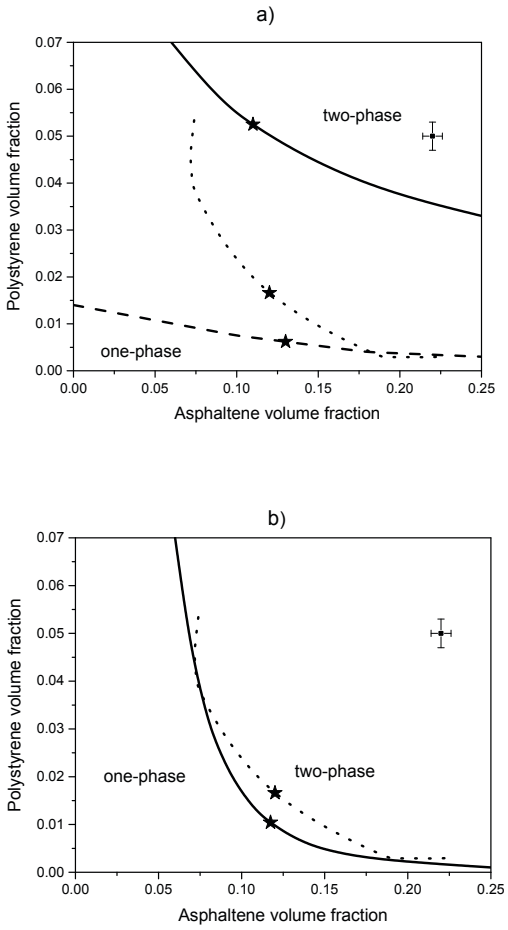

Figure 5.2 *Two-phase to one-phase boundary for mixtures of Maya asphaltenes + toluene + polystyrene (M_w =393,000 g/mol) at T=298 K: a) the Fleer–Tuinier model with the asphaltene nanoparticle radii set at 5.5 nm (solid curve) and 22 nm (dashed curve),[5,10] and the experimental boundary (dotted curve); b) The modified Fleer–Tuinier model[9] (solid curve) and the experimental boundary (dotted curve). The symbol (★) denotes a liquid-liquid critical point. Maximum composition uncertainty is inset.*

2. Phase Behavior Model Development

2.1 Impact of Temperature Variation on Mean Asphaltene Aggregate size

The asphaltene fraction of a crude oil is partitioned from saturate, aromatic, resin fractions using one of many operational protocols that include dilution (in an n-alkane) followed by macroscopic filtration and washing of the retentate (with an aromatic hydrocarbon) to obtain a filtrate that passes through the macroscopic filter. For example, ASTM D4055 is one such protocol. While asphaltenes obtained according to such protocols are deemed insoluble in n-alkanes and soluble in aromatic hydrocarbons, there are diverse sets of experimental data highlighting the nanostructured nature of asphaltenes in toluene at the ppm level at room temperature.[11-16] Small-angle X-ray scattering (SAXS), small-angle neutron scattering (SANS), and photon correlation spectroscopy (PCS) have been used to study the temperature dependence of Safaniya vacuum residue asphaltene aggregate size in toluene.[14] Based on SANS and SAXS experiments, the radius of gyration of asphaltenes extracted from Safaniya vacuum residue increase from 3.5 nm at 570 K to 5.0 nm at 350 K at 15 wt%. PCS measurements show an increase in hydraulic radius from 10 nm at 273 K to 500 nm at 253 K at 0.5 wt%. Care must be taken not to over interpret such results[14] but it would appear that asphaltene aggregates can be expected to increase in size as temperature is reduced. This qualitative result informs model development.

2.2 Possible Impacts of Temperature on Asphaltene-Aggregate Interaction

The formation and structure of asphaltene aggregates remain subjects of debate in the literature. However, asphaltenes may be viewed conceptually as biplex, comprising cores of unresolved density and shape, and surface layers from which molecular fragments protrude,

as illustrated in Figure 5.1. Many studies have employed analogies with macromolecules,[17-19] a field where interactions among macromolecules in organic solvents can be explored using the surface force apparatus.[20-25] For polymer–solvent mixtures, solvent type, temperature and other intensive and extensive variables impact macromolecule conformation and the nature of interactions among them, e.g.: steric repulsion, van der Waals attraction and electrostatic repulsion. Competition between proximate chains for the same volume tends to lead to short range repulsive interactions among macromolecules.[26] Wang et al.[27] probed colloidal forces between surfaces coated with asphaltenes immersed in toluene using atomic force microscopy and found that the repulsive interaction between asphaltene surfaces in toluene was steric in nature and independent of temperature between 298 K to 318 K. In this work, possible impacts of electrostatic repulsion are probed by zeta potential measurements[28] and as van der Waals attraction becomes more important at low temperature,[29] investigation of asphaltene particle stability in toluene at low temperatures is used to test the significance of this type of interaction.

2.3 Impact of Temperature Variation on Polymer Radius of Gyration (Rg)

The radii of gyration of polymer molecules depend on the solvent. In poor solvents, molecules maintain compact conformations. In good solvents, molecules adopt looser conformations. In the limit of very poor solvents polymer molecules behave like hard spheres, while in good solvents the molecules maximize the number of polymer–fluid contacts. Temperature can affect the quality of solvent.[29] For a polymer like polystyrene, increasing temperature improves the quality of toluene as a solvent and above a temperature, called the theta (θ) temperature, the polymer behaves like an ideal chain.[30] The radius of gyration of polystyrene molecules in toluene is well described by:[31]

$$R_g(T) = R_g^\theta \left[\chi\left(1 - \exp\left(\frac{T_\theta - T}{\tau}\right)\right) + 1\right] \qquad (5.19)$$

where χ=0.998 and τ= 131°C and χ=1.002 and τ= 94°C are fitting constants for polystyrene M_w of 393,000 g/mol and 700,00 g/mole respectively obtained using literature data: R_g^θ =17 nm, T_θ = –78°C, $R_g^{393,000}$(22°C) = 26 nm, and $R_g^{700,000}$(22°C) = 28 nm.[10, 30, 32] The impact of temperature variation over the range of interest in this work is illustrated in Figure 5.3 for polystyrene (M_w= 390,000 g/mole and M_w= 700,000 g/mole).

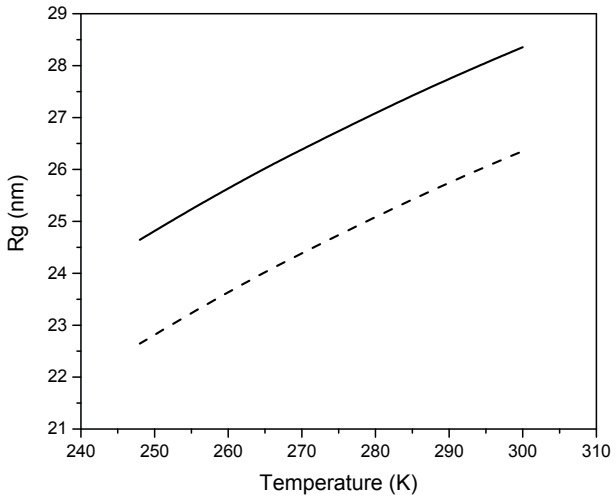

Figure 5.3 *The impact of temperature on the radius of gyration, R_g, of polystyrene in toluene, (dashed curve): M_w= 390,000 g/mole; (solid curve): M_w= 700,000 g/mole according to equation (5.19).*

2.4 Phase Behavior Modeling Approach

In the present study the impact of temperature on the phase behavior of Maya asphaltene + polystyrene (M_w = 393,000 g/mole) + toluene mixtures is explored experimentally and then theoretically once primary dependencies are identified. The known impact of temperature

variation on the radius of gyration of polystyrene is included in the model from the outset, while the unknown impacts of temperature variation on mean asphaltene aggregate size at lower temperatures is excluded. Possible impacts of temperature variation on the nature and intensity of asphaltene–asphaltene interactions are evaluated prior to their exclusion from the model.

3. Experimental

3.1 Sample Preparation

Toluene (99%) was purchased from Fisher Scientific. Pentane asphaltenes were prepared from Maya heavy oil according to ASTM standard D4055.[33-34] Polystyrene with a M_w = 390,000 g/mole was purchased from Aldrich. Asphaltenes were added to toluene in vials. The vials were mixed using a vortex mixer for 1 hour and then placed in an ultrasonic shaker for 120 minutes. The volume fractions of toluene, asphaltenes and polystyrene, needed to construct and simulate the phase diagram, were calculated from mass fractions, used for mixture preparation, by assuming densities for asphaltenes (1200 kg/m^3) and polystyrene (1050 kg/m^3) and using the known density for toluene (895 kg/m^3) at 248 K.[35, 36]

3.2 Zeta Potential Measurement

A DT 1200 electroacoustic spectrometer manufactured by Dispersion Technology Inc. with operating temperature range of 273-373 K was used to measure the zeta potential of asphaltenes in toluene at 288, 298, and 308 K. In this device an oscillating electric field is applied to particles in dispersions. The field exerts a force on the particles that is proportional to their charge. Particle movement displaces fluid in the opposite direction. If particles have a

density different from that of the fluid there is a net momentum transfer in line with the applied electric field. Momentum transfer at the electrode/dispersion interface creates a sound wave that is detected by an acoustic transducer behind the electrode. The frequency of the sound wave is the same as the frequency of the applied electric field and the amplitude of the sound wave is related to particle mobility and hence to the zeta potential.[37-38]

3.3 Phase Behaviour Measurements

Acoustic measurements are non-intrusive, accurate, and sensitive to the composition of liquid mixtures and to the presence of interfaces. The acoustic view cell employed in this work, described in detail elsewhere,[39] includes two multi-element acoustic sensors spaced at 0.6 mm intervals over a total length of 35 mm coupled to a polybenzimidazole walled view cell. The internal temperature of the cell is controlled using copper block immersion heaters/coolers. A mixture of ethylene glycol + water is circulated from a thermostat and through the immersion heaters/coolers at a constant temperature with a tolerance of ± 0.1 K. The probes are used in sender–receiver mode where the emitter probe is stimulated and the received signal is interpreted using a custom signal generation/interpretation software package (TomoView™, Olympus NDT) through a custom data transmission and acquisition interface (TomoScan Focus LT™, Olympus NDT). Liquid–liquid and liquid–vapour interfaces are detected as peaks in waveform amplitude (Figure 5.4.a) and discontinuities in the speed of sound data (Figure 5.4.b), with elevation.[10, 40-41] The two sets of measurements yield volume fractions that agree to within +/- 0.01.

Boundaries between the single-phase and two-phase regions were identified primarily using the method of Bodnar et al.[42] This approach relies on the quality of relative phase volume

fraction data obtained for three composition trajectories within the two-phase region. An accurate calibration curve for the relationship between measured elevation and volume must be available. A calibration curve for the view cell at 248 K is shown in Figure 5.5. The uncertainty of interface elevations is +/- 0.3 mm. The trajectories are created by adding aliquots of toluene to samples with three initial mixtures comprising toluene + polystyrene + asphaltene. For each measurement along the three trajectories, mixtures were prepared and stirred for 30 minutes. The stirrer is then removed and progress to a steady state volume distribution is observed at 5 minutes intervals for a minimum of one hour. If no phase boundary is observed after 1 hour then the sample is deemed to be single phase. If two phases are observed after one hour, the interface elevation is tracked until no further movement is detected, typically after 20 hours from the start of the experiment, and relative phase volumes are then recorded. Supplemental phase behavior measurements were performed adjacent to the phase boundary locations identified using the Bodnar et al. [42] method, in both the single- and two phase regions to verify boundary position.

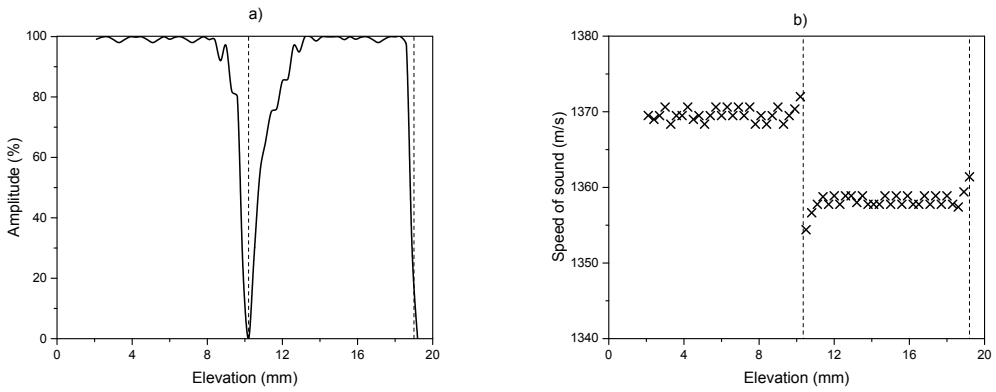

Figure 5.4 *Liquid–liquid and liquid–vapour interface detection for pentane asphaltenes (16.4 wt. %) + toluene (80.8 wt. %) + polystyrene Mw = 390,000 g/mole (2.8 wt. %) exhibiting liquid–liquid phase behaviour T=248 K: a) based on acoustic waveform amplitude peaks, b) based on discontinuities in speed of sound values.*

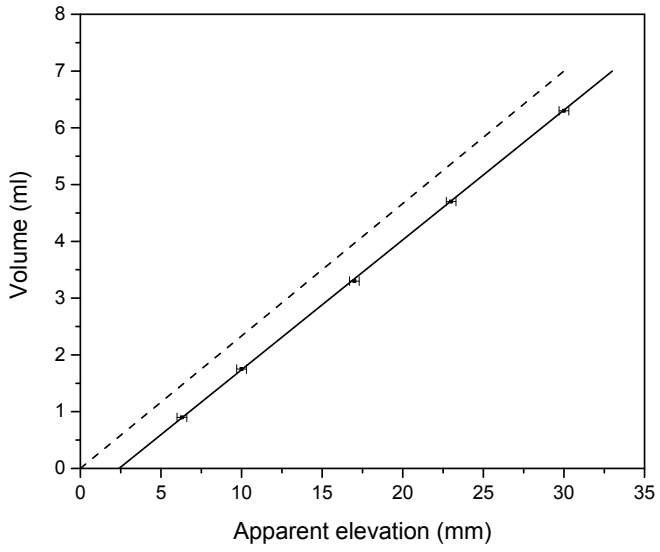

Figure 5.5 *Volume calibration based on toluene–air interface detection from speed of sound profiles at 248 K. (Solid line): apparent elevation; (Dotted line): elevation from the bottom of the cell.*

3.4 Experimental Phase Boundary Construction

With reference to Figure 5.6 and according to the Bodnar et al.[42] method, the upper phase volume fraction, R_P, at point P in the two-phase region is:

$$R_P = \frac{V_{II}}{V_{II}+V_I} = \frac{\eta_I-\eta_P}{\eta_I-\eta_{II}} = \frac{\phi_P-\phi_I}{\phi_{II}-\phi_I} \qquad (5.20)$$

and the polystyrene volume fraction at point P, ϕ_p, is:

$$\phi_P = \left(\frac{\eta_I\phi_{II}-\eta_{II}\phi_I}{\eta_I-\eta_{II}}\right) + \left(\frac{\phi_I-\phi_{II}}{\eta_I-\eta_{II}}\right)\eta_P = d + n\eta_P \qquad (5.21)$$

where V is volume, η is asphaltene volume fraction, ϕ is polystyrene volume fraction, subscripts I and II indices refer to the asphaltene-rich phase and polymer-rich phase respectively, n is the tie line slope, and d is the intercept of the tie line with the polymer volume fraction axis.

The phase compositions according to the three trajectories are:

$$\eta_I(p) = \eta_P + \frac{f_P^P \times l}{\sqrt{n^2+1}} \qquad (5.22.a)$$

$$\eta_{II}(p) = \eta_P - \frac{(1-f_P^P)\times l}{\sqrt{n^2+1}} \qquad (5.22.b)$$

$$\eta_I(q) = \eta_P \frac{C_p-n}{C_q-n} + \frac{f_q^Q \times l}{\sqrt{n^2+1}} \qquad (5.23.a)$$

$$\eta_{II}(q) = \eta_P \frac{C_p-n}{C_q-n} - \frac{(1-f_q^Q)\times l}{\sqrt{n^2+1}} \qquad (5.23.b)$$

$$\eta_I(r) = \eta_P \frac{C_p-n}{C_q-n} + \frac{f_r^R \times l}{\sqrt{n^2+1}} \qquad (5.24.a)$$

$$\eta_{II}(r) = \eta_P \frac{C_p-n}{C_q-n} - \frac{(1-f_r^R)\times l}{\sqrt{n^2+1}} \qquad (5.24.b)$$

where f_p^P, f_q^Q, and f_r^R are the volume fraction of the upper phase at point P along trajectory p, at point Q along trajectory q, and at point R along trajectory r respectively, l is the length of tie line, and c_p, c_q, and c_r are the slopes of the trajectories p, q and r respectively:

$$c_p = \frac{\phi^P}{\eta^P}, c_q = \frac{\phi^Q}{\eta^Q}, c_r = \frac{\phi^R}{\eta^R} \qquad (5.25)$$

The length (l) and slope (n) of tie lines, such as *I-II* in Figure 5.6, are determined using an objective function to minimize the difference between average and measured asphaltene volume fractions:[10, 41]

$$Obj(n,l) = \sum_{x=p,q,r}\left[(n^2+1)\left(\eta_{I(x)} - \bar{\eta}_I\right)\right]^2 + \sum_{x=p,q,r}\left[(n^2+1)\left(\eta_{II(x)} - \bar{\eta}_{II}\right)\right]^2 \qquad (5.26)$$

The phase boundaries identified in this way using data from Table 5.1 are then validated using supplemental phase behavior measurements, Table 5.2, at compositions adjacent to the boundaries identified using the Bodnar et al.[42] method.

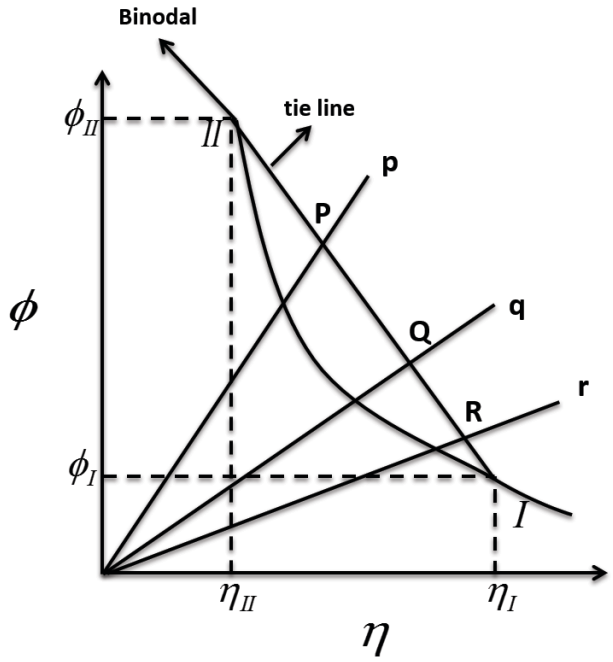

Figure 5.6 *Phase compositions identification using the method of Bodnar et al.* [42]

Table 5.1 *Compositions and associated polymer-rich phase volume fraction data (based on waveform amplitude and speed of sound measurements) for trajectories p, q, and r.*

	Asphaltene volume fraction	Polystyrene volume fraction	Volume fraction of the polymer rich phase (wave form amplitude /speed of sound)
p	0.0987	0.0461	0.84
	0.0937	0.0442	0.86
	0.0857	0.0404	0.92/0.91
	0.0786	0.0372	0.94
	0.0776	0.0364	0.96
q	0.149	0.0293	0.44
	0.143	0.0280	0.45
	0.135	0.0266	0.48
	0.128	0.0252	0.52
	0.1189	0.0234	0.57
	0.1139	0.0223	0.61/0.60
r	0.197	0.0127	0.26
	0.188	0.0118	0.28
	0.168	0.0108	0.29
	0.154	0.0098	0.32
	0.147	0.0094	0.32/0.33

Table 5.2 *Phase behavior measurements used to verify phase boundary placement.*

Asphaltene volume fraction	Polystyrene volume fraction	Observed Phase Behaviour	Volume fraction of the polymer rich phase (wave form amplitude)
0.0716	0.0340	LL	0.97
0.068	0.0319	L	
0.131	0.0082	L	
0.121	0.0073	L	
0.071	0.055	LL	0.97
0.109	0.0214	L	
0.1008	0.0196	L	
0.1412	0.0093	LL	0.22
0.054	0.004	L	
0.176	0.006	LL	0.12

4. Results and Discussion

4.1 Phase Behavior Measurement at 248 K

The construction of the two-phase to one-phase boundary for Maya asphaltene + toluene + polystyrene mixtures at 248 K is illustrated in Figure 5.7.a. Two phase and one phase points on trajectories p, q and r are shown along with supplemental phase behavior measurements adjacent to the phase boundary compositions identified from the trajectories using the method of Bodnar et al.[42] The computed locus for equal volumes of both phases that terminates at a liquid–liquid critical point on the two-phase to one-phase boundary is also shown. Trajectories p and q trend toward the polymer-rich phase while trajectory r tends toward the asphaltene-rich phase. The experimental phase diagram is illustrated as a smooth curve, without construction points, in Figure 5.7.b, where it is compared with the corresponding phase diagram for Maya asphaltenes at 298 K.[10, 40] The phase diagrams are quantitatively similar with respect to phase boundary and critical point placement, and tie line slope. Differences fall well within measurement uncertainty.

4.2 Asphaltene Aggregate Interaction Measurement

Zeta potential measurements, related to electrostatic repulsion, and phase stability measurements, related to van der Waals attraction, were performed for toluene + Maya asphaltene (5 to 30 wt %) mixtures. The results are shown in Table 5.3. The measured zeta potentials are small in absolute terms, invariant within experimental error over the temperature range 288-308 K, and trend toward zero with increasing asphaltene mass fraction. This implies that electrostatic repulsion does not play a significant rule in asphaltene colloid stability.[43] As all mixtures of toluene + asphaltene exhibit only one phase from 248 to

298 K, the van der Waals attractive interaction, expected to cause aggregation at low temperatures if significant, can also be neglected. This leaves steric repulsion[27] as the dominant interaction type.

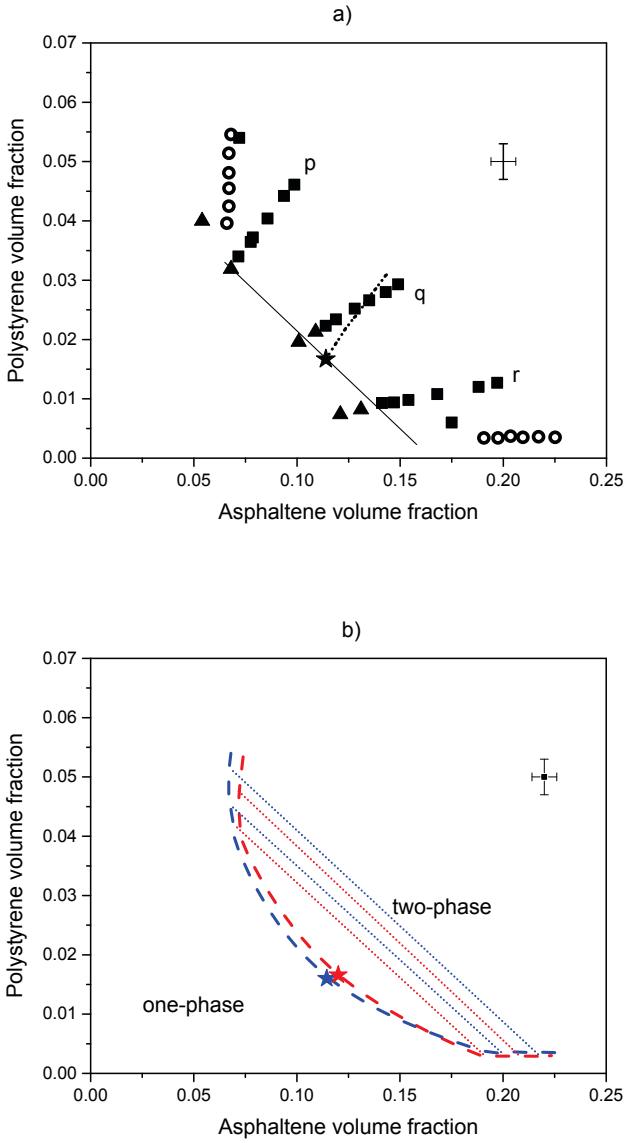

Figure 5.7 *One-phase to two-phase boundaries for Maya asphaltene + polystyrene (Mw = 393,000 g/mole) + toluene mixtures: a) phase boundary construction details at T=248 K (square: two-phase; triangle: one-phase; dotted curve: 50 vol % locus; circle: binodal points), b) Experimental phase boundaries for Maya asphaltene + polystyrene (Mw = 393,000 g/mole) + toluene at T= 248 K (blue) and T=298 K (red) curve. Stars indicate critical points and short dotted lines indicate tie lines. Maximum measurement uncertainty is inset.*

Table 5.3 *Zeta potential and phase stability tests for Maya asphaltenes + toluene mixtures.*

Asphaltene weight fraction in toluene	zeta potentials at 288, 298, and 308 K +/– 0.5 (mV)	phase stability (from 248K to 298K)
0.05	–13.2	1 stable phase
0.11	–10.7	1 stable phase
0.16	–9.9	1 stable phase
0.21	–8.7	1 stable phase
0.3	–7.4	1 stable phase

4.3 Phase Behaviour Model

4.3.1 Temperature Dependence of Asphaltene Aggregates size

Asphaltene aggregate mean size is expected to increase with decreasing temperature at fixed mass fraction. This should move the critical point of the two-phase region closer to the origin. However, the extent of the impact is unclear and this effect is neglected in the development of the phase behavior model. Given the near coincidence of the phase boundaries at 248 K and 298 K, Figure 5.7, this simplification would appear to be justified.

4.3.2 Interactions between Asphaltene Aggregates

Based on the experimental outcomes above, two interactions are considered: the short-range steric repulsion between asphaltene aggregates in toluene, and the long-range depletion attraction arising in asphaltene + toluene + polystyrene mixtures. From a model development

perspective, asphaltenes are viewed as the "hairy balls" - depicted in Figure 5.1, with molecules protruding from the surface. For a preliminary interaction calculation, asphaltene aggregates are assumed to possess a radius of 5 nm, the "hairs" are assumed to possess the nominal dimensions of asphaltene molecules (~1.5 nm) and the steric repulsion effect is assumed to be temperature independent.[27] From the work of Lekkerkerker and Tuinier[29] and Wijmans et al.,[44] the relative impacts of depletion attraction and steric repulsion on the total interaction between hairy particles where the radius of gyration of the polymer, R_g, is large (more than 22 nm in the present case) compared to the hair size (1.5 nm), are sketched in Figure 5.8. The presence of the hairs reduces the net attraction, but the depletion attraction term with an effective range exceeding 25 nm dominates and the repulsion interaction effect can be neglected for depletion flocculation driven phase behavior calculations. This outcome is insensitive to assumptions related to the size and surface properties of asphaltene nano aggregates, and the radius of gyration of the polymer in toluene but is not universal. Clearly, for small polymer molecules, this would not be the case, and the importance of steric repulsion between asphaltene films sorbed on substrates, for example, has been reported.[27]

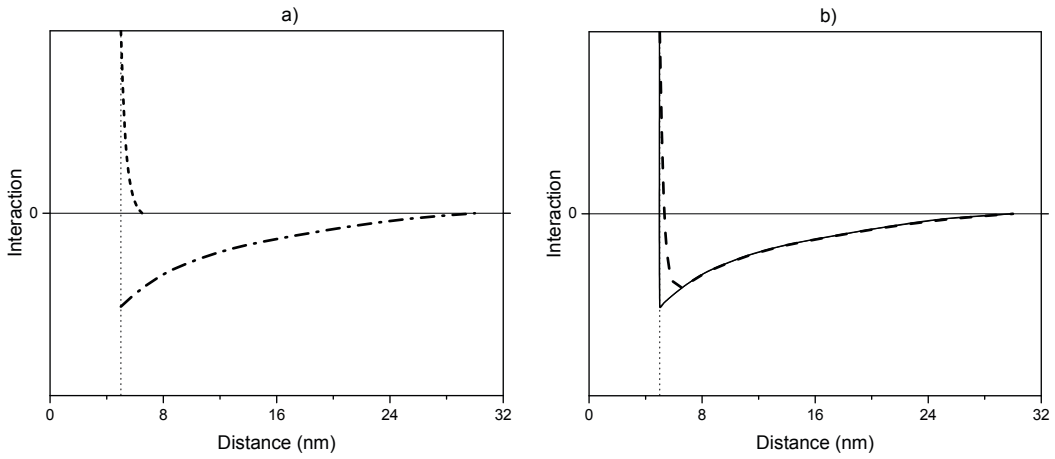

Figure 5.8 *Qualitative illustration of the interactions between a pair of particles with a radius of 5 nm and hairs of 1.5nm: a) steric repulsion (short dashed curve) and depletion attraction (dashed dotted curve), and b) total interaction including steric repulsion (dashed curve) and neglecting steric repulsion (solid curve).*

4.3.3 Predicted Phase Boundary Variation with Temperature

The phase diagram for Maya asphaltenes + polystyrene (Mw = 390,000 g/mole) + toluene at T=248 K is predicted using the modified Fleer–Tuinier model where the polystyrene radius of gyration varies according to equation (5.19), and the asphaltene properties fitted at 298 K (equations (5.17) and (5.18)). The predicted phase diagram at 248 K is compared with the simulated phase diagram in Figure 5.9. The placement of the one-phase to two-phase boundary is effectively temperature independent. However, there are two secondary impacts: the tie line slopes increase and the critical point moves to higher polymer and lower asphaltene volume fractions. The change of tie line slopes and critical point location is

attributed to the change of polymer radius of gyration, and consequently depletion interaction, with temperature.

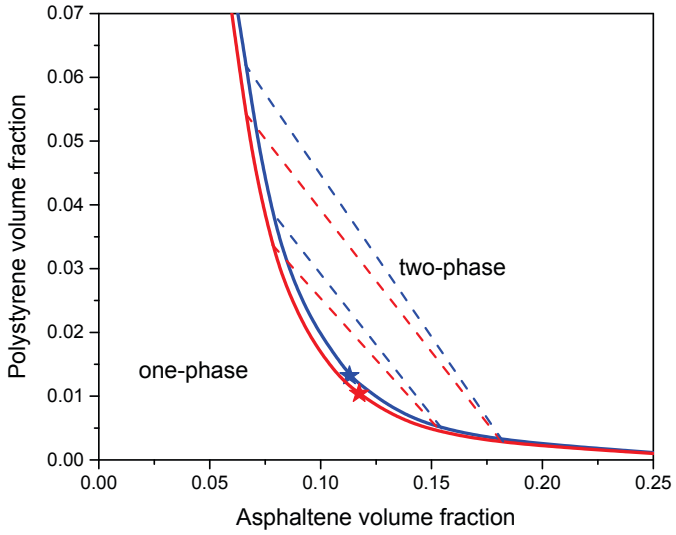

Figure 5.9 *Predicted phase diagram for mixtures of Maya asphaltenes + polystyrene (Mw = 390,000 g/mole) + toluene at T=248 K (blue solid curve), simulated phase diagram at T = 298 K (red solid curve), critical points (★), tie lines (dashed line).*

4.4 Comparison of Predicted and Measured Phase Behaviours

The predicted phase diagram for Maya asphaltenes + toluene + polystyrene (Mw = 393,000 g/mole) at T=248 K is compared with the experimental one in Figure 5.10. The placement of the one-phase to two-phase boundaries and the critical points agree to within the uncertainty of the experimental measurements. However, the predicted tie line slopes are greater than the experimental ones. While this difference is not large, refinement of the model is needed to resolve it. Tie line slopes are sensitive to both R_s, the average asphaltene particle size and γ,

the asphaltene fraction participating in the separation mechanism. Small changes to local values of either parameter, or both parameters concurrently, permit alignment of tie line slopes. For example, increasing γ and R_s reduces the slopes of tie lines. A comparison between predicted and measured upper phase volume fractions at T=248 K provides an additional test of the model. For most compositions, shown in Figure 5.11, predicted values agree with the measured values to within twice the measurement error. This outcome further reinforces the robustness of the model, and its global goodness of fit in the present form.

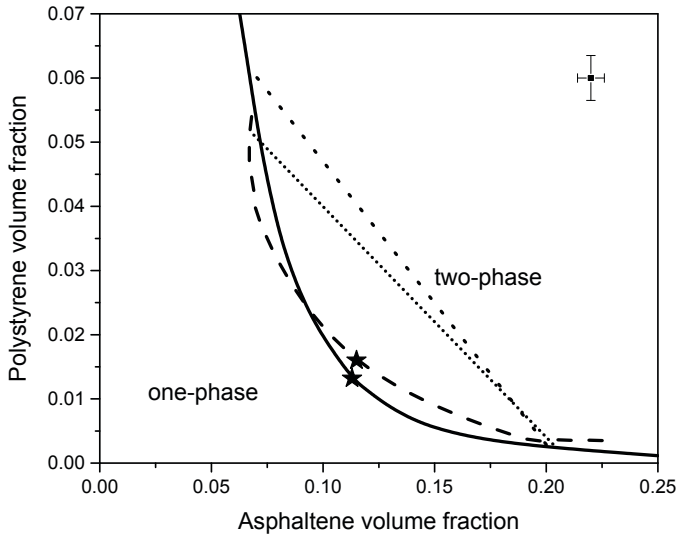

Figure 5.10 *The predicted (solid curve) and experimental (dashed curve) phase diagrams for mixtures of Maya asphaltenes + toluene + polystyrene (Mw = 393,000 g/mole) at T=248 K. (★): critical points; (large dotted line): calculated tie line; (small dotted line): experimental tie line. Maximum measurement uncertainty is inset.*

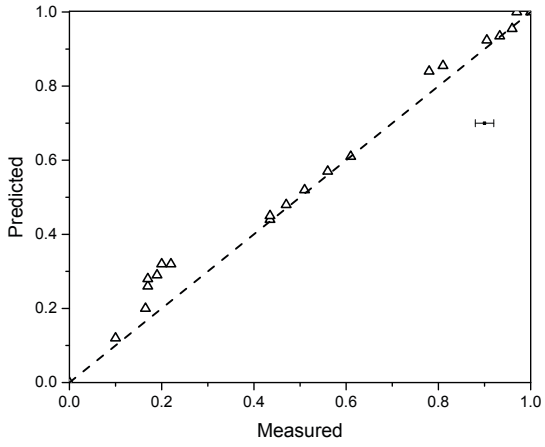

Figure 5.11 *Parity plots for measured and predicted polymer-rich phase volume fractions for Maya asphaltene + polystyrene (M_w=393,000 g/mole) + toluene mixtures at 248 K. Maximum measurement uncertainty is inset.*

5. Conclusions

The phase behavior of Maya asphaltene + toluene + polystyrene (Mw = 393,000 g/mole) mixtures is shown experimentally to be temperature invariant over the temperature interval 248 K to 298 K. The origin of this invariance was identified through a combination of experimental measurements and comparative calculations to be the dominance of the depletion attraction effect arising in these mixtures. van der Waals attraction, electrostatic repulsion and steric repulsion effects between asphaltene particles were found to be negligible compared to this effect. Depletion attraction is impacted by the radius of gyration of the polymer, a known but weak function of temperature, and colloid properties. Only the variation of polymer radius of gyration with temperature was included in the modified Fleer–Tuinier model, used to simulate the phase behaviour of Maya asphaltenes + toluene + polystyrene mixtures at 298 K, and the phase diagram at 248 K was predicted quantitatively.

This outcome suggests that Maya asphaltene properties are essentially invariant over this temperature range and that depletion flocculation driven phase behavior is insensitive to temperature variation. Application of the depletion flocculation concept to whole crude + diluent mixtures and generalization of parameters appearing in the depletion flocculation model comprise planned future work.

Acknowledgements

The authors gratefully acknowledge financial support from the sponsors of the NSERC Industrial Research Chair in Petroleum Thermodynamics: the Natural Sciences and Engineering Research Council of Canada (NSERC), Alberta Innovates Energy and Environment Solutions, British Petroleum Canada, ConocoPhillips Canada Resources Corp., Nexen Energy ULC, Shell Canada Ltd., Total E&P Canada Ltd., Virtual Materials Group.

Glossary

c_p slope of dilution line p

c_q slope of dilution line q

c_r slope of dilution line r

d intercept of tie line

f $\frac{\eta}{1-\eta}$

f_p^P volume fraction of upper phase at point P along dilution line p

f_q^Q volume fraction of upper phase at point Q along dilution line q

f_r^R volume fraction of upper phase at point R along dilution line r

l length of tie line

L nominal length of an asphaltene molecule

M_w polystyrene mean molar mass

n slope of the tie line

p pressure

$(pv)^0$ hard sphere contribution to pressure times particle volume

$(pv)^p$ polymer contribution to pressure times particle volume

q size ratio δ/R_s

q_R size ratio R_g/R_s

R volume fraction of the upper phase

R_P volume fraction of the upper phase at point P

R_g radius of gyration of polymer

R_s colloidal particle radius, asphaltene radius

y normalized particle-free polymer volume fraction φ/φ_{ov}

Y $yq_R^{-1/k}$

Z smallest particle size participating in phase separation during depletion flocculation

α free volume fraction

γ the fraction of asphaltene colloidal particles causing phase separation

δ depletion thickness around a sphere; range of the depletion interaction

η colloid volume fraction, asphaltene volume fraction

η_{FT} asphaltene volume fraction calculated by Fleer–Tuinier model

κ De Gennes exponent in the Fleer–Tuinier model

μ colloid chemical potential

μ^0 hard sphere contribution to colloid chemical potential

μ^p polymer contribution to colloid chemical potential

v colloid volume

$\rho_{asph.}$ asphaltene density

$\rho_{poly.}$ polystyrene density

$\rho_{tol.}$ toluene density

φ particle-free volume fraction of polymer

φ_{ov} particle-free overlap volume fraction of polymer

ϕ polymer volume fraction, $\alpha\ \varphi$

ω weight fraction of asphaltene

REFERENCES

(1) Lima, A.F.; Mansur, C.R.E.; Lucas, E.F.; Gonzalez, G. Polycardanol or Sulfonated Polystyrene as Flocculants for Asphaltene Dispersions. Energy Fuels 2010, 24, 2369–2375.

(2) Myakonkaya, O.; Eastoe, J. Low Energy Methods of Phase Separation in Colloidal Dispersions and Microemulsions. Adv. Colloid Interface Sci. 2009, 149, 39–46.

(3) Poon, W.C.K. The Physics of a Model Colloid-Polymer Mixture. J. Phys. Condens. Matter 2002, 14, 859–880.

(4) Lekkerkerker, H.N.W.; Poon, W.C.K.; Pusey, P.N.; Stroobants, A.; Warren, P.B. Phase Behavior of Colloid + Polymer Mixtures. Europhys. Lett. 1992, 20, 559–564.

(5) Fleer, G.J.; Tuinier, R. Analytical Phase Diagrams for Colloids and Non-adsorbing Polymer. Adv. Colloid Interface Sci. 2008, 143, 1–47.

(6) Carnahan, N.F.; Starling, K.E. Equation of State for Nonattracting Rigid Spheres, J. Chem. Phys. 1969, 51, 635–636.

(7) Fasolo, M.; Sollich, P. Effects of Polymer Polydispersity on the Phase behavior of Colloid-Polymer Mixtures. J. Phys. Condens. Matter. 2005, 17, 797–812.

(8) Paricaud, P. Phase Equilibria in Polydisperse Nonadditive Hard-sphere Systems. Phys. Rev. E 2008, 78, 021202.

(9) Pouralhosseini, S.; Shaw, J.M. Simulating Depletion Flocculation in Asphaltene + Toluene + Polystyrene Mixtures, In Preparation.

(10) Khammar, M.; Shaw, J.M.; Estimation of Phase Composition and Size of Asphaltene Colloidal Particles in Mixtures of Asphaltene + Polystyrene + Toluene at 293K and Atmospheric Pressure, Fluid Phase Equilib. 2012, 332,105–119.

(11) Mostowfi, F.; Indo, K.; Mullins, O.C.; McFarlane, R. Asphaltene Nanoaggregates Studied by Centrifugation. Energy Fuels 2009, 23, 1194–1200.

(12) Yarranton, H.W. Investigation of Asphaltene Association with Vapor Pressure Osmometry and Interfacial Tension Measurements. Ind. Eng. Chem. Res. 2000, 39(8), 2916–2924.

(13) Yarranton, H.W.; Ortiz, P.D.; Barrera, D.M.; Stasik, E.N.; Barre, L.; Frot, D.; Eyssautier, J.; Zeng, H.; Xu, G.; Dechaine, G.; Becerra, M.; Shaw, J.M.; McKenna, A.M.; Mapolelo, M.M.; Bohne, C.; Yang, Z.; Oake, J. On the Size Distribution of Self-Associated Asphaltenes. Energy Fuels 2013, 27(9), 5083–5106.

(14) Espinat, D.; Fenistein, D.; Barre, L; Frot, D.; Briolant, Y. Effects of Temperature and Pressure on Asphaltenes Agglomeration in Toluene. A Light, X-ray, and Neutron Scattering Investigation, Energy Fuels 2004, 18, 1243–1249.

(15) Barre, L.; Simon, S.; Palermo, T. Solution Properties of Asphaltenes. Langmuir 2008, 24, 3709–3717.

(16) Sheu, E.Y. Small Angle Scattering and Asphaltenes. J. Phys.: Condens. Matter 2006, 18, 2485–2498.

(17) Pazuki, G.R.; Nikookar, M.A Modified Flory-Huggins Model for Prediction of Asphaltenes Precipitation in Crude Oil, Fuel 2006, 85, 1083–1086.

(18) Li, M.Y.; Xu, M.J.; Ma, Y.; Wu, Z.L.; Christy, A.A. The Effect of Molecular Parameters on the Stability of Water-in-Crude Oil Emulsions Studied by IR and UV Spectroscopy, Colloids Surf. A 2002, 197, 193–201.

(19) Agrawala, M.; Yarranton, H.W. Asphaltene Association Model Analogous to Linear Polymerization, Ind. Eng. Chem. Res. 2001, 40, 4664–4672.

(20) Johnson, H. E.; Hu, H.W.; Granick, S. Surface Excess and Surface Forces in Ternary Solution, Macromolecules 1991, 24, 1859–1867.

(21) Marra, J.; Hair, M.L. Interactions between Adsorbed Polystyrene Layers in Toluene-Heptane Mixtures. Effect of Solvent Quality, Macromolecules 1988, 21, 2349–2355.

(22) Marra, J.; Hair, M.L. Interaction between Adsorbed Polystyrene Layers in Acetone-Heptane Solvent Mixtures. Effect of Segment-Surface Adsorption Affinity. Macromolecules 1988, 21, 2356–2362.

(23) Costello, B.A.D.; Luckham, P.F.; Tadros, T.F. Investigation of the Interaction Forces of Polymer-Coated Surfaces Using Force Balance, Rheology, and Osmotic Pressure Results. Langmuir 1992, 8, 464–468.

(24) Plunkett, M.A.; Rutland, M.W.J. Dynamic Adhesion of Grafted Polymer Surfaces as Studied by Surface Force Measurements. Adhes. Sci. Technol. 2002, 16, 983–996.

(25) Plunkett, M.A.; Rodner, S.; Bergstrom, L.; Rutland, M.W.J. Surface Forces and Characterization of Glass Surfaces Bearing Grafted Polymers: Solvent Depence. Adhes. Sci. Technol. 2002, 16, 965–981.

(26) Fischer, E.W. Elektronenmikroskopische Untersuchungen zur Stabilität von Suspensionen in Makromolekularen Lösungen. Kolloid Z 1958, 160, 120-141.

(27) Wang, S.; Liu, J.; Zhang, L.; Xu, Z.; Masliyah, J. Colloidal Interactions between Asphaltene Surfaces in Toluene. Energy Fuels 2009, 23, 862–869.

(28) Uchikawa, H; Hanehara, S; Sawaki, D. The Role of Steric Repulsive Force in the Dispersion of Cement Particles in Fresh Paste Prepared with Organic Admixture. Cement Concrete Res. 1997, 27(1), 37–50.

(29) Lekkerkerker, H.N.W.; Tuinier, R. Colloids and the Depletion Interaction; Springer: New York, 2011, DOI 10.1007/978-94-007-1223-2.

(30) Teraoka, I. Polymer Solutions: An Introduction to Physical Properties; John Wiley & Son Inc.: New York, 2002, 103–105.

(31) Taylor, S.; Evans, R.; Royall, C.P. Temperature as an External Field for Colloid-Polymer Mixtures: 'Quenching' by Heating and 'Melting' by Cooling. J. Phys. Condens. Matter 2012, 24(46), 464128.

(32) Mark, J. E. Physical Properties of Polymers Handbook; Springe: USA, 2007, 268-271.

(33) Buenrostro-Gonzalez, E.; Lira-Galeana, C.; Gil-Villegas, A.; Wu, J. Asphaltene Precipitation in Crude oils: Theory and Experiments. AIChE J. 2004, 50(10), 2552–70.

(34) Fulem, M.; Becerra, M.; Hasan, M.D.A.; Zhao, B.; Shaw, J.M. Phase Behaviour of Maya Crude Oil Based on Calorimetry and Rheometry. Fluid Phase Equilib. 2008, 272(1–2), 32–41.

(35) Nikooyeh, K. Phase Behavior of Asphaltenes in Organic Media; PhD Thesis: University of Alberta, Fall 2012.

(36) Goodwin, R.D. Toluene Thermophysical Properties from 178 to 800 K at Pressures to 1000 Bar, J. Phys. Chem. Ref. Data 1989, 18(4), 1565.

(37) Dukhin A.S.; Goetz, P.J. Method for Determining Electric Properties of Particles in Liquids by Means of Combined Electroacoustics and Complex Conductivity Measurements. U.S. Patent 6,915,214 B2, 2005.

(38) Dukhin A.S.; Goetz, P.J. Particle Size Distribution and Zeta Potential Using Acoustic and Electroacoustic Spectroscopy. U.S. Patent 6,109,098, 2000.

(39) Khammar, M.; Shaw J.M. Phase Behaviour and Phase Separation Kinetics Measurement Using Acoustic Arrays. Rev. Sci. Instrum. 2011, 82(10), 104902.

(40) Khammar, M.; Shaw, J.M. Liquid–Liquid Phase Equilibria in Asphaltene + Polystyrene + Toluene Mixtures at 293 K. Energy Fuels 2012, 26 (2), 1075–1088.

(41) Pouralhosseini, S.S; Alizadehgiashi, M; Shaw, J.M. On the Phase Behavior of Athabasca Asphaltene + Polystyrene + Toluene Mixtures at 298 K, Submitted to Energy Fuels 2015.

(42) Bodnar, I.; Oosterbaan, W. Indirect Determination of the Composition of the Coexisting Phases in a Demixed Colloid Polymer Mixture. J. Chem. Phys. 1997, 106, 7777–7780.

(43) Greenwood, R; Kendall, K. Electroacoustic Studies of Moderately Concentrated Colloidal Suspensions. J. Eur. Ceram. Soc. 1999, 19 (4), 479–488.

(44) Wijmans, C.M; Zhulina, E.B.; Fleer, G.J. Effect of Free Polymer on the Structure of a Polymer Brush and Interaction between Two Polymer Brushes. Macromolecules 1994, 27, 3238–3248.

Chapter 6: Conclusions and Recommendations

1. Conclusions

The Fleer–Tuinier[1] model was modified to accommodate the variation of the mean particle size and the fraction of particles large enough to participate in the depletion flocculation mechanism. Two sets of experimental phase behaviour data for Maya asphaltenes + polystyrene (Mw = 393,000 and 700,000 g/mole)[2] + toluene and one set for Athabasca asphaltenes + polystyrene (Mw = 393,000) + toluene were fit quantitatively using the modified Fleer and Tuinier model. Temperature and polymer size independent functions for the participating fractions and mean sizes identified for these two asphaltenes differ. According to the model, the Athabasca asphaltenes are smaller and a smaller fraction participate in the depeletion flocculation mechanism than for the Maya asphaltenes. The phase boundaries, tie lines and critical points for both mixtures were all well represented by the model. The model parameters for the asphaltene samples were validated based on the relative phase volume data (not directly regressed), and calorimetric data.[3] The Ostwald–Freundlich equation[4-5] was used to refine, simplify and generalize the functional form of the model.

Zeta potential measurements and cryogenic phase stability experiments showed that van der Waals attraction and electrostatic repulsion interactions are negligible between asphaltene particles in toluene and that the main interaction between asphaltene particles is steric repulsion. After including the temperature effect on polymer radius of gyration, which decreases with decreasing temperature, and evaluating the steric repulsion interaction

compared to the depletion interaction, the Fleer–Tuinier model, developed to describe the behavior of monodispersed non-interacting hard spheres in liquids, was generalized to account for the impact of temperature. Theoretically and experimentally, it was shown that temperature has a negligible effect on the phase boundaries, critical points and tie lines associated with asphaltene + asphaltene + polystyrene mixtures. It had been anticipated that it would be necessary to account for variations in asphaltene properties with temperature, as suggested by the literature, to fit the phase boundaries within experimental error but this proved not to be the case.

2. Future Work

- Measuring asphaltene mean size and size distributions as a function of temperature.
- Testing whether the phenomenon, the computational approaches, and the equations identified are applicable to whole crudes + polystyrene + toluene.

REFERENCES

(1) Fleer, G.J.; Tuinier, R. Analytical Phase Diagrams for Colloids and Non-adsorbing polymer. Adv. Colloid Interface Sci., 2008, 143, 1-47.

(2) Khammar, M.; Shaw, J.M.; Estimation of Phase Composition and Size of Asphaltene Colloidal Particles in Mixtures of Asphaltene + Polystyrene + Toluene at 293K and Atmospheric Pressure, Fluid Phase Equilib., 2012, 332,105-119.

(3) Nikooyeh, K.; Shaw, J.M. On Enthalpies of Solution of Athabasca Pentane Asphaltenes and Asphaltene Fractions. Energy Fuels, 2013, 27(1), 66-74.

(4) Ostwald, W. On the Assumed Isomerism of Red and Yellow Mercury Oxide and the Surface-Tension of Solid Bodies. Zeitschrift Fur Physikalische Chemie-Stochiometrie Und Verwandtschaftslehre, 1900, 34, 495-503.

(5) Freundlich, H. Kapillarchemie. Akademische Verlagsgessellschaft, 1909, Leipzig.

Full References

Chapter 1:

(1) Everett, D.H. Manual of Symbols and Terminology for Physicochemical Quantities and Units, Appendix 2: Definitions, Terminology and Symbols in Colloid and Surface Chemistry, Pure Appl. Chem. 1972, 31, 579-638.

(2) Everett, D.H. Basic Principles of Colloid Science, The Royal Society of Chemistry 1988, 243-244.

(3) Russel, W.B.; Saville, D.A.; Schowalter, W.R. Colloidal Dispersions Cambridge Universtity Press, USA, 1999.

(4) Zimmerman, S.; Minton, A. Macromolecular Crowding - Biochemical, Biophysical, and Physiological Consequences, Annu. Rev. Biophys. Biomol. Struct. 1993, 22, 27-65.

(5) Neu, B.; Wenby, R.; Meiselman, H. J. Effects of Dextran Molecular Weight on Red Blood Cell Aggregation, Biophys. J., 2008 95, 3059- 3065.

(6) Doublier, J.; Garnier, C.; Renard, D.; Sanchez, C. Proteinpolysaccharide Interactions, Curr. Opin. Colloid Interface Sci. 2000, 5, 202-214.

(7) Hughes, D.; Robb, I.; Dowding, P. Stability of Copper Phthalocyanine Dispersions in Organic Media, Langmuir 1999, 15, 5227-5231.

(8) Fleer, G.J.; Cohen Stuart, M.A.; Scheutjens, J.M.H.M.; Cosgrove, T.; Vincent, B. Polymers at Interfaces, Chapman & Hall, New York, 1993.

(9) Fischer, E.W. Elektronenmikroskopische Untersuchungen zur Stabilität von Suspensionen in Makromolekularen Lösungen, Kolloid Z 1958, 160, 120-141.

(10) Vrij, A. Polymers at Interfaces and the Interactions in Colloidal Dispersions, Pure Appl. Chem. 1976, 48(4), 471-483.

(11) Evers, O.A.; Scheutjens, J.M.H.M.; Fleer. H.J. Statistical Thermodynamics of Block Copolymer Adsorption. Part 2.—Effect of Chain Composition on the Adsorbed Amount and Layer Thickness, J. Chem. Soc. 1990, 86,1333-1340

(12) Golz P.M. Dynamics of Colloids in Polymer Solutions, Ph.D. Thesis, University of Edinburgh, 1999.

(13) Gögelein, C.; Nägele, G.; Buitenhuis, J.; Tuinier, R.; Dhont, J.K.G. Polymer Depletion-Driven Cluster Aggregation and Initial Phase Separation in Charged Nanosized Colloids, J. Chem. Phys. 2009, 130, 204905.

(14) Yarranton, H.W. Investigation of Asphaltene Association with Vapor Pressure Osmometry and Interfacial Tension Measurements, Ind. Eng. Chem. Res. 2000, 39(8), 2916-2924.

(15) Yarrranton, H.W.; Ortiz, P.D.; Barrera, D.M.; Stasik, E.N.; Barre, L.; Frot, D.; Eyssautier, J.; Zeng, H.; Xu, G.; Dechaine, G.; Becerra, M.; Shaw, J.M.; McKenna, A.M.; Mapolelo, M.M.; Bohne, C.; Yang, Z.; Oake, J. On the Size Distribution of Self-Associated Asphaltenes, Energy Fuels 2013, 27(9), 5083-5106

(16) Nikooyeh, K.; Shaw, J.M., On Enthalpies of Solution of Athabasca Pentane Asphaltenes and Asphaltene Fractions, Energy Fuels 2013, 27(1), 66-74.

(17) Zhang, Y.; Takanohashi, T.; Shishido, T.; Sato, S.; Saito, I. Estimating the Interaction Energy of Asphaltene Aggregates with Aromatic Solvents. Energy Fuels 2005, 19(3), 1023-1028.

(18) Mostowfi, F.; Indo, K.; Mullins, O.C.; McFarlane, R. Asphaltene Nanoaggregates Studied by Centrifugation. Energy Fuels 2009, 23, 1194-1200.

(19) Espinat, D.; Fenistein, D.; Barre, L.; Frot, D.; Briolant, Y. Effects of Temperature and Pressure on Asphaltenes Agglomeration in Toluene. A Light, X-ray, and Neutron Scattering Investigation. Energy Fuels 2004, 18, 1243-1249.

(20) Barre, L.; Simon, S.; Palermo, T. Solution Properties of Asphaltenes. Langmuir 2008, 24, 3709-3717.

(21) Sheu, E.Y. Small Angle Scattering and Asphaltenes. J. Phys.: Condens. Matter 2006, 18, 2485-2498.

(22) McKenna, A.M.; Blakney, G.T.; Xian, F.; Glaser, P.B.; Rodgers, R.P.; Marshall, A.G. Heavy Petroleum Composition 2. Progression of the Boduszynski Model to the Limit of Distillation by Ultrahigh Resolution FT-ICR Mass Spectrometry. Energy Fuels 2010, 24, 2939–2946.

(23) Zhao, B.; Shaw, J.M. Composition and Size Distribution of Coherent Nanostructures in Athabasca Bitumen and Maya Crude Oil. Energy Fuels 2007, 21, 2795-2804..

(24) Ching, M.J.T.M.; Pomerantz, A.E.; Andrews, A.B.; Dryden, P.; Schroeder, R.; Mullins, O.C.; Harrison, C. On the Nanofiltration of Asphaltene Solutions, Crude Oils, and Emulsions. Energy Fuels 2010, 24, 5028-5037.

(25) Lima, A.F.; Mansur, C.R.E.; Lucas, E.F.; Gonzalez, G. Polycardanol or Sulfonated Polystyrene as Flocculants for Asphaltene Dispersions. Energy Fuels 2010, 24, 2369-2375.

(26) Myakonkaya, O.; Eastoe, J. Low Energy Methods of Phase Separation in Colloidal Dispersions and Microemulsions. Adv. Colloid Interface Sci. 2009, 149, 39-46.

(27) Khammar, M.; Shaw, J.M. Liquid–Liquid Phase Equilibria in Asphaltene + Polystyrene + Toluene Mixtures at 293 K. Energy Fuels 2012, 26 (2), 1075–1088.

(28) Chang, C.L.; Fogler, H.S. Stabilization of Asphaltenes in Aliphatic Solvents Using Alkylbenzene—Derived Amphiphiles 1. Effect of the Chemical - Structure of Amphiphiles on Asphaltene Stabilization. Langmuir 1994, 10, 1749-1757.

(29) Hashmi, S.M.; Quintiliano, L.A.; Firoozabadi, A. Polymeric Dispersants Delay Sedimentation in Colloidal Asphaltene Suspensions. Langmuir 2010, 26, 8021-8029.

(30) Noda, I.; Higo, Y.; Ueno, N.; Fujimoto, T. Semidilute Region for Linear-Polymers in Good Solvents. Macromolecules 1984, 17, 1055-1059.

(31) Luckham, P. Measurement of the Interaction Between Adsorbed Polymer Layers—The Steric Effect, Adv. Colloid Interface Sci. 1991, 34, 191-215.

(32) Wang, S.; Liu, J.; Zhang, L.; Xu, Z.; Masliyah, J. Colloidal Interactions between Asphaltene Surfaces in Toluene, Energy Fuels 2009, 23, 862- 869.

(33) Khammar, M.; Shaw, J.M.; Estimation of Phase Composition and Size of Asphaltene Colloidal Particles in Mixtures of Asphaltene + Polystyrene + Toluene at 293K and Atmospheric Pressure. Fluid Phase Equilib. 2012, 332,105-119.

(34) Lekkerkerker, H.N.W.; Poon, W.C.K.; Pusey, P.N.; Stroobants, A.; Warren, P.B. Phase Behaviour of Colloid + Polymer Mixtures. Europhys. Lett. 1992, 20, 559-564.

(35) Fleer, G.J.; Tuinier, R. Analytical Phase Diagrams for Colloids and Non-adsorbing Polymer. Adv. Colloid Interface Sci. 2008, 143, 1-47.

Chapter 2:

(1) Lima, A.F.; Mansur, C.R.E.; Lucas, E.F.; Gonzalez, G. Polycardanol or Sulfonated Polystyrene as Flocculants for Asphaltene Dispersions. Energy Fuels, 2010, 24, 2369-2375.

(2) Myakonkaya, O.; Eastoe, J. Low Energy Methods of Phase Separation in Colloidal Dispersions and Microemulsions. Adv. Colloid Interface Sci., 2009, 149, 39-46.

(3) Poon, W.C.K. The Physics of a Model Colloid-Polymer Mixture. J. Phys. Condens. Matter, 2002,14, 859-880.

(4) Lekkerkerker, H.N.W.; Tuinier, R. Colloids and the Depletion Interaction, Springer, 2011, New York.

(5) Lekkerkerker, H.N.W.; Poon, W.C.K.; Pusey, P.N.; Stroobants, A.; Warren, P.B. Phase Behaviour of Colloid + Polymer Mixtures. Europhys. Lett., 1992, 20, 559-564.

(6) Fleer, G.J.; Tuinier, R. Analytical Phase Diagrams for Colloids and Non-adsorbing polymer. Adv. Colloid Interface Sci., 2008, 143, 1-47.

(7) Carnahan, N.F.; Starling, K.E. Equation of State for Nonattracting Rigid Spheres, J Chem Phys, 1969, 51, 635-636.

(8) Khammar, M. The Phase Behaviour of Asphaltene + Polystyrene + Toluene Mixtures at 293 K. PhD Thesis, University of Alberta, April 2011.

(9) Khammar, M.; Shaw, J.M.; Estimation of Phase Composition and Size of Asphaltene Colloidal Particles in Mixtures of Asphaltene + Polystyrene + Toluene at 293K and Atmospheric Pressure, Fluid Phase Equilib., 2012, 332,105-119.

(10) Zhao, B.; Shaw, J.M. Composition and Size Distribution of Coherent Nanostructures in Athabasca Bitumen and Maya Crude Oil. Energy Fuels, 2007, 21 (5), 2795–2804.

(11) Nikooyeh, K.; Shaw, J.M. On Enthalpies of Solution of Athabasca Pentane Asphaltenes and Asphaltene Fractions. Energy Fuels, 2013, 27(1), 66-74.

(12) Bagheri, S.R.; Bazyleva, A.; Gray, M.R.; McCaffrey, W.C.; Shaw, J.M. Observation of Liquid Crystals in Heavy Petroleum Fractions. Energy Fuels, 2010, 24 (8), 4327–4332.

(13) Bazyleva, A.; Fulem, M.; Becerra, M.; Zhao, B.; Shaw, J.M. Phase Behaviour of Athabasca Bitumen. J. Chem. Eng. Data, 2011, 56 (7), 3242–3253.

(14) Zhang, Y.; Takanohashi, T.; Shishido, T.; Sato, S.; Saito, I. Estimating the Interaction Energy of Asphaltene Aggregates with Aromatic Solvents. Energy Fuels, 2005, 19(3), 1023-1028.

(15) Mostowfi, F.; Indo, K.; Mullins, O.C.; McFarlane, R. Asphaltene Nanoaggregates Studied by Centrifugation. Energy Fuels, 2009, 23, 1194-1200.

(16) Yarranton, H.W. Investigation of Asphaltene Association with Vapor Pressure Osmometry and Interfacial Tension Measurements. Ind. Eng. Chem. Res., 2000, 39(8), 2916-2924.

(17) Yarrranton, H.W.; Ortiz, P.D.; Barrera, D.M.; Stasik, E.N.; Barre, L.; Frot, D.; Eyssautier, J.; Zeng, H.; Xu, G.; Dechaine, G.; Becerra, M.; Shaw, J.M.; McKenna, A.M.; Mapolelo, M.M.; Bohne, C.; Yang, Z.; Oake, J. On the Size Distribution of Self-Associated Asphaltenes. Energy Fuels, 2013, 27(9), 5083-5106.

(18) Espinat, D.; Fenistein, D.; Barre, L.; Frot, D.; Briolant, Y. Effects of Temperature and Pressure on Asphaltenes Agglomeration in Toluene. A Light, X-ray, and Neutron Scattering Investigation. Energy Fuels, 2004, 18, 1243-1249.

(19) Barre, L.; Simon, S.; Palermo, T. Solution Properties of Asphaltenes. Langmuir, 2008, 24, 3709-3717.

(20) Sheu, E. Y. Small Angle Scattering and Asphaltenes. J. Phys.: Condens. Matter, 2006, 18, 2485-2498.

(21) McKenna, A.M.; Blakney, G.T.; Xian, F.; Glaser, P.B.; Rodgers, R.P.; Marshall, A.G. Heavy Petroleum Composition 2. Progression of the Boduszynski Model to the Limit of Distillation by Ultrahigh Resolution FT-ICR Mass Spectrometry. Energy Fuels, 2010, 24, 2939–2946.

(22) Zhao, B.; Shaw, J.M. Composition and Size Distribution of Coherent Nanostructures in Athabasca Bitumen and Maya Crude Oil. Energy Fuels, 2007, 21, 2795-2804.

(23) Ching, M.J.T.M.; Pomerantz, A.E.; Andrews, A.B.; Dryden, P.; Schroeder, R.; Mullins, O.C.; Harrison, C. On the Nanofiltration of Asphaltene Solutions, Crude Oils, and Emulsions. Energy Fuels, 2010, 24, 5028-5037.

(24) Akbarzadeh, K.; Hammami, A.; Kharrat, A.; Zhang, D.; Allenson, S.; Creek, J.; Kabir, S.; Jamaluddin, A.; Marshal, A.G.; Rodgers, R.P.; Mullins, O.C.; Solbakken, T. Asphaltenes-Problematic but Rich in Potential, Oilfield Review, Schlumberger, 2007.

(25) Long, B.; Chadakowski, M.; Shaw, J.M. Impact of Liquid-Vapor to Liquid-Liquid-Vapor Phase Transitions on Asphaltene-Rich Nanoaggregate Behavior in Athabasca Vacuum Residue + Pentane Mixtures, Energy Fuels, 2013, 27(4), 1779-1790.

(26) Lucas, E.F.; Mansur, C.R.E.; Spinelli, L.; Queiros, Y.G.C. Polymer Science Applied to Petroleum Production. Pure Appl. Chem., 2009, 81, 473-494.

(27) Hashmi, S.M.; Quintiliano, L.A.; Firoozabadi, A. Polymeric Dispersants Delay Sedimentation in Colloidal Asphaltene Suspensions. Langmuir, 2010, 26, 8021-8029.

(28) deBoer, R.B.; Leerlooyer, K.; Eigner, M.R.P.; Bergen, A.R.D. Screening of Crude Oils for Asphaltene Precipitation, SPE Prod. Facil., 10(1), 1995, 55-61.

(29) Likhatsky, V.V.; Syunyaev, R.Z. New Colloidal Stability Index for Crude Oils Based on Polarity of Crude Oil Components, Energy Fuels, 24, 2010, 6483–6488.

(30) Panuganti, S.R.; Vargas, F.M.; Gonzalez, D.L.; Kurup, A.S.; Chapman, W.G. PC-SAFT Characterization of Crude Oils and Modeling of Asphaltene Phase Behaviour, Fuel, 2012, 93, 658-669.

(31) Ting, P.D.; Gonzalez, D.; Hiraski, G.; Chapman, W.G. Applications of the SAFT Equation of State to Asphaltene Phase Behaviour. Asphaltenes, Heavy Oils and Petroleomics, 2007, 301-327.

(32) Paricaud, P. Phase Equilibria in Polydisperse Nonadditive Hard-sphere Systems. Phys. Rev. E, 2008, 78, 021202.

(33) Fasolo, M.; Sollich, P. Effects of Polymer Polydispersity on the Phase behaviour of Colloid-Polymer Mixtures. J. Phys. Condens. Matter, 2005, 17, 797-812.

(34) Bodnar, I.; Oosterbaan, W. Indirect Determination of the Composition of the Coexisting Phases in a Demixed Colloid Polymer Mixture. J. Chem. Phys., 1997, 106, 7777-7780.

(35) Khammar, M.; Shaw, J.M. Liquid–Liquid Phase Equilibria in Asphaltene + Polystyrene + Toluene Mixtures at 293 K. Energy Fuels, 2012, 26 (2), 1075–1088.

Chapter 3:

(1) Pouralhosseini, S.S.; Shaw, J.M, Simulating Depletion Flocculation in Asphaltene + Toluene + Polystyrene Mixtures, Submitted to Fluid Phase Equilib. 2015.

(2) Fleer, G.J.; Tuinier, R. Analytical Phase Diagrams for Colloids and Non-adsorbing Polymer. Adv. Colloid Interface Sci. 2008, 143, 1-47.

(3) Lima, A.F.; Mansur, C. R. E.; Lucas, E. F.; Gonzalez, G. Polycardanol or Sulfonated Polystyrene as Flocculants for Asphaltene Dispersions. Energy Fuels 2010, 24, 2369-2375.

(4) Myakonkaya, O.; Eastoe, J. Low Energy Methods of Phase Separation in Colloidal Dispersions and Microemulsions. Adv. Colloid Interface Sci. 2009, 149, 39-46.

(5) Poon, W.C.K. The Physics of a Model Colloid-Polymer Mixture. J. Phys. Condens. Matter 2002,14, 859-880.

(6) Carnahan, N.F.; Starling, K.E. Equation of State for Nonattracting Rigid Spheres, J. Chem. Phys. 1969, 51, 635-636.

(7) Pouralhosseini, S.S.; Alizadehgiashi, M.; Shaw, J.M. On the Phase Behavior of Athabasca Asphaltene + Polystyrene + Toluene Mixtures at 298 K, Energy Fuels. 2015.

(8) Defay, R.; Prigogine, I. Surface Tension and Adsorption / R. Defay and I. Prigogine; London, England : Longmans, 1966; English ed: 1966.

(9) Ostwald, W. On the Assumed Isomerism of Red and Yellow Mercury Oxide and the Surface-Tension of Solid Bodies. ZeitschriFleer-Tuinier Fur Physikalische Chemie-Stochiometrie Und VerwandtschaFleer-Tuinierslehre, 1900, 34, 495-503.

(10) Freundlich, H. Kapillarchemie. Akademische VerlagsgessellschaFleer-Tuinier, 1909, Leipzig.

(11) Johnson, K.C. Comparison of Methods for Predicting Dissolution and the Theoretical Implications of Particle-Size-Dependent Solubility. J. Pharm. Sci. 2012, 101, 681-689.

(12) Letellier, P.; Mayaffre, A.; Turmine, M. Solubility of Nanoparticles: Nonextensive Thermodynamics Approach. J. Phys-Condens. Mat. 2007, 19, 436229.

(13) Shchekin, A.K.; Rusanov, A. I. Generalization of the Gibbs-Kelvin-Kohler and Ostwald–Freundlich Equations for a Liquid Film on a Soluble Nanoparticle. J. Chem. Phys. 2008, 129, 154116.

(14) Shchekin, A.K.; Shabaev, I.V.; Rusanov, A.I. Thermodynamics of Droplet Formation Around a Soluble Condensation Nucleus in the Atmosphere of a Solvent Vapor. J. Chem. Phys. 2008, 129, 214111.

(15) Ely, D.R.; Garcia, R.E.; Thommes, M. Ostwald-Freundlich Diffusion-limited Dissolution Kinetics of Nanoparticles. Powder Technol. 2014, 257, 120-123.

(16) Wamatsu, M. Nucleation and Growth by Diffusion under Ostwald-Freundlich Boundary Condition. J. Chem. Phys. 2014, 140, 064702.

(17) Eslami, F; Elliott, J.A.W. Role of Precipitating Solute Curvature on Microdrops and Nanodrops during Concentrating Processess; The Non-Ideal Ostwald–Freundlich Equation, J. Phys. Chem. B, 2014, 118, 14675-14686.

(18) McKenna, A.M.; Donald, L.J.: Fitzsimmons, J.E.; Juyal, P.; Spicer, V.; Standing, K.G.; Marshall, A.G.; Rodgers, R.P. Heavy Petroleum Composition. 3. Asphaltene Aggregation, Energy Fuels, 2013, 27 (3), 1246–1256.

(19) Bagheri, S.R.; Bazyleva, A.; Gray, M.R.; McCaffrey, W.C.; Shaw, J.M. Observation of Liquid Crystals in Heavy Petroleum Fractions, Energy Fuels, 2010, 24 (8), 4327–4332.

(20) Bazyleva, A.; Fulem, M.; Becerra, M.; Zhao, B.; Shaw, J.M., Phase Behavior of Athabasca Bitumen, J. Chem. Eng. Data, 2011, 56. (7), 3242-3253.

(21) Bagheri, S.R.; Masik, B.; Arboleda, P.; Wen, Q.; Michaelian, K.H.; Shaw, J.M. Physical Properties of Liquid Crystals in Athabasca Bitumen Fractions, Energy Fuels, 2012, 26(8), 4978-4987.

(22) Bazyleva, A.; Becerra, M.; Stratiychuk-Dear, D.: Shaw, J.M., Phase Behavior of Safaniya Vacuum Residue, Fluid Phase Equilib., 2014, 80, 28-38.

Chapter 4:

(1) Mehranfar, M.; Gaikwad, R.; Das, S.; Mitra, S.K.; Thundat, T. Effect of Temperature on Morphologies of Evaporation-Triggered Asphaltene Nanoaggregates. Langmuir 2014, 30(3), 800–804.

(2) Mostowfi, F.; Indo, K.; Mullins, O.C.; McFarlane, R. Asphaltene Nanoaggregates Studied by Centrifugation. Energy Fuels 2009, 23(3), 1194–1200.

(3) Espinat, D.; Fenistein, D.; Barré, L.; Frot, D.; Briolant, Y. Effects of Temperature and Pressure on Asphaltenes Agglomeration in Toluene. A Light, X-ray, and Neutron Scattering Investigation. Energy Fuels 2004,18(5), 1243–1249.

(4) Barré, L.; Simon, S.; Palermo, T. Solution Properties of Asphaltenes. Langmuir 2008, 24(8), 3709–3717.

(5) Lisitza, N.V.; Freed, D.E.; Sen, P.N.; Song, Y.Q. Study of Asphaltene Nanoaggregation by Nuclear Magnetic Resonance (NMR). Energy Fuels 2009, 23(3), 1189–1193.

(6) Andreatta, G.; Bostrom, N.; Mullins, O.C. High-Q Ultrasonic Determination of the Critical Nanoaggregate Concentration of Asphaltenes and the Critical Micelle Concentration of Standard Surfactants. Langmuir 2005, 21(7), 2728–2736.

(7) Branco, V.A.M.; Mansoori, G.A.; De Almeida Xavier, L.C.; Park, S.J.; Manafi, H. Asphaltene Flocculation and Collapse from Petroleum Fluids. J. Pet. Sci. Eng. 2001, 32(2–4), 217–230.

(8) Myakonkaya, O.; Eastoe, J. Low energy Methods of Phase Separation in Colloidal Dispersions and Microemulsions. Adv. Colloid Interface Sci. 2009, 149(1–2), 39–46.

(9) Gast, A.P.; Hall, C.K.; Russel, W.B. Polymer-Induced Phase Separations in Nonaqueous Colloidal Suspensions. J. Colloid Interface Sci. 1983, 96(1), 251–267.

(10) Mason, T.G. Osmotically Driven Shape-Dependent Colloidal Separations. Phys. Rev. E 2002, 66(6), 060402.

(11) Wang, S.; Liu, J.; Zhang, L.; Xu, Z.; Masliyah, J. Colloidal Interactions between Asphaltene Surfaces in Toluene. Energy Fuels 2009, 23(2), 862–869.

(12) Lima, A.F.; Mansur, C.R.E.; Lucas, E.F.; González, G. Polycardanol or Sulfonated Polystyrene as Flocculants for Asphaltene Dispersions. Energy Fuels 2010, 24(4), 2369–2375.

(13) Khammar, M.; Shaw, J.M. Estimation of Phase Composition and Size of Asphaltene Colloidal Particles in Mixtures of Asphaltene + Polystyrene + Toluene at 293 K and Atmospheric Pressure. Fluid Phase Equilib. 2012, 332, 105–119.

(14) Khammar, M.; Shaw, J.M. Liquid–Liquid Phase Equilibria in Asphaltene + Polystyrene + Toluene Mixtures at 293 K. Energy Fuels 2012, 26(2), 1075–1088.

(15) Asakura, S.; Oosawa, F. Interaction Between Particles Suspended in Solutions of Macromolecules. J. Polym Sci. 1958, 33(126), 183–192.

(16) Oosawa, F.; Asakura, S. Surface Tension of High-Polymer Solutions. J. Chem. Phys. 1954, 22(7), 1255–1255.

(17) Vrentas, J.S.; Duda, J.L. Diffusion in Polymer–Solvent Systems. I. Reexamination of the Free-Volume Theory. J Polym. Sci. Polym. Phys. Ed. 1977, 15(3), 403–416.

(18) Hsu, C.C.; Prausnitz, J.M. Thermodynamics of Polymer Compatibility in Ternary Systems. Macromolecules 1974, 7(3), 320–324.

(19) Sieglaff, C.L. Phase Separation in Mixed Polymer Solutions. J. Polym. Sci. 1959, 41(138), 319–326.

(20) Clarke, J.; Vincent, B. Stability of Non-aqueous Microgel Dispersions in the Presence of Free Polymer. J. Chem. Soc. Faraday Trans 1 Phy.s Chem. Condens. Phases 1981, 77(8), 1831.

(21) Saunders, B.R.; Vincent, B. Microgel Particles as Model colloids: Theory, Properties and Applications. Adv. Colloid Interface Sci. 1999, 80(1), 1–25.

(22) Bolhuis, P.G.; Meijer, E.J.; Louis, A.A. Colloid-Polymer Mixtures in the Protein Limit. Phys. Rev. Lett. 2003, 90(6), 068304.

(23) Pelissetto, A.; Hansen, J-P. An Effective Two-Component Description of Colloid−Polymer Phase Separation. Macromolecules 2006, 39(26), 9571–9580.

(24) Fuchs, M.; Schweizer, K.S. Structure of Colloid-polymer Suspensions. J. Phys. Condens. Matter. 2002, 14(12), R239, doi:10.1088/0953-8984/14/12/201.

(25) Fleer, G.J.; Tuinier, R. Analytical Phase Diagrams for Colloids and Non-adsorbing Polymer. Adv. Colloid Interface Sci. 2008, 143(1-2), 1–47.

(26) Pouralhosseini, S.S.; Shaw, J.M, Simulating Depletion Flocculation in Asphaltene + Toluene + Polystyrene Mixtures. (in preparation).

(27) Boduszynski Mieczyslaw, M. Asphaltenes in Petroleum Asphalts. Chemistry of Asphaltenes. Adv. Chem. 1981, 10.1021/ba-1981-0195.ch007.

(28) Groenzin, H.; Mullins, O.C. Molecular Size and Structure of Asphaltenes from Various Sources. Energy Fuels 2000,14(3), 677–684.

(29) Miller, J.T.; Fisher, R.B.; Thiyagarajan, P.; Winans, R.E.; Hunt, J.E. Subfractionation and Characterization of Mayan Asphaltene. Energy Fuels 1998, 12(6), 1290–1298.

(30) Andersen, S.I. Effect of Precipitation Temperature on the Composition of N-Heptane Asphaltenes. Fuel Sci. Technol. Int. 1994, 12(1), 51–74.

(31) Zhao, B.; Shaw, J.M. Composition and Size Distribution of Coherent Nanostructures in Athabasca Bitumen and Maya Crude Oil. Energy Fuels 2007, 21(5), 2795–2804.

(32) Yarrranton, H.W.; Ortiz, P.D.; Barrera, D.M.; Stasik, E.N.; Barre, L.; Frot, D.; Eyssautier, J.; Zeng, H.; Xu, G.; Dechaine, G.; Becerra, M.; Shaw, J.M.; McKenna, A.M.; Mapolelo, M.M.; Bohne, C.; Yang, Z.; Oake, J. On the Size Distribution of Self-Associated Asphaltenes. Energy Fuels 2013, 27(9), 5083–5106.

(33) Long, B.; Chadakowski, M.; Shaw, J. Impact of Liquid-Vapor to Liquid-Liquid-Vapor Phase Transitions on Asphaltene-Rich Nanoaggregate Behavior in Athabasca Vacuum Residue + Pentane Mixtures, Energy Fuels 2013, 27(4), 1779–1790.

(34) Khammar, M.; Shaw J.M. Phase Behaviour and Phase Separation Kinetics Measurement Using Acoustic Arrays. Rev Sci Instrum. 2011, 82(10), 104902.

(35) Alizadehgiashi, M.; Shaw J.M. Fickian and Non-Fickian Diffusion in Heavy Oil + Light Hydrocarbon Mixtures. Energy Fuels, 2015, 29(4), 2177–2189.

(36) Buenrostro-Gonzalez, E.; Lira-Galeana, C.; Gil-Villegas, A.; Wu, J. Asphaltene Precipitation in Crude oils: Theory and Experiments. AIChE J. 2004, 50(10), 2552–70.

(37) Fulem, M.; Becerra, M.; Hasan, M.D.A.; Zhao, B.; Shaw, J.M. Phase behaviour of Maya Crude Oil Based on Calorimetry and Rheometry. Fluid Phase Equilib. 2008, 272(1–2), 32–41.

(38) Bodnár, I.; Oosterbaan W.D. Indirect Determination of the Composition of the Coexisting Phases in a Demixed Colloid Polymer Mixture. J. Chem. Phys. 1997, 106(18), 7777–7780.

(39) Nikooyeh, K.; Shaw, J.M. On Enthalpies of Solution of Athabasca Pentane Asphaltenes and Asphaltene Fractions. Energy Fuels 2013, 27(1), 66-74.

(40) Hennequin, Y.; Evens, M.; Angulo, C.; Van Duijneveldt, J. Miscibility of small colloidal spheres with large polymers in good solvent. J. Chem. Phys., 2005, 123(5), 054906.

(41) Annunziata, O.; Ogun, O.; Benedek, G. Observation of liquid–liquid Phase Separation for Eye Lens Gamma S-crystallin. Proc. Natl. Acad. Sci. USA 2003, 100, 970–974.

Chapter 5:

(1) Lima, A.F.; Mansur, C.R.E.; Lucas, E.F.; Gonzalez, G. Polycardanol or Sulfonated Polystyrene as Flocculants for Asphaltene Dispersions. Energy Fuels 2010, 24, 2369–2375.

(2) Myakonkaya, O.; Eastoe, J. Low Energy Methods of Phase Separation in Colloidal Dispersions and Microemulsions. Adv. Colloid Interface Sci. 2009, 149, 39–46.

(3) Poon, W.C.K. The Physics of a Model Colloid-Polymer Mixture. J. Phys. Condens. Matter 2002, 14, 859–880.

(4) Lekkerkerker, H.N.W.; Poon, W.C.K.; Pusey, P.N.; Stroobants, A.; Warren, P.B. Phase Behavior of Colloid + Polymer Mixtures. Europhys. Lett. 1992, 20, 559–564.

(5) Fleer, G.J.; Tuinier, R. Analytical Phase Diagrams for Colloids and Non-adsorbing Polymer. Adv. Colloid Interface Sci. 2008, 143, 1–47.

(6) Carnahan, N.F.; Starling, K.E. Equation of State for Nonattracting Rigid Spheres, J. Chem. Phys. 1969, 51, 635–636.

(7) Fasolo, M.; Sollich, P. Effects of Polymer Polydispersity on the Phase behavior of Colloid-Polymer Mixtures. J. Phys. Condens. Matter. 2005, 17, 797–812.

(8) Paricaud, P. Phase Equilibria in Polydisperse Nonadditive Hard-sphere Systems. Phys. Rev. E 2008, 78, 021202.

(9) Pouralhosseini, S.; Shaw, J.M. Simulating Depletion Flocculation in Asphaltene + Toluene + Polystyrene Mixtures, In Preparation.

(10) Khammar, M.; Shaw, J.M.; Estimation of Phase Composition and Size of Asphaltene Colloidal Particles in Mixtures of Asphaltene + Polystyrene + Toluene at 293K and Atmospheric Pressure, Fluid Phase Equilib. 2012, 332,105–119.

(11) Mostowfi, F.; Indo, K.; Mullins, O.C.; McFarlane, R. Asphaltene Nanoaggregates Studied by Centrifugation. Energy Fuels 2009, 23, 1194–1200.

(12) Yarranton, H.W. Investigation of Asphaltene Association with Vapor Pressure Osmometry and Interfacial Tension Measurements. Ind. Eng. Chem. Res. 2000, 39(8), 2916–2924.

(13) Yarranton, H.W.; Ortiz, P.D.; Barrera, D.M.; Stasik, E.N.; Barre, L.; Frot, D.; Eyssautier, J.; Zeng, H.; Xu, G.; Dechaine, G.; Becerra, M.; Shaw, J.M.; McKenna, A.M.; Mapolelo, M.M.; Bohne, C.; Yang, Z.; Oake, J. On the Size Distribution of Self-Associated Asphaltenes. Energy Fuels 2013, 27(9), 5083–5106.

(14) Espinat, D.; Fenistein, D.; Barre, L; Frot, D.; Briolant, Y. Effects of Temperature and Pressure on Asphaltenes Agglomeration in Toluene. A Light, X-ray, and Neutron Scattering Investigation, Energy Fuels 2004, 18, 1243–1249.

(15) Barre, L.; Simon, S.; Palermo, T. Solution Properties of Asphaltenes. Langmuir 2008, 24, 3709–3717.

(16) Sheu, E.Y. Small Angle Scattering and Asphaltenes. J. Phys.: Condens. Matter 2006, 18, 2485–2498.

(17) Pazuki, G.R.; Nikookar, M.A Modified Flory-Huggins Model for Prediction of Asphaltenes Precipitation in Crude Oil, Fuel 2006, 85, 1083–1086.

(18) Li, M.Y.; Xu, M.J.; Ma, Y.; Wu, Z.L.; Christy, A.A. The Effect of Molecular Parameters on the Stability of Water-in-Crude Oil Emulsions Studied by IR and UV Spectroscopy, Colloids Surf. A 2002, 197, 193–201.

(19) Agrawala, M.; Yarranton, H.W. Asphaltene Association Model Analogous to Linear Polymerization, Ind. Eng. Chem. Res. 2001, 40, 4664–4672.

(20) Johnson, H. E.; Hu, H.W.; Granick, S. Surface Excess and Surface Forces in Ternary Solution, Macromolecules 1991, 24, 1859–1867.

(21) Marra, J.; Hair, M.L. Interactions between Adsorbed Polystyrene Layers in Toluene-Heptane Mixtures. Effect of Solvent Quality, Macromolecules 1988, 21, 2349–2355.

(22) Marra, J.; Hair, M.L. Interaction between Adsorbed Polystyrene Layers in Acetone-Heptane Solvent Mixtures. Effect of Segment-Surface Adsorption Affinity. Macromolecules 1988, 21, 2356–2362.

(23) Costello, B.A.D.; Luckham, P.F.; Tadros, T.F. Investigation of the Interaction Forces of Polymer-Coated Surfaces Using Force Balance, Rheology, and Osmotic Pressure Results. Langmuir 1992, 8, 464–468.

(24) Plunkett, M.A.; Rutland, M.W.J. Dynamic Adhesion of Grafted Polymer Surfaces as Studied by Surface Force Measurements. Adhes. Sci. Technol. 2002, 16, 983–996.

(25) Plunkett, M.A.; Rodner, S.; Bergstrom, L.; Rutland, M.W.J. Surface Forces and Characterization of Glass Surfaces Bearing Grafted Polymers: Solvent Depence. Adhes. Sci. Technol. 2002, 16, 965–981.

(26) Fischer, E.W. Elektronenmikroskopische Untersuchungen zur Stabilität von Suspensionen in Makromolekularen Lösungen. Kolloid Z 1958, 160, 120-141.

(27) Wang, S.; Liu, J.; Zhang, L.; Xu, Z.; Masliyah, J. Colloidal Interactions between Asphaltene Surfaces in Toluene. Energy Fuels 2009, 23, 862–869.

(28) Uchikawa, H; Hanehara, S; Sawaki, D. The Role of Steric Repulsive Force in the Dispersion of Cement Particles in Fresh Paste Prepared with Organic Admixture. Cement Concrete Res. 1997, 27(1), 37–50.

(29) Lekkerkerker, H.N.W.; Tuinier, R. Colloids and the Depletion Interaction; Springer: New York, 2011, DOI 10.1007/978-94-007-1223-2.

(30) Teraoka, I. Polymer Solutions: An Introduction to Physical Properties; John Wiley & Son Inc.: New York, 2002, 103–105.

(31) Taylor, S.; Evans, R.; Royall, C.P. Temperature as an External Field for Colloid-Polymer Mixtures: 'Quenching' by Heating and 'Melting' by Cooling. J. Phys. Condens. Matter 2012, 24(46), 464128.

(32) Mark, J. E. Physical Properties of Polymers Handbook; Springe: USA, 2007, 268-271.

(33) Buenrostro-Gonzalez, E.; Lira-Galeana, C.; Gil-Villegas, A.; Wu, J. Asphaltene Precipitation in Crude oils: Theory and Experiments. AIChE J. 2004, 50(10), 2552–70.

(34) Fulem, M.; Becerra, M.; Hasan, M.D.A.; Zhao, B.; Shaw, J.M. Phase Behaviour of Maya Crude Oil Based on Calorimetry and Rheometry. Fluid Phase Equilib. 2008, 272(1–2), 32–41.

(35) Nikooyeh, K. Phase Behavior of Asphaltenes in Organic Media; PhD Thesis: University of Alberta, Fall 2012.

(36) Goodwin, R.D. Toluene Thermophysical Properties from 178 to 800 K at Pressures to 1000 Bar, J. Phys. Chem. Ref. Data 1989, 18(4), 1565.

(37) Dukhin A.S.; Goetz, P.J. Method for Determining Electric Properties of Particles in Liquids by Means of Combined Electroacoustics and Complex Conductivity Measurements. U.S. Patent 6,915,214 B2, 2005.

(38) Dukhin A.S.; Goetz, P.J. Particle Size Distribution and Zeta Potential Using Acoustic and Electroacoustic Spectroscopy. U.S. Patent 6,109,098, 2000.

(39) Khammar, M.; Shaw J.M. Phase Behaviour and Phase Separation Kinetics Measurement Using Acoustic Arrays. Rev. Sci. Instrum. 2011, 82(10), 104902.

(40) Khammar, M.; Shaw, J.M. Liquid–Liquid Phase Equilibria in Asphaltene + Polystyrene + Toluene Mixtures at 293 K. Energy Fuels 2012, 26 (2), 1075–1088.

(41) Pouralhosseini, S.S; Alizadehgiashi, M; Shaw, J.M. On the Phase Behavior of Athabasca Asphaltene + Polystyrene + Toluene Mixtures at 298 K, Submitted to Energy Fuels 2015.

(42) Bodnar, I.; Oosterbaan, W. Indirect Determination of the Composition of the Coexisting Phases in a Demixed Colloid Polymer Mixture. J. Chem. Phys. 1997, 106, 7777–7780.

(43) Greenwood, R; Kendall, K. Electroacoustic Studies of Moderately Concentrated Colloidal Suspensions. J. Eur. Ceram. Soc. 1999, 19 (4), 479–488.

(44) Wijmans, C.M; Zhulina, E.B.; Fleer, G.J. Effect of Free Polymer on the Structure of a Polymer Brush and Interaction between Two Polymer Brushes. Macromolecules 1994, 27, 3238–3248.

Chapter 6:

(1) Fleer, G.J.; Tuinier, R. Analytical Phase Diagrams for Colloids and Non-adsorbing polymer. Adv. Colloid Interface Sci., 2008, 143, 1-47.

(2) Khammar, M.; Shaw, J.M.; Estimation of Phase Composition and Size of Asphaltene Colloidal Particles in Mixtures of Asphaltene + Polystyrene + Toluene at 293K and Atmospheric Pressure, Fluid Phase Equilib., 2012, 332,105-119.

(3) Nikooyeh, K.; Shaw, J.M. On Enthalpies of Solution of Athabasca Pentane Asphaltenes and Asphaltene Fractions. Energy Fuels, 2013, 27(1), 66-74.

(4) Ostwald, W. On the Assumed Isomerism of Red and Yellow Mercury Oxide and the Surface-Tension of Solid Bodies. Zeitschrift Fur Physikalische Chemie-Stochiometrie Und Verwandtschaftslehre, 1900, 34, 495-503.

(5) Freundlich, H. Kapillarchemie. Akademische Verlagsgessellschaft, 1909, Leipzig.

Appendix A. MATLAB Code for Calculation of the Phase Diagram of Asphaltene Aggregates + Polystyrene

```
close all;
clear all;




Mw=393000;% Polystyrene molecular weight (g/mol)
T=-25;
Rg=(17*(0.998*(1-exp((-78-(T))/131))+1));% Radius of gyration of the
polymer (nm)
NA=6.0221417930e23; % Avogrado number
Cp_over=3*Mw/(4.*pi*((Rg*1.e-9)^3)*NA);% Polymer overlap concentration
phi_over=Cp_over/(1.047e6);% Polymer overlap volume fraction




Y_star=1.464;
eta_star=0.317;
f_star=eta_star/(1-eta_star);
eta_stars=0.594;
f_stars=eta_stars/(1-eta_stars);
```

```
%----- parameters for minimization:
opts.tol=1.e-8;
opts.maxevals=100;
opts.maxits=100;
opts.maxdeep=100;
opts.globalmin=0.;

fs_star=1.465;

 %------- Critical Point Calculation ------

myfunc_crit = @(vec)integ_object_critical(vec,Rg);

X0=[Y_star f_star];

[X f_valX]=fminsearch(myfunc_crit,X0,optimset('TolX',1e-8,'MaxFunEvals',...
    50000,'MaxIter',50000))

Yc=X(1)
fcritical=X(2)
%-------------------------------------------

gama=0.77;
etasmin=0.542;
fsmin=etasmin/(1.-etasmin);

    lb=[0.4*Y_star 0.];
```

```
ub=[1.6*Y_star fcritical];


bounds(:,1)=lb;
bounds(:,2)=ub;


opts.tol=1.e-8;
opts.maxevals=5000;
opts.maxits=5000;
opts.maxdeep=50;
opts.globalmin=0.;


fLvec2=fcritical:0.02:0.45;


for j=1:length(fLvec2)




    myfunc_LL= @(vec) Obj_LL_integr(vec,fLvec2(j),Rg);


    Problem.f=myfunc_LL;
    [ret_minval,final_xatmin]=Direct(Problem,bounds,opts)


      Y_LG(j)=final_xatmin(1);
      fLvec1(j)=final_xatmin(2);
      qR(j)=qR_Cal(fLvec1(j),Rg);
      y_LG(j)=Y_LG(j)./(qR(j).^(-1./gama));
      qRd(j)=qRd_Cal(fLvec2(j),Rg);
```

```
        yd_LG(j)=Y_LG(j)./(qRd(j).^(-1./gama));


    end


%---------------------------------
qRc=qR_Cal(fcritical,Rg);
yc=Yc./(qRc^(-1./gama));



open('1.fig')




   aa =     0.99    ;
   bb =     0.001835;
   cc =    -1.112   ;
   dd =    -31.05   ;


  %---- Liquid Gas ------
  etaLvec1=(fLvec1./(1+fLvec1))./((aa.*exp(bb.*fLvec1) +...
    cc.*exp(dd.*fLvec1))).^1;
  etaLvec2=(fLvec2./(1+fLvec2))./((aa.*exp(bb.*fLvec2) +...
    cc.*exp(dd.*fLvec2))).^1;
```

```
   [alphaG]=cal_alpha_y(fLvec1,Rg,Y_LG);
   [alphaL]=cal_alpha_yd(fLvec2,Rg,Y_LG);

   phi_LG=y_LG.*phi_over;
   phid_LG=yd_LG.*phi_over;
   fi_LG_G=alphaG.*phi_LG;
   fi_LG_L=alphaL.*phid_LG;




%---------------------------------
etacritical=(fcritical./(1+fcritical))./((aa.*exp(bb.*fcritical) +...
    cc.*exp(dd.*fcritical))).^1;
f_critical= etacritical./(1-etacritical);

[alphacritical]=cal_alpha_y(fcritical,Rg,Yc);

phi_crit=yc*phi_over;
fi_critical=alphacritical*phi_crit;
      k=1;

for i=1:length(eta)
```

```
    for j=1:length(etaLvec2)
       del=(((fi_LG_G(j)-fi_LG_L(j))./(etaLvec1(j)-etaLvec2(j)))...
           .*(eta(i)-etaLvec1(j)))+fi_LG_G(j)-PHI(i);
       if abs(del)<0.003



       Rc(k)=(etaLvec2(j)-eta(i))./(etaLvec2(j)-etaLvec1(j));
       RR(k)=R(i);
       k=k+1;
       end
    end
end
  for j=1:length(etaLvec2)


eta50(j)=etaLvec2(j)+(0.5.*(etaLvec1(j)-etaLvec2(j)));
PHI50(j)=fi_LG_L(j)+(0.5.*(fi_LG_G(j)-fi_LG_L(j)));



  end
  for j=1:length(etaLvec2)
  etaL_vec1(j+1)=etaLvec1(j);
  etaL_vec2(j+1)=etaLvec2(j);


  fi_LG_GG(j+1)=fi_LG_G(j);
  fi_LG_LL(j+1)=fi_LG_L(j);
  end
```

```
  etaL_vec2(1)=eta50(1);
  fi_LG_LL(1)=PHI50(1);
  etaL_vec1(1)=eta50(1);
  fi_LG_GG(1)=PHI50(1);

  plot(etaL_vec1,fi_LG_GG,'r--','Linewidth',2);hold on;
  plot(etaL_vec2,fi_LG_LL,'b--','Linewidth',2);hold on;
  ylim([0. 0.07]);
  xlim([0 0.30]);
  xlabel('   Asphaltene Volume Fraction ','FontSize',16);
  ylabel('Polymer Volume Fraction  ','FontSize',16);
for j=1:2:10
plot([etaLvec1(j),etaLvec2(j)],[fi_LG_G(j),fi_LG_L(j)]);hold on;
end
plot(f_critical./(f_critical+1), fi_critical,'ms','MarkerSize',20);hold on;
plot(eta50(1), PHI50(1),'g*','MarkerSize',40);hold on;

plot(eta50,PHI50,'g--','Linewidth',2);




function [alpha]=cal_alpha_y(f,Rg,Y)

c1=3.95;
```

```
gama=0.77;
qR=qR_Cal(f,Rg);
q=0.865*((qR.^(-2.)+c1*(Y.^(2*gama))).^(-0.44));



A=3*q+3*(q.^2)+(q.^3);
B=3*(q.^2).*(q+(3/2));
C=3*(q.^3);


Q=A.*f+B.*(f.^2)+C.*(f.^3);


eta=(f./(1+f));


     beta=exp(-Q);
       aa =        0.99  ;
       bb =     0.001835  ;
       cc =      -1.112  ;
       dd =      -31.05  ;
  etaLvec1=(f./(1+f))./(aa.*exp(bb.*f) + cc.*exp(dd.*f)).^1;


  flvec1=etaLvec1./(1-etaLvec1);
       p1 =    0.001274  ;
       q1 =    -0.1051  ;
       q2 =    0.003985  ;
       an =   0.4808 ;
       bn =   -6.6 ;
       cn =   15.48  ;
```

```
       dn =  -25.56 ;
  for j=1:length(flvec1)

    if flvec1(j)<0.005
      alpha(j)=((p1) ./ (flvec1(j).^2 + q1.*flvec1(j) + q2)).^0.*(1.-
eta(j)).*beta(j);
  else
 alpha(j)=((p1) ./ (flvec1(j).^2 + q1.*flvec1(j) + q2)).^1.*(1.-
eta(j)).*beta(j);
    end
  end
    return




function [pv mu]=cal_pv_mu(Y,f,qR,flag)

[mu0,pv0]=f_mupv0_int(f,flag);

YY=0:0.001*Y:Y;

myfunc_pv =fun_pvp(YY,f,qR);
integral_pv= trapz(YY,myfunc_pv);

pv=pv0+integral_pv;
```

```
myfunc_mu =fun_mup(YY,f,qR);
integral_mu=trapz(YY,myfunc_mu);

mu=mu0+integral_mu;



return









function [funct_mup]=fun_mup(Y,f,qR)

gama=0.77;
c1=3.95;

term=(qR.^(-2.))+c1*(Y.^(2*gama));

q=0.865*(term.^(-0.44));



A=3*q+3*(q.^2)+(q.^3);%
```

```
B=3*(q.^2).*(q+(3/2));
C=3*(q.^3);

Q=A*f+B*(f.^2)+C*(f.^3);
Q1=A+2*B*f+3*C*(f.^2);
Q2=2*B+6*C*f;
Q3=6*C;

eta=(f./(1+f));

    beta=exp(-Q);

  beta1=-beta.*Q1;
  beta2=-beta.*Q2-beta1.*Q1;
  beta3=-beta.*Q3-2*beta1.*Q2-beta2.*Q1;


  psi=1+q;

  c2=1.62;
  dpidY=(qR^(-3+(1/gama)))+3*gama*c2*(Y.^(3*gama-1));

  funct_mup=(beta-(1+f)*beta1).*dpidY;


  end
```

```
function [funct_pvp]=fun_pvp(Y,f,qR)


gama=0.77;

c1=3.95;

af=ac(f);

term=(qR.^(-2.))+c1*(Y.^(2*gama));


q=0.865*(term.^(-0.44));


A=3*q+3*(q.^2)+(q.^3);%

B=3*(q.^2).*(q+(3/2));

C=3*(q.^3);


Q=A*f+B*(f.^2)+C*(f.^3);

Q1=A+2*B*f+3*C*(f.^2);

Q2=2*B+6*C*f;

Q3=6*C;


eta=(f./(1+f));


    beta=exp(-Q);


  beta1=-beta.*Q1;

  beta2=-beta.*Q2-beta1.*Q1;
```

```
  beta3=-beta.*Q3-2*beta1.*Q2-beta2.*Q1;

  psi=1+q;

  h=beta-f.*beta1;
  c2=1.62;

  dpidY=(qR^(-3+(1/gama)))+3*gama*c2*(Y.^(3*gama-1));
  af=ac(f);
  funct_pvp=(h./(4./3.*pi.*af.^3)).*dpidY;

  end



function [funct_pvp1]=fun_pvp1(Y,f,Rg)

gama=0.77;
c1=3.95;
qR=qR_Cal(f,Rg);

term=(qR^(-2.))+c1*(Y.^(2*gama));

q=0.865*(term.^(-0.44));

qR1=qR1_Cal(f,Rg);
```

```
qR2=qR2_Cal(f,Rg);
qR3=qR3_Cal(f,Rg);

q1=-0.44*0.865.*(term.^(-0.44-1)).*(-2.*qR.^-3).*qR1;
q2=((-0.44).*0.865.*(term.^-1.44)).*(6.*qR.^-4.*qR1.^2+qR2.*(-2.*qR.^-
3))...
   +(-1.44.*-0.44.*0.865.*term.^-2.44.*-2.*qR.^-3.*qR1).*(-2.*qR.^-3.*qR1);
q3=(2.*(-1.44.*-0.44.*0.865.*term.^-2.44.*-2.*qR.^-3.*qR1).*(6.*qR.^-4.*...
   qR1.^2+qR2.*(-2).*qR.^-3))+((-0.44.*0.865.*term.^1.44).*(-24.*qR.^-5....
.*qR1.^2+2.*qR1.*qR2.*6.*qR.^-4+qR3.*(-2).*qR.^-3+(-3).*(-2).*qR.^-4....
.*qR1.*qR2))+(-2.44.*-1.44.*-0.44.*0.865.*term.^-3.44.*-2.*qR.^-3.*qR1...
.*-2.*qR.^-3.*qR1+(6.*qR.^-4.*qR1.^2+qR2.*(-2.*qR.^-3.*qR1)).*(-1.44.*...
-0.44.*0.865.*term.^-2.44.*-2.*qR.^-3.*qR1)).*(-2.*qR.^-3.*qR1);

A=((1.+q).^3)-1.;%
B=3*(q.^2).*(q+(3/2));
C=3*(q.^3);

A1=3.*(1.+q).^2.*q1;
B1=(9.*q.^2.+9.*q).*q1;
C1=9.*q.^2.*q1;

A2=6.*(1+q).*q1.^2+q2.*3.*(1+q).^2;
B2=(18.*q+9).*q.^2+q2.*(9.*q.^2+9.*q);
C2=18.*q.*q1.^2+9.*q2.*q.^2;

A3=6.*q1.^3+2.*q.*q3.*6.*(1+q)+q3.*(3.*(1+q).^2)+6.*(1+q).*q1.*q2;
B3=18.*q.*q1.^3+2.*18.*q1.*q2.*q+q3.*9.*q.^2+18.*q.*q1.*q2;
```

```
C3=18.*q1.^3+2.*q1.*q2.*18.*q+q3.*9.*q.^2+18.*q.*q1.*q2;


Q=A*f+B*(f.^2)+C*(f.^3);
Q1=(A1.*f+A)+(B1.*f.^2+2*B*f)+(3*C.*(f.^2)+C1.*f.^3);
Q2=(A2.*f+A1+A2)+(B2.*f.^2+2.*2.*f.*B1+2*B)+(C2.*f.^3+3.*f.^2.*C1+6*C*f+3.*
f.^2.*C1);
Q3=(A3.*f+3.*A2)+(B3.*f.^2+3.*2.*f.*B2+6.*B1)+(C3.*f.^3+3.*f.^2.*C2+3.*...
    6.*f.*C1+6.*C);


eta=(f./(1+f));


    beta=exp(-Q);



  beta1=-beta.*Q1;
  beta2=-beta.*Q2-beta1.*Q1;
  beta3=-beta.*Q3-2*beta1.*Q2-beta2.*Q1;



  c2=1.62;



  dpivdY=(qR^(-3+(1/gama)))+3*gama*c2*(Y.^(3*gama-1));


  af=ac(f);
  syms d;
  af1=subs(diff(ac(d),d),d,f);
```

```
  funct_pvp1=((((-f.*beta2).*(4./3.*pi.*af.^3))-(4.*pi.*af.^2.*af1.*...
      (beta-f.*beta1))).*dpivdY;/(4./3.*pi.*af.^3).^2).



end



function [funct_pvp2]=fun_pvp2(Y,f,Rg)

gama=0.77;
c1=3.95;
qR=qR_Cal(f,Rg);

term=(qR^(-2.))+c1*(Y.^(2*gama));

q=0.865*(term.^(-0.44));

qR1=qR1_Cal(f,Rg);
qR2=qR2_Cal(f,Rg);
qR3=qR3_Cal(f,Rg);

q1=-0.44*0.865.*(term.^(-0.44-1)).*(-2.*qR.^-3).*qR1;
q2=((-0.44).*0.865.*(term.^-1.44)).*(6.*qR.^-4.*qR1.^2+qR2.*(-2.*qR.^-
```

```
3))...
   +(-1.44.*-0.44.*0.865.*term.^-2.44.*-2.*qR.^-3.*qR1).*(-2.*qR.^-3.*qR1);
q3=(2.*(-1.44.*-0.44.*0.865.*term.^-2.44.*-2.*qR.^-3.*qR1).*(6.*qR.^-4.*...
   qR1.^2+qR2.*(-2).*qR.^-3))+((-0.44.*0.865.*term.^1.44).*(-24.*qR.^-5....
.*qR1.^2+2.*qR1.*qR2.*6.*qR.^-4+qR3.*(-2).*qR.^-3+(-3).*(-2).*qR.^-4....
.*qR1.*qR2))+(-2.44.*-1.44.*-0.44.*0.865.*term.^-3.44.*-2.*qR.^-3.*qR1...
.*-2.*qR.^-3.*qR1+(6.*qR.^-4.*qR1.^2+qR2.*(-2.*qR.^-3.*qR1)).*(-1.44.*...
-0.44.*0.865.*term.^-2.44.*-2.*qR.^-3.*qR1)).*(-2.*qR.^-3.*qR1);

A=((1.+q).^3)-1.;%
B=3*(q.^2).*(q+(3/2));
C=3*(q.^3);

A1=3.*(1.+q).^2.*q1;
B1=(9.*q.^2.+9.*q).*q1;
C1=9.*q.^2.*q1;

A2=6.*(1+q).*q1.^2+q2.*3.*(1+q).^2;
B2=(18.*q+9).*q.^2+q2.*(9.*q.^2+9.*q);
C2=18.*q.*q1.^2+9.*q2.*q.^2;

A3=6.*q1.^3+2.*q.*q3.*6.*(1+q)+q3.*(3.*(1+q).^2)+6.*(1+q).*q1.*q2;
B3=18.*q.*q1.^3+2.*18.*q1.*q2.*q+q3.*9.*q.^2+18.*q.*q1.*q2;
C3=18.*q1.^3+2.*q1.*q2.*18.*q+q3.*9.*q.^2+18.*q.*q1.*q2;

Q=A*f+B*(f.^2)+C*(f.^3);
Q1=(A1.*f+A)+(B1.*f.^2+2*B*f)+(3*C*(f.^2)+C1.*f.^3);
Q2=(A2.*f+A1+A2)+(B2.*f.^2+2.*2.*f.*B1+2*B)+(C2.*f.^3+3.*f.^2.*C1+6*C*f+3.*
```

```
f.^2.*C1);
Q3=(A3.*f+3.*A2)+(B3.*f.^2+3.*2.*f.*B2+6.*B1)+(C3.*f.^3+3.*f.^2.*C2+3.*...
    6.*f.*C1+6.*C);

eta=(f./(1+f));

    beta=exp(-Q);

  beta1=-beta.*Q1;
  beta2=-beta.*Q2-beta1.*Q1;
  beta3=-beta.*Q3-2*beta1.*Q2-beta2.*Q1;



  psi=1+q;

  c2=1.62;



  dpivdY=(qR^(-3+(1/gama)))+3*gama*c2*(Y.^(3*gama-1));

  af=ac(f);
  syms d;
  af1=subs(diff(ac(d),d),d,f);
  af2=subs(diff(ac(d),d,2),d,f);

  funct_pvp2=(((((-beta2-f.*beta3).*(4./3.*pi.*af.^3)+(4.*pi.*...
      af.^2.*af1).*(-f.*beta2))-
```

```
(((8.*pi.*af.*af1.^2)+(4.*pi.*af.^2.*af2)...
      ).*(beta-f.*beta1)+(-f.*beta2).*(4.*pi.*af.^2.*af1))).*(4./3.*pi.*...
      af.^3).^2)-((2.*(4./3.*pi.*af.^3).*(4.*pi.*af.^2.*af1)).*(((-f.*...
      beta2).*(4./3.*pi.*af.^3))-(4.*pi.*af.^2.*af1.*(beta-
f.*beta1))))).*...
      ((4./3.*pi.*af.^3).^4).*dpivdY;



  end
```